Stony Brook University

Energy Efficient Ethanol Dehydration Using Nanofiborus Based Membranes

A Dissertation Presented

by

Tsung-Ming Yeh

to

The Graduate School

in Partial Fulfillment of the

Requirements

for the Degree of

Doctor of Philosophy

in

Materials Science and Engineering

Stony Brook University

December 2013

Stony Brook University

The Graduate School

Tsung-Ming Yeh

We, the dissertation committee for the above candidate for the

Doctor of Philosophy degree, hereby recommend

acceptance of this dissertation.

Devinder Mahajan – Dissertation Advisor
Professor, Department of Materials Science and Engineering

Benjamin S. Hsiao – Dissertation Advisor
Professor, Chemistry Department

Benjamin Chu – Dissertation Advisor
Distinguished Professor, Stony Brook University

Tae Jin Kin
Assistant Professor, Department of Materials Science and Engineering

Ashutosh Gupta – External Examiner
Senior Scientist, Pfizer Inc.

This dissertation is accepted by the Graduate School

Charles Taber

Dean, Graduate School

Abstract of the Dissertation

Energy Efficient Ethanol Dehydration Using Nanofiborus Based Membranes

by

Tsung-Ming Yeh

Doctor of Philosophy

in

Materials Science and Engineering

Stony Brook University

2013

In this study, nanofibrous based membranes were designed, fabricated, characterized and then evaluated for ethanol dehydration in terms of flux, separation factor and energy efficiency. The developed pervaporation (PV) membranes comprise of a barrier layer and a thin-film nanofibrous composite (TFNC) as the supporting scaffold. The TFNC scaffold consisted of three layers: an ultra-fine cellulose nanofibrous (CN) layer, a polyacrylonitrile (PAN) electrospun nanofibrous mid-layer and a polyethylene terephthalate (PET) nonwoven microfibrous bottom layer. The TFNC scaffold had high bulk porosity (up to 80% on electrospun nanofibers) and high surface to volume ratio, and formed a fully interconnected pore structure with 52% - 80% of pressure drop from the similar class of commercial membranes. The nanofibrous scaffold also provided lower transport resistance and minimized the Kundson diffusion behavior for pervaporation (PV). A barrier layer of polyvinyl alcohol (PVA) cross-linked by fumaric acid, was coated on TFNC to form a PV membrane, which showed superior performance during evaluation for ethanol dehydration, when compared with the same conventional PV membranes with cross-linked PVA

barrier layer. The ethanol dehydration results of this new class of PV membranes under varying operating conditions were also investigated.

Another type of barrier layer based on multilayered grapheme oxide (GO), was deposited onto the TFNC scaffold to form a high flux PV membrane, by taking advantage of the unique property of GO sheets. The ethanol dehydration experiments showed that the permeate flux doubled and the separation factor quadrupled, compared to commercial (PVA)-based membranes. The morphology of the GO-TFNC membranes and the mechanism of water transport in the GO layer were also elucidated. Further modification of GO was achieved by using an optimal amount of borate to cross-link GO and thereby to stabilize GO. This treatment could improve the thermal stability without affecting the permeability due to the interplay between the enlarged nanocapillary and the reduced hydrophilicty of the GO layer. Both PVA-TFNC and GO-TFNC membrane systems showed promise for possible replacement of the expensive distillation step in the commercial fermentation ethanol production process.

Table of Content

List of Figure

List of Table

Acknowledgment

For these years of my long journey to pursue the degree, I am sincerely grateful to my advisers, Professors Devinder Mahajan, Benjamin Hsiao, and Benjamin Chu, for supporting me and providing immeasurable assistance, not just with my research, also with my parts of life in Stony Brook. It is rare to have three advisers for a PhD thesis, especially when they are experts in dissimilar fields and have profound knowledge in individual aspects. Therefore, I felt lucky to have them to mentor me through this study; also I learned much interdisciplinary experiences and knowledge from them, which developed my various expertise and broadened my profession. I am also grateful to my committee members, Dr. Ashutosh Gupta and Professor Tae-Jin Kim for their insightful comments, suggestions, and encouragements.

I would like acknowledge the support given by the senior scientists and faculty, Drs. Dufei Fang, Christian Burger, Hongyang Ma, Lixia Rong and Shigeyuki Toki. They provided me crucial assistance in technical aspects and valuable suggestion over these years.

Many thanks to all members of two groups for helping with each other and sharing a good time together: Low Carbon Energy Management (L-CEM) Group: Saurabh, Wei, Kristine, Julia, Celest, Andrew, Jeff, and Prasad. Hsiao's & Chu's Group: Xiao, Justin, Zhe, Ying, Ray, Hui, Xiaowei, Edward, Ran, Yang, Yimin, Alex, Vivian, Hao. And too many friends in SB to name here.

I expressed my deepest gratitude to my parents and family for their endless love and support. Besides, I especially thank to my dear wife for her always company and cares. I would not have completed this journey without them.

Chapter 1

Introduction

Table of Content

§ 1.1. Biofuel

Biofuels represent a broad range of fuels that can be derived from biomass, such as wood waste, animal waste, municipal solid waste and vegetable oil. Biofuels are considered environmentally friendly fuels because the fixed carbon in plants when burned is recycled back. As a renewable source of energy, it reduces demand on fossil fuels while it burns more cleanly, resulting in reduced emissions of CO_2, a greenhouse gas.

There is a global effort to reduce energy consumption and develop renewable energy sources, including energy produced from biomass, ocean, wind, and solar. According to the World Committee of Energy Council, by 2070, about 60% of total world energy will come from renewable energy resources.[1] In the U.S., the Energy Independence and Security Act of 2007 (EISA) set targets for renewable fuels at 9 billion gallons annually for 2008, expanding to 36 billion gallons per year by 2022 [2]. Similarly, the European Union recommendations will raise ethanol production and subsidize it over the next several years

Bioethanol is presently the most used commercial biofuel. It is used as an additive to gasoline because it can also raise the octane number and combustibility of gasoline. At 10 wt% of ethanol in gasoline, present car engines do not need any modifications to adjust the fuel composition. In January 2011, the Environmental Protection Agency (EPA) granted a new waiver to increase the ethanol volume to 15% in gasoline for vehicles built after 2000. For the above reasons, ethanol consumption is growing rapidly. According to the U.S. Energy Information Administration (EIA) statistics, ethanol consumption grew by 440% between 2002 and 2009 (Table 1-1). The U.S. government has further set a goal to displace 1/3 petroleum usage

to substitute by renewables by 2022 (Figure 1.1). The US ethanol consumption was at 12.8 billion gallons in 2010, though it is purely produced from corn.

Table 1-1 Ethanol consumption and production [3]

Annual U.S. ethanol production and consumption

Year	Production	Consumption
2002	2140	2173
2003	2804	2826
2004	3404	3552
2005	3904	4059
2006	4884	5481
2007	6521	6886
2008	9309	9683
2009	10938	11037
2010	13298	12858
2011	13929	12893
2012	13218	12882
2013*	8656	8709

(million U.S. gallons)
*Till August, 2013

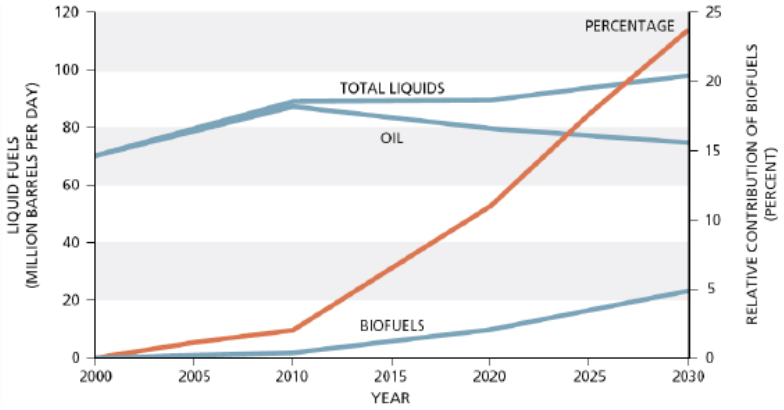

Figure 1-1 Proceeded fuel consumption in U.S. [4]

§ 1.2. Ethanol production methods

§ 1.2.1 Ethanol process flow sheet

The main processes involving ethanol production are storage and preparation of raw materials, pre-treatment, cellulose hydrolysis, fermentation of ethanol and ethanol refining. For example, the lignocellulosic raw materials, such as barley and wheat straw, are milled, cleaned and then pre-treated. The pre-treated biomass is then digested by enzymes to release sugar molecules, which are further fermented by yeast to produce ethanol, CO_2 and a large quantity of water. Further conventional processing involves distillation that results in an azeotrope. In the final treatment to produce fuel-grade ethanol, the azeotrope is subjected to treatment, such as molecular sieve, and ethanol of purity (99.9%) is obtained. The water removal steps are energy intensive and it is the subject of the present study.

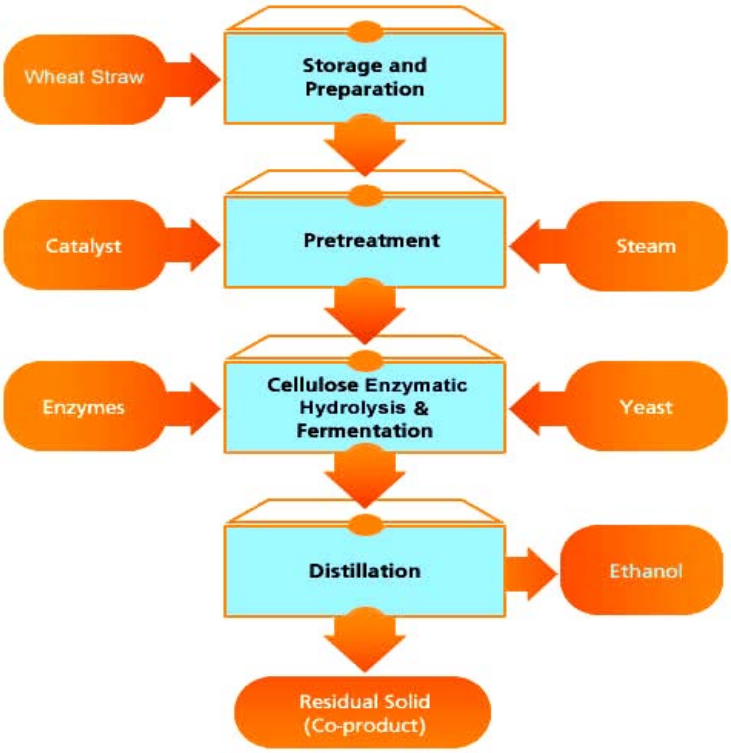

Figure 1-2 Schematics of ethanol production.[5]

§ 1.2.2 Ethanol purification methods

Ethanol with water content of < 0.5% is regarded as a fuel for blending with gasoline. For most industrial and fuel uses, the ethanol must be purified after the fermentation step. Conventional corn fermentation produces ethanol that can be subjected to conventional distillation, which is based on the difference between boiling points of water and ethanol. The distillation process produces an azeotrope (95% ethanol and water) (Table 1-2). Production of anhydrous ethanol requires overcoming the barriers of a positive azeotrope. Various alcohols form azeotropes with water (Table 1-2).

Table 1-2 Different azeotropes between water and alcohols[6]

Components	Boling point (℃)	Azetrope point (℃)	Compositions of Azetrope (wt%)
Water	100.0	78.15	4.4
Ethanol	78.3		95.6
Water	100.0	80.3	12.3
Isopropanol	82.3		87.4
Water	100.0	93.0	44.5
1-Butanoal	117.7		55.5

Dehydration of ethanol is a separate manufacturing step requiring additional labor, energy, and expense. Below we first consider various options of dehydration (not including pervaporation) that include absorption methods (e.g. dehydration by molecular sieves), extraction, pressure reduced distillation, and azeotropic distillation.

Adsorption

Liquid phase adsorption and vapor phase adsorption by membranes are two water removal techniques used in the separation of water/ethanol mixtures. Adsorbents employed in liquid phase are generally type A zeolites, cellulose based materials, etc. Vapor phase water adsorption widely relies on inorganic adsorbents, such as zeolite molecular sieves (3A and 4A), lithium chloride, and silica gel. Substances of biological origin are considered only as potential adsorbents for this application.

Synthetic molecular sieves offer some technological advantages, like long service life of up to 5 years, regeneration, and high economic efficiency due to high adsorption capacity and high water diffusion rate. However, compared to pervaporation, water adsorption is now attracting much less attention. But using zeolite membranes with high adsorption ability in pervaporation have been emphasized for a period of time

Besides zeolite based materials, carbon is another efficient water adsorbent. It can dehydrate water from 1.6% – 50.9% water/ethanol mixtures. The process is more stable if heated by air or nitrogen in the 80 – 120 °C temperature range.

A commercial process named “Pressure Swing Adsorption” (PSA), is conducted in an adsorption/desorption column through pressure difference. Adsorption is carried out on zeolites at an elevated pressure of 379.2 kPa and a temperature of 440 K. The feed, which contains 92 wt % ethanol, is introduced in the top section of the column at a rate of 10410 kg/h. The ethanol concentration in the product stream is above 99.5 wt%.[7]

However, due to high total cost of ethanol production by adsorption, current efforts are focused on experimental determination of the capacity of various zeolites for separating ethanol/water mixtures and on simulation of adsorption in particular systems.[8]

Extraction

The solvents used in the liquid/liquid extraction of ethanol from dilute aqueous fermentation solutions must meet many requirements, including low solubility in the aqueous phase, short separation time, chemical inertness, and environmental friendliness. Generally, extraction of ethanol from fermentation broths is processed by hexadecane. The extracting agent is completely soluble above the upper critical solution temperature (UCST) and is partially soluble at lower temperatures (in the two phase region between 60~100 °C). The hot solvent is brought into contact with the water–ethanol mixture at 115 °C (15° above UCST) to extract ethanol. The ethanol/solvent mixture is then cooled to 30 °C in a separator, and the solvent is returned to the extractor. According to experimental data, this separation process affords ethanol containing <1% water [9].

Separation of water/ethanol mixtures with supercritical CO_2 ($ScCO_2$) has not been commercialized. It is only used in the separation of organics in pharmaceutical industry. $ScCO_2$ has a comparatively low critical point (7.38 MPa, 304.25K) (Figure 1.3) and is relatively inexpensive. Furthermore, it is environmentally friendly and CO_2 is easy to recover. Using $ScCO_2$, the extraction is readily separable from ethanol in a distillation column under elevated pressures. Since the CO_2/ethanol/water mixture is azeotropic at 333.2 K and 10 MPa, it can also be separated by conventional distillation. According to Figure 3-1, $ScCO_2$ extraction consumes less energy than azetropic distillation, but it still wastes more energy than other alternatives.

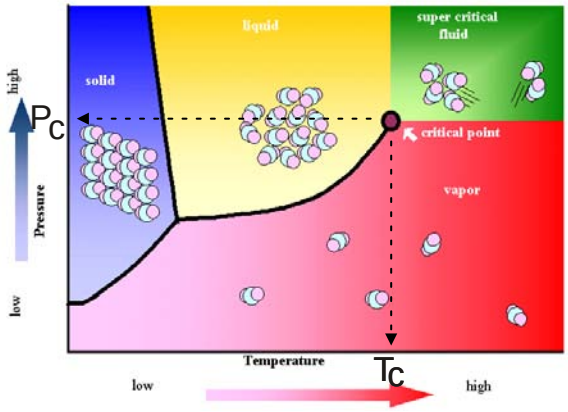

Figure 1-3 Phase diagram of supercritical carbon dioxide. [77]

Pressure Reduction (Pressure Swing) Distillation

At pressures less than 1 atmospheric, the composition of the ethanol-water azeotrope shifts to more ethanol-rich mixtures, and at pressures less than 70 torr (9.333 kPa), there is no azeotrope. Thus, it is possible to distill absolute ethanol from an ethanol-water mixture. While vacuum distillation of ethanol is not presently economical, pressure-swing distillation is a topic of current research. In this technique, a reduced-pressure distillation first yields an ethanol-water mixture of more than 95.6% ethanol. Then, fractional distillation of this mixture at atmospheric pressure distills off the 95.6% azeotrope, leaving anhydrous ethanol at the bottom.

Figure 1-4 shows the typical distillation flow sheet for the ethanol (1)/water (2) mixture with the composition X_F. The appropriateness of this flow sheet is governed by the value of the azeotropic shift $\Delta x = x''–x'$ (the change in azeotrope composition) caused by the change in pressure from P_1 to P_2. The maximum Δx value in the technologically acceptable pressure range minimizes the recycle rate and reduces the energy required for separation [10].

Pressure reduction is not presently economical, and just used in the dehydration of ethanol resulting from fermentation by combing with the distillation step.

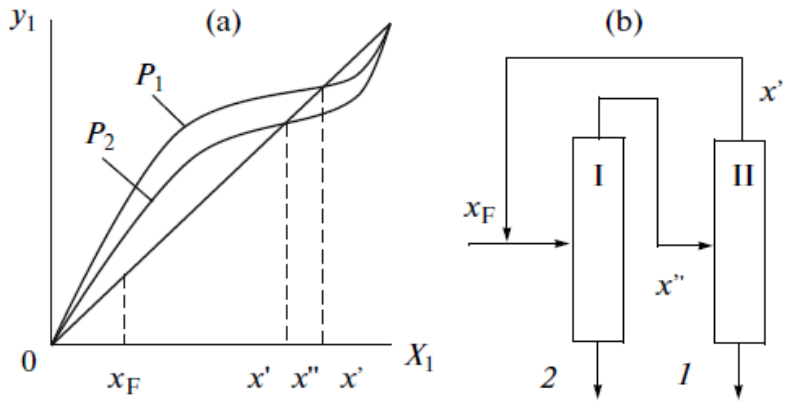

Figure 1-4 Pressure swing distillation of the azeotropic mixture ethanol (1) water (2): (a) liquid–vapor equilibrium diagram; y_1 and x_1 means vapor and water composition of ethanol, respectively. (b) distillation flow sheet involving (I) a column operating at pressure P_1 and (II) a column operating at pressure P_2 [11]

Azeotropic Distillation

Presently, fractional distillation can concentrate ethanol to 95.6 wt %. though refining distillated techniques, such as extractive, azetropic, and vacuum, and can extract ethanol to 99.5%, the minimum purity needed to produce fuel-grade ethanol. Among these techniques, azeotropic distillation is one of the most widespread and efficient processes.

In azeotropic distillation, a substance forming homogeneous or heterogeneous azeotrope with components of the initial mixture is introduced into the column. The separation of the new azeotropic mixture requires a special technique. It is commonly thought that azeotropic distillation in most cases is less economical in terms of energy because the azeotrope-forming agent undergoes multiple evaporations.

Homoazeotropic distillation is considered to be appropriate when the mixture of the azeotrope forming agent with one of the components is usable without being separated. For dehydration of ethanol/water mixtures, the only separation agent of this kind is ethylenediamine. It forms a homogeneous, maximum boiling azeotrope with water and is unstable without water.

Heteroazeotropic distillation is the azeotropic distillation technique in which the liquid is separated deliberately into two phases by introducing a heteroazeotrope forming agent into the system. A classic example of heteroazeotropic distillation is ethanol dehydration with benzene. In this process, benzene (3), which has limited solubility in water, is added to the azeotropic ethanol (1) water (2) mixture (Fig. 1.5a). In the steady state operation of the separation complex, the organic (benzene) layer plays the role of the heteroazeotrope forming agent. Other separation agents, including dichloroethane, isobutyl alcohol, butyl acetate, propyl acetate, diethyl ether, diisopropyl ether, cyclohexane, 2,2,4 trimethylpentane, toluene, n-pentane, cyclopentane, methylcyclopentane, n-hexane, 2- methylpentane, and 2, 2, 3-trimethylbutane can be used [11, 12]. Because the fermentation of bio-feedstock, biowaste, polysaccharides, sugar, and other biomaterials produces dilute aqueous ethanol solutions, it needs a distillation process for pre-concentration prior to the heteroazeotropic distillation (Fig. 1-5b).

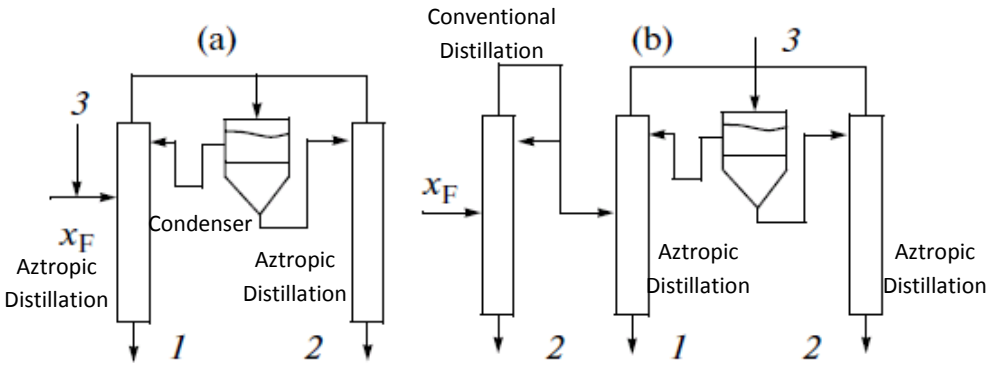

Figure 1-5 Dehydration of ethanol with the feed composition X_F (1)–water,(2)–mixtures by heteroazeotropic distillation, (3) –benzene : Diagram of normal separation complex (a) and (b) a complex with an conventional distillation for concentration of feed.[12]

Among all techniques mentioned above, based on the cost comparison (Table 1-3), adsorption, vapor permeation, and pervaporation are highly competitive to distillation. Adsorption needs the least energy to produce ethanol but expensive equipment makes it less competitive. Therefore, pervaporation is one of the most economical technologies.

Table 1-3 Comparison of the cost of ethanol dehydration (94 wt. %- 99.8 wt. %) by various techniques (Costs were estimated in US$ per ton of dehydrated ethanol)[13]

cost	**Vapor Permeation**	**PV.**	**Az. Distil.**	**Adsorption**
Operation	11	8.6	44	23.8
Reloading cost	4.75	6	n/a	12.5
Total	15.75	14.6	44	36.3

§ 1.3. Statement of problem

Bioethanol is wildly used as a fuel-additive and the demand for ethanol is increasing rapidly. Hence, an efficient and clean ethanol recovery technique to replace distillation is desirable. For all potential technologies to replace distillation, meeting the economic aspect is the basic requirement. Besides, from the engineering point of view, present tendency in separation techniques is toward combining a chemical reaction and a separation mass transfer process in one apparatus, that usually exhibits better performance than the process based only on physical mechanism. The membrane techniques have those characteristics, and are highly studied in the past two decades.

In terms of concerns including economics, eco-friendliness, and engineering concepts, pervaporation is the most promising technique to produce fuel-grade ethanol. Hence, in this study, pervaporation was developed and used for ethanol dehydration with designed membranes. More details on pervaporation and designed membranes will be discussed in the following sections.

§ 1.4. Pervaporation

§ 1.4.1 Economic aspects of ethanol dehydration by pervaporation

According to the comparison of energy consumptions (Table 1-4) between distillation and PV with different membranes, the energy consumption for ethanol dehydration (going from 95 wt.% to 99.5 wt.%) by azerotropic distillation is around thirteen times higher than that for pervaporation with polymer membranes. For this reason, many existing plants use a hybrid process - conventional distillation followed by PV. These processes could enable reductions in operational cost and energy consumption without substantially changing the production process.

Table 1-4 Energy Requirements of Ethanol Purification[14]

Process	Stream concentration (wt %) (Feed)	(Final)	Energy consumption (GJ/m^3)	(Btu/gal)	Ref.
Reverse osmosis	4.0	10.0	0.64	2,300	Bitter (1988)
Conventional distillation	10.0	95.0	4.7	17,000	Serra (1987)
Azeotropic distillation	95.0	99.9	2.0	7,200	Serra (1987)
Total	4.0	99.9	7.3	26,500	
Reverse osmosis	2.5	8.0	0.30	1,100	
Conventional distillation	8.0	92.4	6.64	23,800	
Azeotropic distillation	92.4	99.5	1.95	7,000	Leeper and Tsao (1987)
Total	2.5	99.5	8.89	31,900	
Conventional distillation	2.0	92.4	22.32	80,100	
Azeotropic distillation	92.4	99.5	1.95	7,000	Leeper and Tsao (1987)
Total	2.0	99.5	24.27	87,100	
Conventional distillation	7.0	92.4	6.2	22,200	Collura (1988)
Azeotropic distillation	92.4	99.5	1.95	7,000	Leeper and Tsao (1987)
Total	7.0	99.5	8.2	29,200	
Conventional distillation	10.0	95.0	4.74	17,000	Serra (1987)
Azeotropic distillation	95.0	99.9	2.0	7,200	Serra (1987)
Total	10.0	99.9	6.74	24,200	
Vapor recompression distillation	10.0	95.0	1.70	6,100	
Azeotropic dist (ether)	95.0	99.9	0.84	3,000	
Total	10.0	99.9	2.54	9,100	
Supercritical extraction w/CO_2	10.0	91.0	2.51	9,000	
Azeotropic distillation	92.5	99.9	>2.01	>7,200	
Total	10.0	99.9	>4.5	>16,200	Serra (1987)
Conventional distillation	8.0	80.0	—	—	
Pervaporation	80.0	99.5	—	—	
Total	8.0	99.5	3.68	13,200	Serra (1987)
Conventional distillation	10.0	87.5	—	—	
Water adsorption (cornmeal)	87.5	99.5	—	—	
Total	10.0	99.5	3.34	12,000	Serra (1987)
Two step extraction	10.0	26.0	—	—	
Conventional distillation	26.0	98.0	—	—	
Total	10.0	98.0	4.90	17,600	Serra (1987)
Conventional distillation	10.0	90.0			
Extraction with gasoline to produce gasohol	90.0	10.0	5.52	19,800	Leeper and Wankat (1982)

Azt. Dist. #4

SCO2. #3

PV. #2

Ad. #1

§ 1.4.2 Characteristics of pervaporation

Pervaporation is a new membrane technique that combines permeation and vaporization. The experimental setup (Figure 1-6) is similar to water filtration; the major difference is that there is a vacuum pump connecting to the back end of the membrane cell. During the process, a pressure difference between the feed and the permeate of the membrane is introduced, which is also the

driving force for pervaporation, in addition to the difference in the chemical potential between the solution and the membrane.

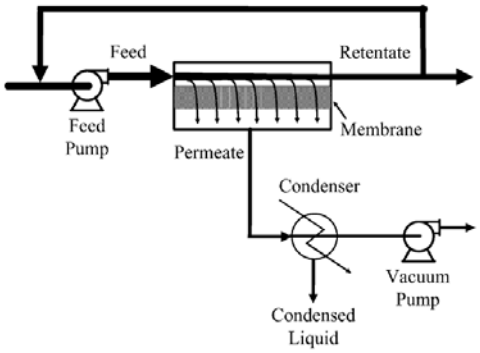

Figure 1-6 The process set-up for PV[15]

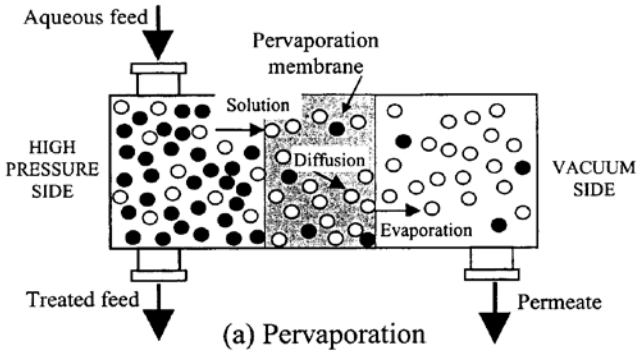

Figure 1-7 Mass transfer during pervaporation [16]

During the process (Figure 1-7), a liquid stream feeds a cell which has a semi-permeable membrane (hydrophilic or hydrophobic), the liquid separates into two streams: gas permeates through the membrane due to the pressure difference introduced by a vacuum pump and for the liquid retentate that is recycled. A permeate is enriched with a component transmitted preferentially by the membrane, compared to the retentate which has a smaller amount of the

component. Since separation by the membrane does not depend on liquid-vapor equilibrium, the process can be used efficiently for separating azeotropes and liquids with close boiling points.

In pervaporation, the separation process consists of several steps: (1) transport from bulk to the membrane interface, (2) preferential sorption on the membrane, (3) diffusion through the membrane, (4) desorption from the permeate side of the membrane [17]. Membrane transport of a species is the rate-controlling process, which is generally governed by Fick's first law:

$$N = -D\frac{dCm}{d\delta} \qquad \text{(Equation 1-1)}$$

where N is the permeation flux of a species through the membrane, Cm is the concentration of a species in the membrane, D is the diffusion coefficient of the species in the membrane, and δ is the position value for the diffusion distance.

Depending on the membrane affinity, pervaporation membranes are categorized into hydrophilic membranes and hydrophobic (organophilic) membranes. For dehydration of ethanol aqueous solution with the minority being water, hydrophilic membranes are more favored than hydrophobic membranes due to their better affinity to water and higher diffusion rate of water in the membrane.

When characterizing the performance of a pervaporation membrane, two important parameters – permeation flux J and separation factor are defined.

$$J = \frac{Q}{A\Delta t} \qquad \text{(Equation 1-2)}$$

$$\alpha = \frac{Y_W/Y_E}{X_W/X_E} \qquad \text{(Equation 1-3)}$$

where Q is weight of the permeate collected in a time interval Δt, A is the effective membrane area, X and Y represent mass fractions in the feed and the permeate, respectively. The subscripts, W and E, denote water and ethanol, respectively.

There are two principal approaches to describe the mass transport in pervaporation: (1) the solution-diffusion model and (2) the pore flow model.

§ 1.4.3 Solution-diffusion theory

The solution-diffusion model is accepted by majority of researchers (Kataoka et al., 1991a,b; Wijmans and Baker, 1995) to describe the PV process, which consists of three steps: (i) sorption of permeate from feed liquid to membrane, (ii) diffusion of permeate in membrane and (iii) desorption of permeate in the vapor phase on the downstream side of membrane. (Figure 1-8)

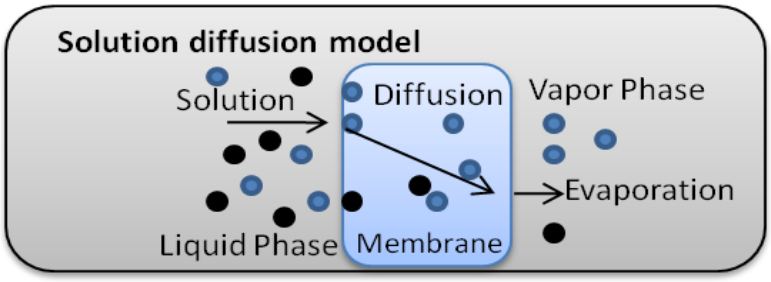

Figure 1-8 Solution-Diffusion Model.

Membrane has no pores but relies on the thermally agitated motion of chain segments comprising the polymer matrix to generate penetrant-scale transient gaps in the matrix, thereby allowing diffusion from the upstream to the downstream side of the membrane.

On the basis of Fick's Law and thermodynamics, the mass transport in a barrier layer of the membrane can be written in terms of chemical potentials [18]

$$J_i = k_{ov,i}(\mu_{b,i} - \mu_{p,i}) = \frac{\mu_{b,i} - \mu_{p,i}}{R_{ov,i}}$$

(Equation 1-4)

where $k_{ov,i}$ is the overall mass transfer coefficient of component i, $\mu_{b,i}$ and $\mu_{p,i}$ are the chemical potentials of component i in the bulk (feed) and the permeate side, respectively and $R_{ov,i}$ is the overall resistance to mass transfer of component i ($R_{ov,i} = 1/k_{ov,i}$)

During the separation process, the mass transport resistance mainly comes from the feed boundary layer and the membrane itself, while the front one can usually be neglected ($R_{bl,i}$) if the boundary effect is depleted by introducing turbulent flow. So the overall resistance can be written as [18]:

$$R_{ov,i} = R_{bl,i} + R_{m,i}$$

(Equation 1-5)

$R_{m,i}$ is the resistance from the membrane for component i. The membrane mass transfer coefficient, $k_{m,i}$, can be found easily once the resistance is known ($k_{m,i} = 1/R_{m,i}$).

$$R_{m,i} = \frac{L}{D_i S_i}$$

(Equation 1-6)

where L is the membrane thickness, D_i is the diffusion coefficient and Si is the solubility coefficient of component i in the membrane. Usually, $R_{m,i}$ is the rate-determining step assuring the pervaporation process. [19] The diffusion selectivity can thus be written as

$$(\alpha)^{diff.} = \frac{D_{i0}}{D_{j0}}\left\{1 + \frac{(\alpha_{ii} - \alpha_{ij})KC_T}{2!}X_i + \frac{[(\alpha_{ii} - \alpha_{ij})KC_T]^2}{3!}X_i^2 + \cdots\right\}$$

(Equation 1-7)

The overall diffusion selectivity of a membrane is a function of water content X_i in the feed. The diffusion selectivity decreases as the water content X_i in the feed increases, and it can thus be judged that $\alpha_{ii} < \alpha_{ij}$. The physical meaning of this inequality is that the diffusion coefficient of the more permeable species (e.g., water) is less enhanced by plasticization or membrane swelling than that of the less permeable species (e.g., alcohols). The above equation offers a theoretical interpretation on why a swollen membrane shows reduced overall diffusion selectivity.

The transport of a single component through a non-porous homogeneous membrane has been relatively well described, but for binary mixtures, the mass transport is complicated by the permeant-permeant and permeant-membrane interactions, and no overall theory exists. Base on the single-component approach and the assumption that fluid on both sides of the membrane are considered to be in equilibrium with their respective membrane interfaces, there are various modified models to the mechanism. However, the models do not specify where the phase change occurs, and it is difficult to determine which transport regime (e.g., surface diffusion, viscous flow, and slip flow) dominates the water transport in these watery regions.

§ 1.4.4 Pore-flow theory

For the reasons discussed in the previous section, the pore flow model was developed to overcome the some shortcomings of the solution-diffusion model (Okada and Matsurra, 1991). The pore flow model assumes that there are many bundles of cylinder pores on the membrane surface. There are three steps for the process: (i) liquid transport from the pore inlet to a liquid-vapor phase boundary, (ii) evaporation at the phase boundary, and (iii) vapor transport from the boundary to the pore outlet. The most important feature of the pore flow model is that it assumes the process to occur at the interface between liquid and vapor, (Figure 1-9) with a combination of

liquid transport and vapor transport in series [20]. Viscous flow takes place in the liquid section, while diffusion occurs in the vapor section.

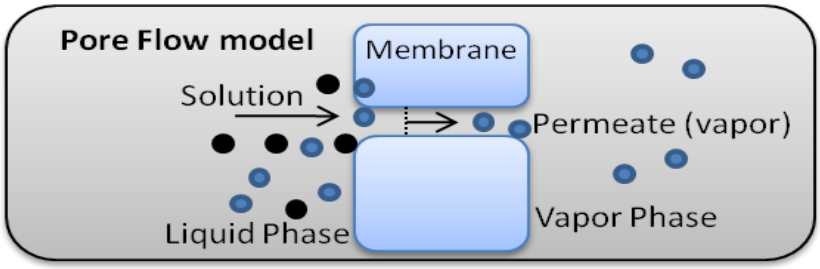

Figure 1-9 Pore Flow model

The solution-diffusion model considers the pores as passageways, allowing communication between upstream and downstream membrane face by Knudsen flow or the viscous flow mechanism. However, a dense membrane has no pores but relies on the thermally agitated motions of chain segments. Although this model offers a very good insight for understanding the modified Solution-Diffusion theory, this model oversimplifies the complex progressive change in the state/phase of the transporting species in the membrane as implied in the modified solution-diffusion model. As a transport theory, the pore-flow model lacks precision for understanding the actual mass transport in pervaporation membranes.

§ 1.4.5 Molecular view of mass transport in membrane

In the presence of strong membrane–species interactions, the pervaporation membrane can no longer be treated as a uniform medium for permeation. Shimidzu [20] et al reported that polar groups in the membrane matrix, responsible for the membrane hydrophilicity, act as fixed

carriers for mass transport in the membrane. Unlike the random walk of the less polar species Sj (Figure 1-10), the water molecule (Si) jumps from one polar site to another. The fixed carrier theory implies that water and the less polar species in the liquid mixture take different paths while diffusing through the membrane.

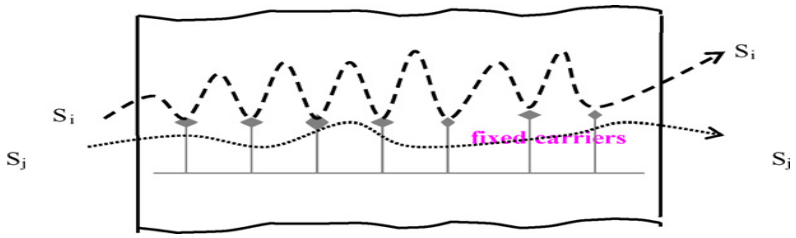

Figure 1-10 Depiction of fixed carrier theory. Si: polar species (i.e. water); Sj: less polar species [19]

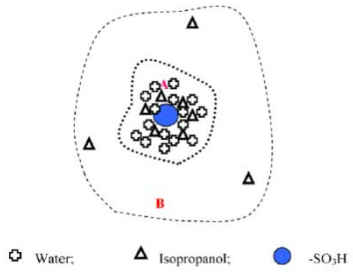

Figure 1-11 Mechanism of water dissolution in hydrophilic environment A and isopropanol dissolution in both hydrophilic and hydrophobic environment A+ environment B.[19]

On the basis of above assumptions, Cabasso and Liu [21] studied the sorption and transport behavior of water and isopropanol in Nafion hollow fiber ion membranes. They believed that water preferentially interacted with sulfonic groups, while isopropanol interacted better with –O–CF2– in the side chains, indicating that water and isopropanol transport in the membrane through different channels (Figure 1-11). It was also found that the permeation activation energies of

water and isopropanol through the membrane were essentially the same, a finding analyzed based on the aggregate model. It was concluded that the water channel in the Nafion membrane used was discrete, since otherwise water would have a smaller permeation activation energy than isopropanol.

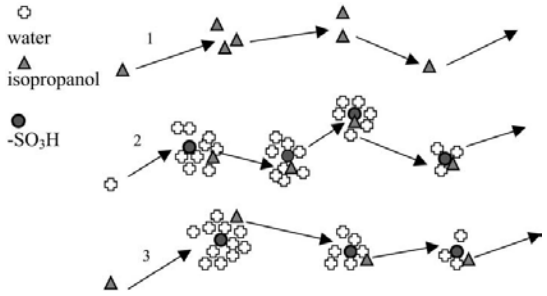

Figure 1-12 Three types of transport processes through sulfonated poly(ether ketone) membranes. [19]

Huang [22] proposed a novel model observed in the pervaporation dehydration of isopropanol by using the sulfonated poly(ether ether ketone) membranes to describe the molecular transfer mechanism in the membrane based on the fixed carrier theory and the cluster theory. When a water molecule jumped from one cluster to another, the vacancy left in the cluster could be filled by either one water molecule or one isopropanol molecule in the previous neighboring cluster (Figure 1-12), implying that the filling of the vacancy was non-selective, and the total concentration difference between the two neighboring clusters acted as the driving force for transport of both water and isopropanol. This composite driving force formed the basis of the coupled transport of the non-general type. For a specific vacancy in a cluster, the probability that the vacancy would be filled by a species (water or isopropanol) was assumed to be proportional to its local concentration. Therefore, the local diffusion coefficients of water and isopropanol

should be corrected by their respective jump probability, and the apparent local diffusion coefficient. Then, the permeation flux of water or isopropanol could be written, respectively as:

$$D_i^{\text{app.}} = D_i \frac{C_i}{C_i + C_j}$$

$$N_i = -D_i \frac{C_i}{C_i + C_j} \frac{\mathrm{d}(C_i + C_j)}{\mathrm{d}\delta}$$

(Equation 1-8)

Though experiments showed that this model provided a reasonable explanation for the coupled transport, it could not offer a picture of how the coupled transport took place in the membrane, and the physical meaning of the coupled transport was thus not well defined. However, the model did provide a valuable description of the phenomena from diffusion under molecular motion.

§ 1.5. Polymeric membranes

§ 1.5.1 Poly (vinyl alcohol) (PVA)

PVA is often used in the pervaporation of water-alcohol mixtures for its good film-forming ability, hydrophilicity, chemical and mechanical stability and low manufacturing cost [23]. However, it has to be properly cross-linked. Huang et al [76] were the first to study PVA membranes for pervaporation applications. They investigated the effects of the degree of cross-linking on pervaporation performances. A separation factor of about 100 with a flux of 0.25 kg m^{-2} h^{-1} was achieved at an operating temperature of 45 ℃ using a 50% ethanol feed mixture..

Praptowidodo et al. [24] also studied how the cross-linking degree affected the PVA pervaporation performance. Glutaraldehyde was used as the cross-linking reagent and HCl was used as the catalyst. They concluded that increased cross-linking and reduced swelling in the PVA membrane led to a reduction in flux and an increase in separation factor. But the prepared membranes suffered from swelling (more than 30%) that led to a lower separation factor of 104 at 40 ℃ using 90% of ethanol as the feed solution.

Kang et al [25] reported the surface modified PVA membrane with carboxylic acid for pervaporation. The permeate selectivity of the surface-modified membrane was almost double when compared with the unmodified cross-linked PVA membrane, and the flux was also slightly increased.

The effect of membrane layer thickness on pervaporation of composite PVA-Polysulfone (PSf) membrane was studied by Hyder et al [18]. They first reviewed the effect of thickness of the homogenous membrane on the pervaporation performance and found that the flux was inversely proportional to the membrane thickness but the selectivity remained nearly unaffected for these membranes. Later, they prepared the PVA membrane with different thicknesses (4μm, 11μm, 23μm, 38μm, and, 52μm) on the PSf ultrafiltration membrane support. Due to different surface roughness which changed with the PVA layer thickness, the membrane hydrophilicity also changed, leading to a slight selectivity variation from 95 to 110. The total flux increased by more than two-fold from the PVA membrane thickness of 4 μm to 52 μm at an operating temperature of 25 ℃ and by using 85% ethanol solution.

§ 1.5.2 Chitosan

Chitosan (1,4)-2-amino-2-deoxy-D-glucose) is the deacrylated form of chitin. It contains both hydroxyl and amino groups in the structure, which makes it extremely hydrophilic and easily modified. Many chitosan-based pervaporation membranes were prepared. The results have been summarized below.

Zhang et al. [26] prepared the glutaraldehyde cross-linked chitosan (CS-GA) membranes and then modified the surface with maleic anhydride (MA) in acetone solution. For the separation of 90 wt% ethanol/water mixture at 60 ℃, the separation factor of the CS-GA-MA membrane was 634, significantly improved by a factor of 4 compared to the CS-GA membrane, and the flux was also slightly increased.

Huang et al. [27] prepared the chitosan composite membrane having a microporous polysulfone substrate and tested for the dehydration of isopropanol. They cross-linked the chitosan membranes with GA/H_2SO_4 solution. With a thickness of the selective layer of 1 μm, the membrane yielded a moderate separating factor of around 300 and a flux of 1 kg m^{-2} h^{-1} at the operating temperature of 50 ℃ using the feed solution of 90% ethanol solution.

To suppress the membrane swelling and to enhance the membrane stability, Shieh and Huang [28] mixed the chitosan solution with polyacrylic acid and obtained very stable separatiom performance. It is known an amine group exists in each repeat unit of chitosan, and thus chitosan is polycationic. When chitosan is blended with polyanions (PAA), the amine groups in chitosan can form stable complex linkages with other anions in the polyanions, resulting in polyelectrolyte complex linkage which acts as the “ionic cross-linking” for the membrane [19]. They used the membranes for dehydration of 95% ethanol aqueous solution at

30 ℃. For the homogeneous membrane, the permeation flux was 0.033 kg $m^{-2}.h^{-1}$ and separation factor was 2216. For the composite membrane with a phase-inverted polysulfone membrane as the substrate, the permeation flux was 0.132 $kg.m^{-2}.h^{-1}$ and the separation factor was 1008. Similar work has been done by Nam et al [29]. The membrane prepared with chitosan and PPA with a weight ratio of 75:25 yielded a separation factor of more than 4,000 with a flux of 0.277 $kg.m^{-2}.h^{-1}$ at the operating temperature of 80 ℃ and by using 80% ethanol aqueous solution. When this membrane was used for the dehydration of 95% ethanol aqueous solution, the separation factor reached to more than 19,000, but the flux was only 0.022 $kg.m^{-2}.h^{-1}$ due to the thick dense membrane.

§ 1.5.3 Alginate

Alginate is a block polymer consisting of two acid residues, α-(1-4)-linked L-guluronic acid and β-(1-4)-linked D-mannuronic acid[30]. The hydrophilic nature of the polymer makes it a good material candidate for pervaporation membrane.

Sodium alginate (Na-Alg) was the first studied for the application of alcohol dehydration by pervaporation. As a membrane material, however, it lacks mechanical strength and stability in aqueous solution. Yeom et al. [31-34] improved the membrane stability by thermal treatment of the membrane at 100 ℃ for hours. They also cross-linked the membrane with glutaraldehyde. To control the solubility of the membrane, Huang et al. [35] cross-linked sodium alginate ionically by using various divalent and trivalent ions. These multivalent metal ions could interact with the carboxyl groups of the polymer and thereby limiting the mobility of polymer chains. Results showed that sodium alginate membranes cross-linked with Ca^{2+} showed the best performance in

terms of flux and separation factor for the dehydration of 90% ethanol aqueous solution (separation factor = 320, permeation flux = 0.23 $kg.m^{-2}.h^{-1}$ at an operating temperature of 50 ℃).

§ 1.5.4 Other polymeric materials

PVA, chitosan and alginate are the most commonly used polymeric materials of pervaporation membranes. Apart from them, other materials include polysulfone [36-38], polyimides [39, 40], polyamides [41], polyelectrolyte [42], and et al [43, 44]. These materials, however, either has to be modified, or, when made into membranes, show relatively poor pervaporation performance compared to those hydrophilic polymers summarized above.

Up to now, PVA, chitosan and alginate are still the most desirable polymeric materials for pervaporation membranes used for ethanol dehydration, due to their abundant hydrophilic groups in the structures. To overcome the limitations of pervaporation membranes with single materials on either pervaporation performance or structural stability, many researchers have utilized blending strategies to prepare membranes. For instance, Svang-Ariyaskul et al [45] blended chitosan and PVA to produce dense membrane for isopropyl alcohol. They reported the membrane containing 3:1 chitosan to PVA offered the best separation factor with permeates consisting of close to 100 wt% water. Rao et al [46] also did similar work using chitosan and PVA. They found the blends performed significantly better than either of the materials alone, and the cross-linked membranes provided both good mechanical strength and improved pervaporation performance. The effect of blending Na-Alg and PVA was also tested by Kurkuri et al. [47] and Dong et al [48], which also led to the conclusion that blend materials could perform better than either of the single materials.

So based on different cross-linking agent selection, cross-linking degree tuning and blending strategies, different pervaporation membranes can be obtained with these promising materials.

§ 1.6. Inorganic materials

§ 1.6.1 Ceramics

Ceramics are thermally and chemically stable materials with melting points of over 1000 ℃ and able to operate over a wide range of pH values and in many organic solvents. However, they are either normally used as the support layers of the pervaporation membrane to provide mechanical strength [49-51], or when used as the selective layer, behave relatively poor separation performance in the dehydration of ethanol [52, 53].

§ 1.6.2 Zeolites

Zeolites (aluminasilicates) are excellent inorganic candidate materials for pervaporation membranes due to their highly ordered structures. With different aluminum to silica ratios, the pore sizes of the zeolite structures ranged from about 3-8 angstroms. The pore size variation depends on different cations being attached to the framework. Like type A zeolites form a 3D structure and contain cations making them very hydrophilic (Figure 1-13).

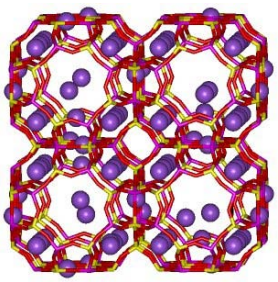

Figure 1-13: A type Zeolite (NaA zeolite), Effective Pore diameter~4A [78]

Zeolites increase the hydphilicity as the contents of Si/Al are decreased. Table 1-5 shows that the attraction of highly polar molecules results in hydrophilicity. Besides the Si/Al issue, larger pores enhance hydrophilcity. So the order of hydrophlicity for zeolites in this table is: silicalite-1< beta < NaY < NaX <COM 3A≈UOP 4A≈COM 5A

Table 1-5 Physical properties of A type zeolites [54]

Zeolite	Pore size (Å)	Atomic composition[a]			
		Si/Al	Na/Al	K/Al	Ca/Al
COM 3A	<4[a]	1.0	0.45	0.55	–
UOP 4A	4[b]	1.0	1.0	–	–
COM 5A	>4[a]	1.0	0.34	–	0.33
NaX	7.4[b]	1.3	1.0	–	–
NaY	7.4[b]	2.5	1.0	–	–
Beta	7.1 × 7.3[b]	16	1.0	–	–
Silicalite-1	5.2 × 5.7[b]	196	1.0	–	–

[a] Based on EDS analysis.
[b] From Ref. [31].

Pervaporation membranes with zeolite A as the selective layer perform significantly better than polymeric membranes. Van den Berg et al. [55] prepared the zeolite A membrane on UV-irradiated TiO_2 coated metal. A separation factor up to 54,000 with a flux of 0.86 $kg.m^{-2}.h^{-1}$ was achieved at 45 ℃ using 95% ethanol aqueous solution. Tanaka et al. [56] reported a separation factor of 10,000 and a flux of 2.15 $kg.m^{-2}.h^{-1}$ with zeolite A membrane coated on α-Alumina to dehydrate 90% ethanol solution at 75 ℃.

Although zeolite membranes showed far better pervaporation performance than polymeric membranes, limitations still remain. They are generally regarded to be difficult for large-scale production and often expensive [30]. The application of zeolite membranes for pervaporation has been studied in a review by Bowen et al. [15]

§ 1.7. Mixed matrix membranes

Mixed matrix membranes consist of a polymeric base membrane through which an inorganic material is dispersed and locked into a polymer matrix. The inorganic component is considered to impart mechanical strength and reduce swelling of hydrophilic membranes. Zhang et al. [57] prepared organic-inorganic hybrid membranes by incorporation of polysilisequioxane (PSS) into a poly(vinyl alcohol) (PVA) matrix in order to solve the trade-off relationship between selectivity and permeability of PVA membranes. Uragami et al [58, 59] produced organic-inorganic hybrid pervaporation membranes from PVA and tetraethyl orthosilicate (TEOS) using the sol-gel reaction. The additions of TEOS into PVA membrane decreased the swelling and improved the water permeate selectivity of the hybrid membrane. Their work also included blended quaternized chitosan (q-Chito) membranes with TEOS via sol-gel reaction. For the membrane with the TEOS content of 45 mol% and a thickness of 76.7 mm, the separation factor reached up to 35,480 at of 40 ℃ using 96.5% ethanol solution, while the permeation flux was only 0.007 $kg.m^{-2}.h^{-1}$.

§ 1.8. Homogeneous membrane and composite membranes

Based on the structure of pervaporation membranes, they fall in to two catalogues: homogeneous membrane and composite membrane. Homogeneous membranes, or self-standing membranes, are typically dense and thick, and therefore, possess very good mechanical properties but relatively low permeation flux during pervaporation. The composite membranes

are made by coating a very thin thickness of homogeneous membrane onto a porous substrate, which is normally a ultrafiltration membrane, to provide enough mechanical strength to the composite membrane.

§ 1.9. Core issue of present membranes: responding solutions

Ideally, the porous substrate of a composite membrane should present negligible resistance to mass transport [60]. Otherwise, the substrate resistance leads to decreased membrane productivity and selectivity [61]. So, the composite pervaporation membranes, tailoring the microstructure of the substrate is important in achieving high performance.

Feng [62] noted that many asymmetric and composite membranes made by the traditional phase inversion process were not very selective for pervaporation. It is frequently assumed that the porous substrate acts only as a mechanical support, and there is a notion that such asymmetric and composite membranes are unsuitable for pervaporation. Moreover, in pervaporation, the permeate side is maintained at vacuum and the flow of permeate vapor through the pores of the substrate is likely to follow the Knudsen flow mechanism. The resistance of the substrate cannot always be neglected.

Hunag and Feng [63] provided a resistance model (Figure 1-14) to analyze the effects of membrane performance from each independent layer in a composite membrane. They demonstrated an analysis of membranes with different substrates and found that the selectivity achievable in an asymmetric pervaporation membrane was determined not only by the resistance of skin layer and substrate but also by the relative resistance of the polymer matrix and the pores

in the substrate. If the resistances offered by the polymer matrix and the pores in the substrate were not well balanced, even a membrane with a defect-free skin layer might still exhibit low selectivity.

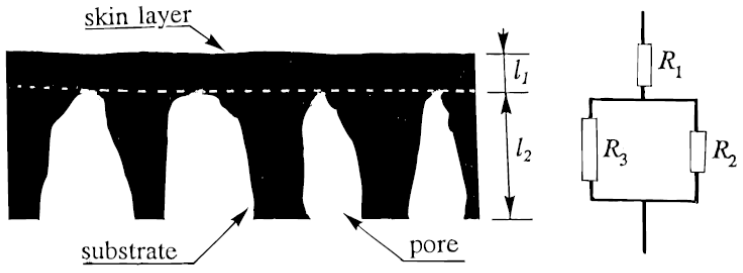

R_1 = resistance of the skin layer (= R_{skin})
R_2 = resistance of the pores in the substrate
R_3 = resistance of the polymer matrix in the substrate
R_{sub} = resistance of the substrate [= $R_2R_3/(R_2+R_3)$]

Figure 1-14 Resistance configuration of mass transport through an asymmetric membrane.[62]

Trifumnovic [64] concluded that increasing porosity and pore diameter of the support, and decreasing the length of Knudsen region, would enhance component mass transfer coefficient, and also minimize the pressure losses during the experiment.

Hence, the multilayer membrane based on electrospun nanofibrous scaffold can be a promising approach to resolve the above problems with following features: Electrospun membranes have unique features, such as high bulk porosity (up to 80%) with fully interconnected pore structures, and high surface to volume ratio. According to the resistance model mentioned above, this structure should benefit mass transport of permeable gas, in addition to providing support.

The application of electrospun membranes in liquid filtration has been successfully demonstrated [65-75]. We have shown that the permeation flux of the pervaporation membrane

can be enhanced with the e-spun membranes as the scaffold. Meanwhile, the e-spun membranes can also act as a separating layer if the hydrophilic material, such as the electrospun PVA membrane, is beneficial to improve the separation performance. Of course, more attention should be paid to the top coating layer, which is the most crucial part determining the performance of the pervaporation membrane.

§ 1.10. References

1. Bauen, A., *Future energy sources and systems acting on climate change and energy security*. J. Power Sources, 2006. **157** p. 893–901.

2. Sissine, F., *Energy Independence and Security Act of 2007: A Summary of Major Provisions*, in *United States Senate Committee on Energy & Natural Resources*. 2007.

3. (EIA), U.E.I.A., *US ethanol comsumption statistics*. 2010.

4. N/A, *National Petroleum Council*. 2007.

5. Available from: http://www.eia.gov/totalenergy/data/monthly/pdf/sec10_7.pdf

6. Fadden, K.M. *Hydrophobic front end Membranes for BiofuelSeparations*. 2009.

7. Simo, M., Brown, C.J., and Hlavacek, V.,, *Simulation of Pressure Swing Adsorption in Fuel Ethanol Production Process.* Comput. Chem. Eng., 2008. **32**(7): p. 1635–1649.

8. Ladisch, M.R., *Cornmeal Adsorber for Dehydrating Ethanol Vapors.* Ind. Eng.Chem. Proc. Des. Dev., 1983. **23**: p. 437-445.

9. Available from: http://www.ethanolindia.net/.

10. Neuhause.S and F. Wolf, *Separation of Alkylpyridine Mixtures .1. Separation of Beta-Gamma-Picoline Fractions by Azeotropic Distillation.* Brennstoff-Chemie, 1968. **49**(12): p. 355-&.

11. Frolkova, A.K. and V.M. Raeva, *Bioethanol dehydration: State of the art.* Theoretical Foundations of Chemical Engineering, 2010. **44**(4): p. 545-556.

12. Pucci, A., *Phase-Equilibria of Alkanol Alkane Mixtures in New Oil and Gas Process-Development.* Pure and Applied Chemistry, 1989. **61**(8): p. 1363-1372.

13. Kaminski, W., J. Marszalek, and A. Ciolkowska, *Renewable energy source - Dehydrated ethanol.* Chemical Engineering Journal, 2008. **135**(1-2): p. 95-102.

14. Li, N.N. and J.M. Calo, *Separation and purification technology*. 1992, New York: M. Dekker. viii, 310 p.

15. Bowen, T.C., R.D. Noble, and J.L. Falconer, *Fundamentals and applications of pervaporation through zeolite membranes.* Journal of Membrane Science, 2004. **245**(1-2): p. 1-33.

16. A.M. Urtiaga, E.D.G., G. Ruiz, I. Ortiz, *Parallelism and differences of pervaporation and vacuum membrane distillation in the removal of VOCs from aqueous streams.* Separation and Purification Technology, 2001. **22-23**: p. 327–337.

17. Smuleac, V., et al., *Novel perfluorinated polymer-based pervaporation membranes for the separation of solvent/water mixtures.* Journal of Membrane Science, 2010. **352**(1-2): p. 41-49.

18. Hyder, M.N., R.Y.M. Huang, and P. Chen, *Effect of selective layer thickness on pervaporation of composite poly(vinyl alcohol)-poly(sulfone) membranes.* Journal of Membrane Science, 2008. **318**(1-2): p. 387-396.

19. Shao, P. and R.Y.M. Huang, *Polymeric membrane pervaporation.* Journal of Membrane Science, 2007. **287**(2): p. 162-179.

20. Okada, T. and T. Matsuura, *A New Transport Model for Pervaporation.* Journal of Membrane Science, 1991. **59**(2): p. 133-150.

21. Cabasso, I., E. Korngold, and Z.Z. Liu, *On the Separation of Alcohol Water Mixtures by Polyethylene Ion-Exchange Membranes.* Journal of Polymer Science Part C-Polymer Letters, 1985. **23**(11): p. 557-581.

22. Huang, R.Y.M., et al., *Pervaporation separation of water/isopropanol mixture using sulfonated poly(ether ether ketone) (SPEEK) membranes: transport mechanism and separation performance.* Journal of Membrane Science, 2001. **192**(1-2): p. 115-127.

23. Yeom, C.K. and K.H. Lee, *Pervaporation separation of water-acetic acid mixtures through poly(vinyl alcohol) membranes crosslinked with glutaraldehyde.* Journal of Membrane Science, 1996. **109**(2): p. 257-265.

24. Praptowidodo, V.S., *Influence of swelling on water transport through PVA-based membrane.* Journal of Molecular Structure, 2005. **739**(1-3): p. 207-212.

25. Kang, Y.S., et al., *Pervaporation of Water Ethanol Mixtures through Cross-Linked and Surface-Modified Poly(Vinyl Alcohol) Membrane.* Journal of Membrane Science, 1990. **51**(1-2): p. 215-226.

26. Zhang, W., et al., *Maleic anhydride surface-modification of crosslinked chitosan membrane and its pervaporation performance.* Journal of Membrane Science, 2007. **295**(1-2): p. 130-138.

27. Huang, R.Y.M., R. Pal, and G.Y. Moon, *Crosslinked chitosan composite membrane for the pervaporation dehydration of alcohol mixtures and enhancement of structural stability of chitosan polysulfone composite membranes.* Journal of Membrane Science, 1999. **160**(1): p. 17-30.

28. Shieh, J.J. and R.Y.M. Huang, *Pervaporation with chitosan membranes .2. Blend membranes of chitosan and polyacrylic acid and comparison of homogeneous and composite membrane based on polyelectrolyte complexes of chitosan and polyacrylic acid for the separation of ethanol-water mixtures.* Journal of Membrane Science, 1997. **127**(2): p. 185-202.

29. Nam, S.Y. and Y.M. Lee, *Pervaporation and properties of chitosan poly(acrylic acid) complex membranes.* Journal of Membrane Science, 1997. **135**(2): p. 161-171.

30. Chapman, P.D., et al., *Membranes for the dehydration of solvents by pervaporation.* Journal of Membrane Science, 2008. **318**(1-2): p. 5-37.

31. Yeom, C.K., J.G. Jegal, and K.H. Lee, *Characterization of relaxation phenomena and permeation behaviors in sodium alginate membrane during pervaporation separation of ethanol-water mixture.* Journal of Applied Polymer Science, 1996. **62**(10): p. 1561-1576.

32. Yeom, C.K. and K.H. Lee, *Characterization of permeation behaviors of ethanol-water mixtures through sodium alginate membrane with crosslinking gradient during pervaporation separation.* Journal of Applied Polymer Science, 1998. **69**(8): p. 1607-1619.

33. Yeom, C.K. and K.H. Lee, *Characterization of sodium alginate and poly(vinyl alcohol) blend membranes in pervaporation separation.* Journal of Applied Polymer Science, 1998. **67**(5): p. 949-959.

34. Yeom, C.K. and K.H. Lee, *Characterization of sodium alginate membrane crosslinked with glutaraldehyde in pervaporation separation.* Journal of Applied Polymer Science, 1998. **67**(2): p. 209-219.

35. Huang, R.Y.M., R. Pal, and G.Y. Moon, *Characteristics of sodium alginate membranes for the pervaporation dehydration of ethanol-water and isopropanol-water mixtures.* Journal of Membrane Science, 1999. **160**(1): p. 101-113.

36. Chen, S.H., et al., *Pervaporation separation of water/ethanol mixture by sulfonated polysulfone membrane.* Journal of Membrane Science, 2001. **183**(1): p. 29-36.

37. Hung, M.Y., et al., *Pervaporation separation of Water/Ethanol mixture by a sodium sulfonate polysulfon membrane.* Journal of Applied Polymer Science, 2003. **90**(12): p. 3374-3383.

38. Hung, M.Y., et al., *Pervaporation separation of water/ethanol mixture by TGN/PSF blending membrane.* European Polymer Journal, 2003. **39**(12): p. 2367-2374.

39. Qiao, X.Y. and T.S. Chung, *Diamine modification of P84 polyimide membranes for pervaporation dehydration of isopropanol.* Aiche Journal, 2006. **52**(10): p. 3462-3472.

40. Wang, Y.C., et al., *Preparation and pervaporation performance of 3,3-bis[4-(4-aminophenoxy)phenyl] phthalide based polyimide membranes.* Journal of Applied Polymer Science, 2005. **96**(6): p. 2046-2052.

41. Lee, K.R., R.Y. Chen, and J.Y. Lai, *Plasma Deposition of Vinyl-Acetate onto Nylon-4 Membrane for Pervaporation and Evaporation Separation of Aqueous Alcohol Mixtures.* Journal of Membrane Science, 1992. **75**(1-2): p. 171-180.

42. Xu, Z.K., et al., *Microporous polypropylene hollow fiber membranes Part II. Pervaporation separation of water/ethanol mixtures by the poly(acrylic acid) grafted membranes.* Journal of Membrane Science, 2003. **214**(1): p. 71-81.

43. Ball, I.J., et al., *The pervaporation of ethanol water feeds with polyaniline membranes and blends.* Synthetic Metals, 1999. **102**(1-3): p. 1311-1312.

44. Chiang, W.Y. and Y.H. Lin, *Properties of modified polyacrylonitrile membranes prepared by copolymerization with hydrophilic monomers for water-ethanol mixture separation.* Journal of Applied Polymer Science, 2003. **90**(1): p. 244-250.

45. Svang-Ariyaskul, A., et al., *Blended chitosan and polyvinyl alcohol membranes for the pervaporation dehydration of isopropanol.* Journal of Membrane Science, 2006. **280**(1-2): p. 815-823.

46. Rao, K.S.V.K., et al., *Blend membranes of chitosan and poly(vinyl alcohol) in pervaporation dehydration of isopropanol and tetrahydrofuran.* Journal of Applied Polymer Science, 2007. **103**(3): p. 1918-1926.

47. Kurkuri, M.D., U.S. Toti, and T.M. Aminabhavi, *Syntheses and characterization of blend membranes of sodium alginate and poly(vinyl alcohol) for the pervaporation separation of water plus isopropanol mixtures.* Journal of Applied Polymer Science, 2002. **86**(14): p. 3642-3651.

48. Dong, Y.Q., et al., *Preparation of poly(vinyl alcohol)-sodium alginate hollow-fiber composite membranes and pervaporation dehydration characterization of aqueous alcohol mixtures.* Desalination, 2006. **193**(1-3): p. 202-210.

49. Song, K.M. and W.H. Hong, *Dehydration of ethanol and isopropanol using tubular type cellulose acetate membrane with ceramic support in pervaporation process.* Journal of Membrane Science, 1997. **123**(1): p. 27-33.

50. Peters, T., et al., *Thin high flux ceramic-supported PVA membranes.* Desalination, 2006. **200**(1-3): p. 37-39.

51. Peters, T.A., et al., *Ceramic-supported thin PVA pervaporation membranes combining high flux and high selectivity; contradicting the flux-selectivity paradigm.* Journal of Membrane Science, 2006. **276**(1-2): p. 42-50.

52. van Veen, H.M., et al., *Dewatering of organics by pervaporation with silica membranes.* Separation and Purification Technology, 2001. **22-3**(1-3): p. 361-366.

53. Sommer, S. and T. Melin, *Performance evaluation of microporous inorganic membranes in the dehydration of industrial solvents.* Chemical Engineering and Processing, 2005. **44**(10): p. 1138-1156.

54. Zhen Huanga, H.-m.G., Wee lee Tan , Xiang-Yi Qiao , Santi Kulprathipanja, *Pervaporation study of aqueous ethanol solution through zeolite-incorporated multilayer*

poly(vinyl alcohol) membranes Effect of zeolites. Journal of Membrane Science 2006. **276**: p. 260-271.

55. van den Berg, A.W.C., et al., *Zeolite A membranes synthesized on a UV-irradiated TiO2 coated metal support: the high pervaporation performance.* Journal of Membrane Science, 2003. **224**(1-2): p. 29-37.

56. Tanaka, K., et al., *Application of zeolite membranes to esterification reactions.* Catalysis Today, 2001. **67**(1-3): p. 121-125.

57. Zhang, Q.G., et al., *Structure and permeation of organic-inorganic hybrid membranes composed of poly(vinyl alcohol) and polysilisesquioxane.* Journal of Materials Chemistry, 2008. **18**(39): p. 4646-4653.

58. Uragami, T., et al., *Structure and permeation characteristics of an aqueous ethanol solution of organic-inorganic hybrid membranes composed of poly(vinyl alcohol) and tetraethoxysilane.* Macromolecules, 2002. **35**(24): p. 9156-9163.

59. Uragami, T., H. Matsugi, and T. Miyata, *Pervaporation characteristics of organic-inorganic hybrid membranes composed of poly(vinyl alcohol-co-acrylic acid) and tetraethoxysilane for water/ethanol separation.* Macromolecules, 2005. **38**(20): p. 8440-8446.

60. Koops, G.H., et al., *Poly(Vinyl Chloride)Polyacrylonitrile Composite Membranes for the Dehydration of Acetic-Acid.* Journal of Membrane Science, 1993. **81**(1-2): p. 57-70.

61. Pinnau, I. and W.J. Koros, *Relationship between Substructure Resistance and Gas Separation Properties of Defect-Free Integrally Skinned Asymmetric Membranes.* Industrial & Engineering Chemistry Research, 1991. **30**(8): p. 1837-1840.

62. Feng, X.S. and R.Y.M. Huang, *Liquid separation by membrane pervaporation: A review.* Industrial & Engineering Chemistry Research, 1997. **36**(4): p. 1048-1066.

63. Huang, R.Y.M.F., X., *Resistance model approach to asymmetric polyetherimide membranes for pervaporation of isopropanol/ water mixtures.* J. Membrane Sci. , 1993. **84**: p. 15.

64. Olivera Trifunovi, G.T., *The influence of support layer on mass transport of homologous series of alcohols and esters through composite pervaporation membranes.* J. Membrane Sci., 2005. **259**: p. 122-134.

65. Ma, H.Y., et al., *High-flux thin-film nanofibrous composite ultrafiltration membranes containing cellulose barrier layer.* Journal of Materials Chemistry, 2010. **20**(22): p. 4692-4704.

66. Tang, Z.H., et al., *Design and Fabrication of Electrospun Polyethersulfone Nanofibrous Scaffold for High-Flux Nanofiltration Membranes.* Journal of Polymer Science Part B-Polymer Physics, 2009. **47**(22): p. 2288-2300.

67. Yoon, Y., B.S. Hsiao, and B. Chu, *High flux ultrafiltration nanofibrous membranes based on polyacrylonitrile electrospun scaffolds and crosslinked polyvinyl alcohol coating.* Journal of Membrane Science, 2009. **338**(1-2): p. 145-152.

68. Yoon, K., B.S. Hsiao, and B. Chu, *Formation of functional polyethersulfone electrospun membrane for water purification by mixed solvent and oxidation processes.* Polymer, 2009. **50**(13): p. 2893-2899.

69. Tang, Z.H., et al., *UV-cured poly(vinyl alcohol) ultrafiltration nanofibrous membrane based on electrospun nanofiber scaffolds.* Journal of Membrane Science, 2009. **328**(1-2): p. 1-5.

70. Yoon, K., B.S. Hsiao, and B. Chu, *High flux nanofiltration membranes based on interfacially polymerized polyamide barrier layer on polyacrylonitrile nanofibrous scaffolds.* Journal of Membrane Science, 2009. **326**(2): p. 484-492.

71. Yoon, K., B.S. Hsiao, and B. Chu, *Functional nanofibers for environmental applications.* Journal of Materials Chemistry, 2008. **18**(44): p. 5326-5334.

72. Chu, B., B.S. Hsiao, and K. Yoon, *Nanofiber and manocomposite-fiber technology for environmental applications.* Aatcc Review, 2008. **8**(2): p. 31-33.

73. Wang, X.F., et al., *High performance ultrafiltration composite membranes based on poly(vinyl alcohol) hydrogel coating on crosslinked nanofibrous poly(vinyl alcohol) scaffold.* Journal of Membrane Science, 2006. **278**(1-2): p. 261-268.

74. Yoon, K., et al., *High flux ultrafiltration membranes based on electrospun nanofibrous PAN scaffolds and chitosan coating.* Polymer, 2006. **47**(7): p. 2434-2441.

75. Wang, X.F., et al., *High flux filtration medium based on nanofibrous substrate with hydrophilic nanocomposite coating.* Environmental Science & Technology, 2005. **39**(19): p. 7684-7691.

76. R. Y. M. Huang, et al., *Pervaporation membrane separation processes using modified poly(vinyl alcohol) membranes.* Polymer Internaltional, 1993, 30 (1),p. 123-128.

77. http://maritzaperez6270.wordpress.com/2010/09/20/first-post-year-2010-2011/

78. http://www.bza.org/zeolites.html

Chapter 2

Pervaporation Process Development

Table of Content

§ 2.1. Design and building of pervaporation unit

A custom lab-scale pervaporation unit was designed and built for this study. The system can be divided into two parts, a liquid-handling system and a vapor-handling system, which are operated by a circulating pump and a vacuum pump, respectively. Of all the parts in the unit, the membrane cell is the critical part that determines other system parameters, such as radius of tubes, tank capacity, and pump flow rate. A larger-area cell could provide much efficiency but the difficulty in preparing larger-sized membranes that usually accompany higher possibility of defects.

Two stages are considered for the unit. First, an essential pervaporation unit with basic functions needed to be built. The goal of this stage was to create a reliable system to test membrane performance. At a later stage, the unit will be upgraded with some advanced modification to make it operate in a continuous mode to produce ethanol. This would include installation of an electronic data acquisition, a sequent cell, and a sample analyzer (gas chromatography).

§ 2.2. Unit description

A custom design and construction of the pervaporation unit was completed in early 2011. Figure 2-1a shows the unit configuration and as shown, most components are compactly installed on a vertical rack on rollers. The membrane cell assembly was purchased from Sulzer Chemtech, and its design is capable to reduce the concentration polarization occurred and boundary layer on the membrane surface [1]. The Reynold number of the cell when operating between 70~90℃ with ethanol aqueous mixture ranges between 1100 - 2500.

[a]

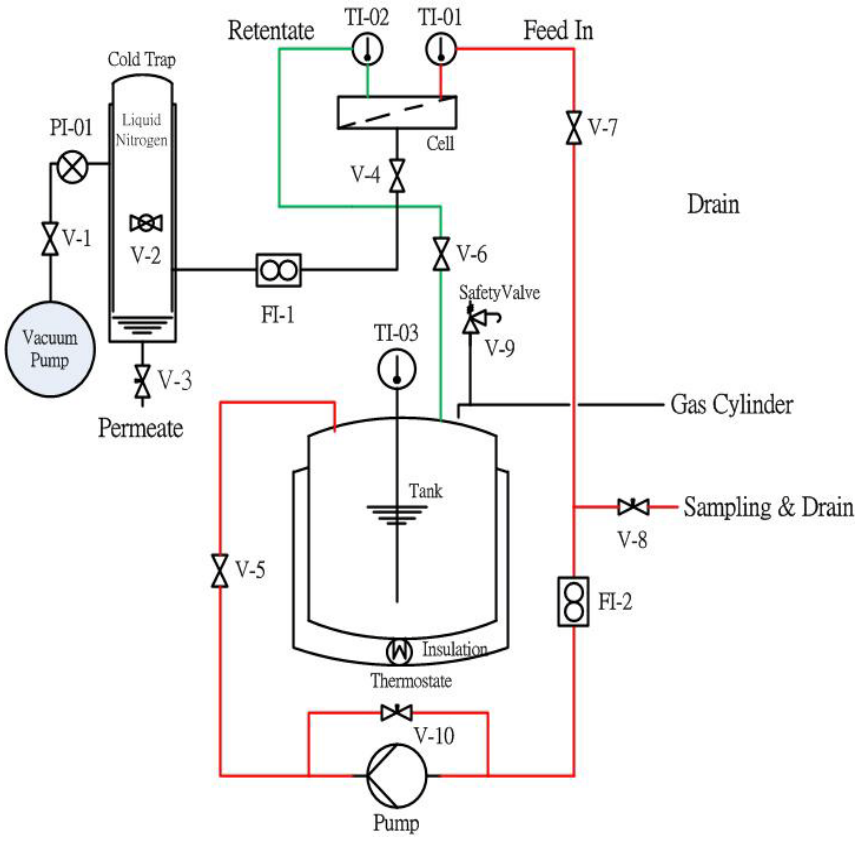

[b]

Figure 2-15 (a) Schematic representation of the pervaporation apparatus, (b) actual set-up of the unit. Also shown is the gas tank on right.

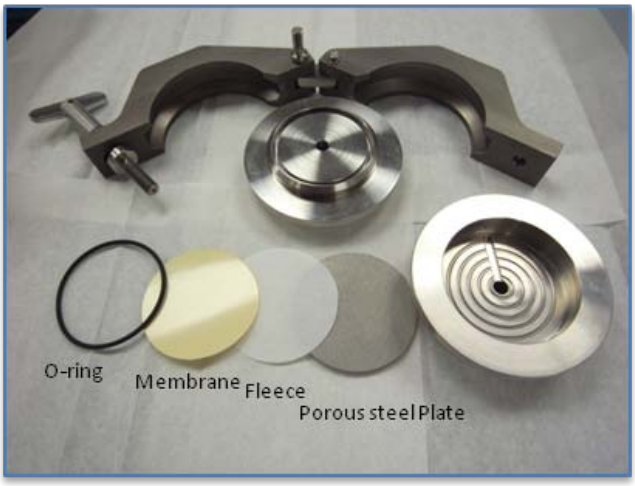

Figure 2-16 Pervaporation membrane cell assembly

Table 2-6 Critical components used in the pervaporation apparatus

Pressurized feed tank (1 gallon)	Test cell (diameter 3.15 inch)
Circulation pump (34 L/hr)	Operation temperature (20℃~90℃)
Vacuum pump (2×10^{-3} mbar)	

The main body includes one gallon feed tank, heating tape & temperature control, 150 psi safety valve, two flow meters, vacuum pump, circulating pump, thermocouples, pressure transmitter, and the unit is assembled close to a fume hood. The safety relief valve was added to the feed tank. Two additional pressure gauges were added; one above the feed tank, and the other after Flow Meter 2 and before Valve 8. The shielding was added around system to prevent liquid spills hitting electrical equipment. The insulation for pumps and the feed tank ensured energy efficiency. The system was properly grounded to prevent any possible sparks that could ignite ethanol vapors. See Table 2-1 for equipment details.

§ 2.3. Standard operating procedure (SOP) of pervaporation unit

Before starting, check that all valves are closed.

1 Star-up and preheating system.

Feed 2 - 4 L target solution (ethanol-water) with known concentration into the tank. Measure the concentration of ethanol before feeding into the tank.

1.1 Turn on the heating tape and set the desired temperature.. This set point should be 5 to 10°C above the operating temperature. It takes about 40 minutes to 1 hour for the temperature of the solution to reach the equilibrium.

1.2 Start the vacuum pump.

1.3 Seal the cold trap. Open V1, leaving V2, V3 and V4 still closed. Open the vacuum pump. The vacuum will reach around 300 millitorr in 1 to 2 minutes. If vacuum can't be reduced below 300 millitorr, check above valves and cold trap seal.

2 Membrane Installation.

2.1 Wear thin plastic gloves in order to avoid fingerprints on the membrane or damage by scratches with fingernails

2.2 Open V4. Insert the pervaporation membrane together with the O ring into the cell. Remember shiny side of the membrane faces the feed, and then put the O-ring on it.

The membrane should be sucked onto the porous metal substrate firmly, leaving any spacing in between. Otherwise, close V4, take out the membrane, and replace it with a new membrane.

2.3 Check that no residual liquid is in the upper cell (feed and retentate), and double check V6 and V7 to ensure they are in the closed status **(Important!).**

2.4 Install the upper part of the membrane cell and seal it. The vacuum will go down to ~800 micron torr in 1-2 minutes.

3 Start circulating

3.1 Open gas tank and apply ~5 psi gas pressure and shut it down. Open V5 and V8, and the solution should start coming out from V8. Close V8 when no air bubbles are trapped in the solution.

3.2 Switch on the circulating pump. Open V6 and V7 at the same time immediately.

3.3 Observe the temperature readings T1 and T2 and their respective difference on the installed digital thermometers. When the difference between TI-02 and TI-03 is 1°C or less, the unit has reached temperature equilibrium.

3.4 Let the unit run at least half an hour without permeate collection. (Not fill liquid nitrogen yet.) We call this period as "*Preconditioning of membranes*"

3.5 After "preconditioning", make sure that T01 reaches the set temperature, then fill cold trap with liquid nitrogen.

This is time zero of the Pervaporation test

2.3.1 Test Procedure

1. Monitor the temperature of thermocouples (T-01, T-02, T-03), the flow rate could vary from 20-30 gallons/h by adjusting bypass (V-10)

2. Check the level of liquid nitrogen in the cold trap, at least every 30 minutes. Add some more, if necessary.

3. To take a sample from the tank, follow the procedure. Close V6&7. Open V8 and take sample from V8. Then close V8 and close V6&7.

2.3.2 Shut down the unit

Remember always apply vacuum (keep V-4 opening) to cell during whole operations until opening the cell.

1. Shut down the circulating pump.

2. Turn off heat to the tape. (the controller near the tank)

3. Close V5. Apply gas pressure ~15 psi. Open V8 to get rid of the solution within the membrane cell and between V6 and V7. Release gas pressure and close V8.

4. Open membrane cell. The membrane should be dry and still firmly sticking onto the metal substrate. Wipe the liquid droplet on the membrane and underneath the O ring thoroughly.

5. Shut down the vacuum pump. Open V2. Take out the membrane carefully from the cell using tweezers.

6. Shut off the thermostat and thermometers.

2.3.3 Permeate collection in the cold trap.

1. After the unit shutdown, open V-2 to vent to ambient pressure.

2. Use hair dryer or heater to expedite cold trap melting and vaporization of liquid nitrogen.

3. When all ice melts into liquid, open V-3 to collect permeate sample.

2.3.4 Mixture collection in the tank

Don't open the tank and sample valve (V-8) (high vapor pressure) and high temperature until temperature reaches ambient temperature or below 40℃. Relieve the safety valve (V-9) before opening it.

2.3.5 Safety

1. Must wear long pants and a protection suit before starting the experiment

2. Open the suction hood above the unit to avoid inhaling too much ethanol vapor.

3. Wear cryogenic protection gloves when handling coolant liquid.

4. Use a funnel to pour coolant liquid in the cold trap to avoid splashing on the unit.

5. Be careful not to touch the tank and tubing when applying heating.

6. When the run is complete, do not open the tank or the valve to take the sample until the temperature drops below 40℃.

7. Check all electronic devices and switch off during unit shutdown.

§ 2.4. Baseline experiment

After the pervporation unit completion, the collection of baseline data with commercial membranes was completed before testing the deigned membranes.

Sulzer 1210, a commercial membrane, was selected for baseline experiments for its well-known performance for dehydration of ethanol and for its thermal stability and durability. The membrane was tested under different operating conditions, including varying feed concentrations (90%, 80% 70%), and varying temperature (60℃-90℃) the most decisive parameters for pervaporation experiments. Adjusting these variables would yield different permenat flux, and ethanol concentrations in the permeate.

The results of the permeant flux at different temperatures and feed concentrations are plotted in Figure 2-3. As temperature increases, the flux increases in a linear correlation. It is expected that higher temperature translate more kinetic energy for molecules, thus greater permeant flux.

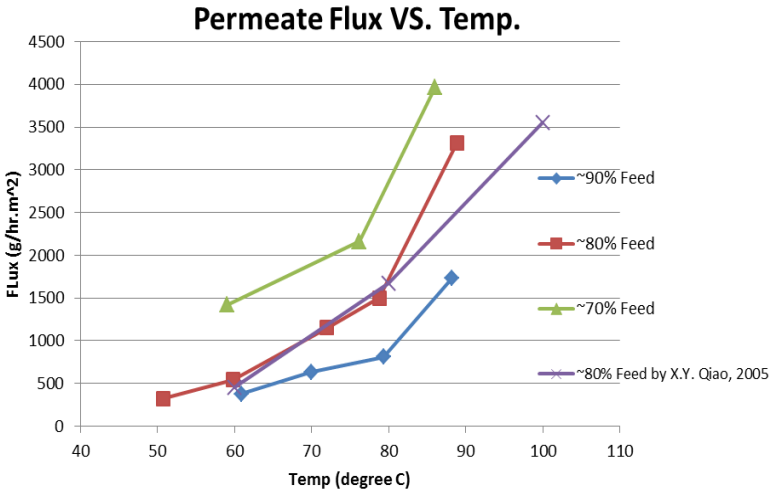

Figure 2-17 Permeate flux vs. temperature at different ethanol feed concentrations.

The purple line in Figure 2-3 represents the data referenced from Qiao, [2], who also tested Sulzer 1210 through pervaporation. From the comparison for the 80% feed, the results are mostly identical below 80℃. One off points might be due to the different testing instruments and working conditions, such as the flow rate and the pressure of feed. The results for flux for our current operation are right on target with the literature.

The results for separation factor vs. temperature at different concentrations of feed solution are shown in Figure 2-4 the data display that higher temperatures result in more ethanol in permeate, thus the separation factor decreases. Because at higher temperatures, ethanol and water molecules have more kinetic energy that allows them to diffuse through the membranes, that causes a higher flux and a poor separation factor.

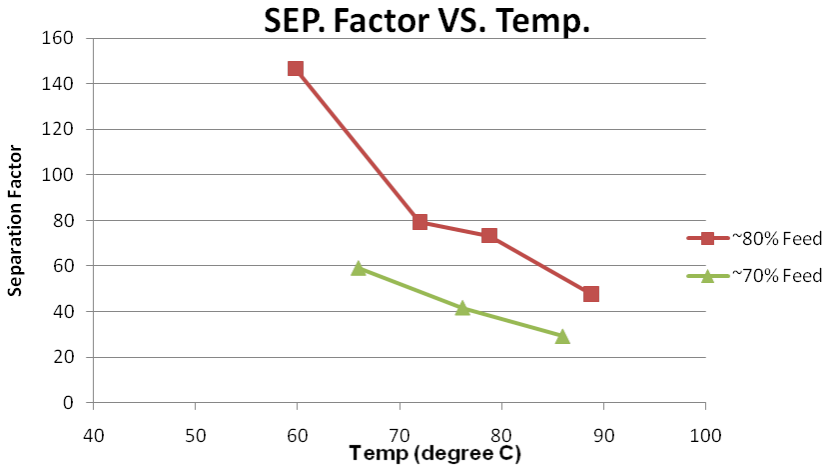

Figure 2-18 Separation factor vs. temperature at different ethanol feed concentrations.

Though the results for our permeate flux line up perfectly with the literature, the results for the selectivity of our Sulzer 1210 membrane are lower than those reported in the literature.

According to Sulzer Chemtech, the precondition during which the membrane sits in contact with the solution for 12 hours before running, may be responsible for the observed difference. It is believed that the time allows the membrane to become equilibrated and yields the actual selectivity results. It is similar to fouling time and compacting time for water-filtration membranes. Therefore, all experiments were conducted after a certain period of preconditioning.

§ 2.5. Experiments with PV-TFNC membranes

Specifically, a cross-linked hydrophilic poly(vinyl alcohol) barrier layer was cast on electrospun nanofibrous scaffolds as well as several conventional porous membrane scaffolds (e.g. nanofiltration membrane NF270 and ultrafiltration PDMS membrane). The results indicated that the permeate flux of the membrane based on the electrospun scaffold was always higher than those based on conventional porous membrane scaffolds, while the separation factors were about the same among all these membranes. Furthermore, when hydrophilic zeolite was added to the barrier layer, the separation factor of the resulting membranes based on conventional NF porous membrane support or nanofibrous scaffold became even higher (by 3 times) than the most successful commercial pervaporation membrane (e.g., Sulzer 1210).

Electrospun nanofibrous scaffolds have high porosity (>80 %), high specific surface area due to fine nanofibers (diameters 0.1 to 1 μm), and interconnected-pore structure. As successfully demonstrated by our group in the past few years, electrospun nanofibrous scaffolds could be used as a supporting layer in the thin-film nanofibrous composite (TFNC) ultra- and nano-filtration membranes, which possess very high permeation flux (increased by a factor of 2 ~ 10 when compared with typical commercial membranes) and high rejection rate. Based on the unique TFNC membrane structure, we have also demonstrated a new class of pervaporation members that have high flux and high separation factor for ethanol dehydration process.

A hydrophilic barrier layer of cross-linked polyvinyl alcohol (thickness 6~8 microns) was incorporated in to zeolite and then cast on a TFNC membrane scaffold containing a very thin cellulose nanofiber top layer, an electrospun mid-layer nanofibrous scaffold (thickness about 40 microns) and a PET non-woven substrate (thickness about 120 microns). For comparison, the

same cross-linked polyvinyl alcohol/zeolite barrier layer was also coated on a nanofiltration membrane (NF270, Dow chemistry). The resulting membranes were cut into 3 inch-diameter round disc samples, which were used to evaluate the pervaporation efficiency of ethanol dehydration. In the pervaporation process, 70% ethanol was used as the feeding mixture and the operating temperature was set at 70℃.

It is recognized that the pervaporation performance is mainly determined by the barrier layer. It has been demonstrated that the incorporation hydrophilic zeolite materials in the barrier layer (called nanocomposite barrier layer) can significantly enhance the separation factor without losing the permeation flux. These results are illustrated in Figure 2-5, where the pervaporation performance of membranes based on the nanocomposite barrier layers (one contains zeolite 3A and one contains zeolite 5A) cast on a nanofiltration (NF) membrane as a support , as well as that of membranes based on the unmodified barrier layer are compared. It is seen that membranes based on the nanocomposite barrier layers (PVA and zeolite) exhibit a much higher separation factor (157.92 for zeolite 5A) than with the unmodified PVA barrier layer (39.09). The separation factor of the typical commercial pervaporation membrane (Sulzer 1210) is 47.12. The permeation flux of the three membranes containing different barrier layers but the same nanofiltration scaffold (NF 270) was about the same (0.8 $kg/m^2.h$). Hence, with a combination of nanocomposite barrier layer (with the same thickness as the commercial pervaporation membrane) and the electrospun nanofibrous scaffold should lead to simultaneous increases in permeation flux and separation factor.

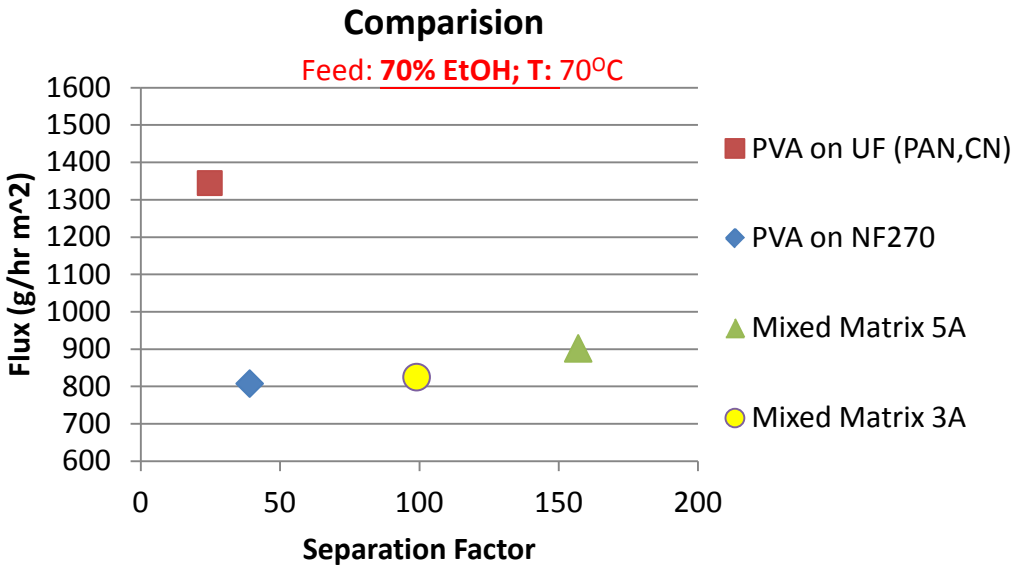

Figure 2-19 Comparison of pervaporation performance of membranes with nanocomposite barrier layer (containing hydrophilic zeolite) on a nanofiltration scaffold (NF 270).

§ 2.6. Conclusions

Based on the above reported results, we conclude that there are two unique features of nanofibrous membranes for pervaporation applications such as separation of water and ethanol. First, the membranes fabricated by using the electrospun nanofibrous scaffolds can have significantly higher permeation flux than those based on conventional porous membranes fabricated by the phase conventional method. Second, the barrier layer containing hydrophilic zeolites of proper pore size and suitable hydrophilic polymer matrix can lead to substantial increase in separation factor for ethanol dehydration. The combined features could lead to a new class of pervaporation membranes with simultaneous enhancements of permeation flux and separation factor. Some examples are illustrated in the following sections.

§ 2.7. References

1. Wijmans, J.G., et al., *The role of boundary layers in the removal of volatile organic compounds from water by pervaporation.* J. Membr. Sci. . 1-10(109): p. 135-146.

2. Zhen Huanga, H.-m.G., Wee lee Tan , Xiang-Yi Qiao , Santi Kulprathipanja, *Pervaporation study of aqueous ethanol solution through zeolite-incorporated multilayer poly(vinyl alcohol) membranes Effect of zeolites.* Journal of Membrane Science 2006. 276: p. 260-271.

Chapter 3

Polymeric Nanofibrous Composite Membranes for Energy Efficient Ethanol Dehydration

Table of Content

§ 3.1. Introduction

Various membranes have been developed for pervaporation applications, including homogeneous, asymmetric, composite, and mixed matrix membranes involving polymeric and/or inorganic materials [1,2,3]. Polymeric composite membranes are the most widely used membranes because they can be processed inexpensively and operated at relatively low operating cost. The composite polymeric pervaporation membrane is produced by casting of a very thin homogeneous barrier layer on a porous substrate that is formed by the phase inversion method. The porous substrate provides the overall mechanical strength for the composite membrane.

Ideally, the porous substrate in a composite pervaporation membrane should yield negligible resistance to the mass transport [4]. Otherwise, the substrate resistance would lead to decreases in permeability and/or selectivity [5]. As a result, the microstructure of the substrate in the composite pervaporation membrane is an important factor to achieve high separation performance. Several articles [3, 6] have pointed out that many asymmetric and composite membranes with substrates fabricated by the phase inversion method did not show the perceived selectivity desired for pervaporation. However, it is important to point out that in pervaporation, the permeate side is operated under vacuum. Thus, the flow of permeate vapor through the tiny pores of the substrate is likely to follow the Knudsen flow mechanism. In this case, the resistance to flow due to the presence of the substrate should not be neglected, which has also reported in the literature. For example, Trifunović [7] concluded that the components of the mass transfer coefficient can be enhanced by increasing the porosity and pore diameter of the substrate and by decreasing the length of the Knudsen region. Such a change can also minimize the pressure loss in the process.

Based on the above reasons, we hypothesize that the use of porous electrospun nanofibrous scaffold as a substrate can lead to the development of more energy efficient pervaporation membranes with higher permeability without the sacrifice of separation efficiency. This is because electrospun scaffolds have high bulk porosity (up to 80%), fully interconnected pore structure and high surface to volume ratio. According to the resistance model mentioned above, this structure should benefit the mass transport of permeable vapor phase.

Applications of electrospun scaffold for water purification using the format of thin-film nanofibrous composite (TFNC) membrane have been successfully demonstrated by us recently [8-18]. For the pervaporation applications, the structure in the TFNC membrane would contain four layers (shown schematically in Figure 3-1): PVA top barrier layer, buffer layer based on cellulose nanofiber, electrospun nanofibrous scaffold, and nonwoven microfibrous substrate, as demonstrated in this study. PVA was chosen as the barrier layer material because it is hydrophilic and a proven polymer for ethanol dehydration. The TFNC structure containing the cellulose nanofibrous top layer, the electrospun nanofibrous scaffold and the polyethylene terephthalate (PET) nonwoven microfibrous-substrate (as the mechanical support) has been demonstrated recently for high-flux ultrafiltration [8-18], and will be used as a scaffold to support the cross-linked PVA barrier layer.

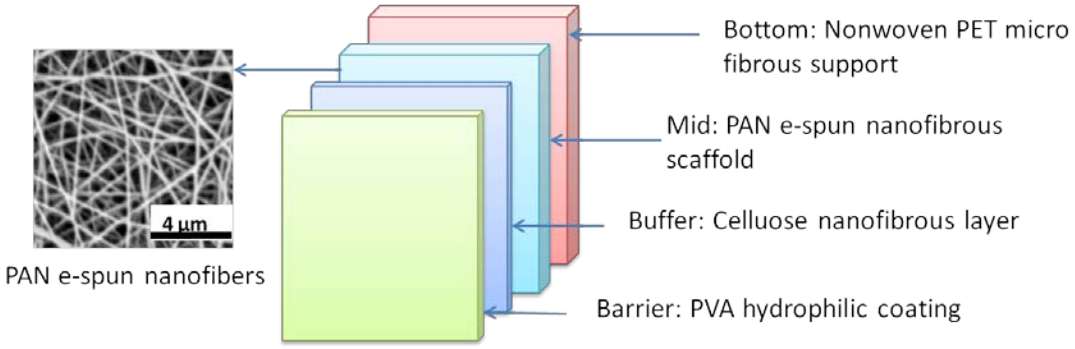

Figure 3-20 Schematic representation of a high flux pervaporation membrane with the four-layered structure

In this study, cellulose nanofibers were modified to form a less hydrophilic surface but can still provide a firmer buffer layer structure between the PVA barrier layer and the electrospun nanofibrous scaffold. In addition, the modified cellulose layer also provides the proper insulation to prevent the penetration (or intrusion) of PVA into the nanofibrous scaffold during the fabrication of barrier layer. More details about the benefits of such composite structure are presented later in this manuscript.

§ 3.2. Experimental

§ 3.2.1 Materials

Polyvinyl alcohol (PVA, degree of hydrolysis = 98.4%, weight-average molecular weight = 195,000 g/mole) was obtained from the Kuraray Company. Polyacrylonitrile (PAN, weight average molecular weight = 150,000 g/mol), glutaraldehyde (GA, 50% weight in water) and hydrochloric acid (HCl) were obtained directly from Aldrich. Nonwoven polyethylene terephthalate (PET) substrate (Hollytex 3242) was kindly provided by the Ahlstrom Mount Holly Springs Company. Commercial nanofiltration (NF) membrane, NF270, was obtained from Dow Chemical. Commercial ultrafiltration membrane containing polyethersulfone (PES) porous layer was provided by the Filtration Solutions Inc. Sulzer 1210 membrane was obtained from Sulzer Chemtech. Cellulose raw material in suspension (Biofloc 92 MV, 22% wt. of wood pulp) was supplied by the Tembec Tartas factory in France.

§ 3.2.2 Pervaporation membrane preparation

The procedures for preparing pervaporation membranes are as follows. An aqueous PVA solution (4 % wt.) was first prepared by dissolving the powder sample in water by stirring at 80°C for 6 hours. Subsequently, HCl (0.1M) was added to the PVA solution at a molar ratio of 0.2 (HCl/PVA) as a catalyst. An appropriate amount of GA (glutaraldehyde), as a cross-linker, was then added to the solution, at different PVA/GA (by mole) ratio, to initiate the cross-linking reaction. In order to prevent the penetration of PVA layer into the porous nanofibrous support during the barrier layer casting, we took advantage of the gelling formation during the PVA/GA crosslinking. The PVA mixture was stirred under the monitoring of a viscometer, where the solution viscosity increased continuously with time. The stirring time was varied depending on the PVA/GA ratio, temperature and humidity. It would usually take about 15-20 minutes for the viscosity to reach 150 centipoises (cP). We discovered that when the viscosity of PVA was above this value, the penetration of the coating layer into the porous nanofibrous mats became minimal.

Procedures of preparing electrospun PAN nanofibrous scaffold on a PET non-woven substrate have been described elsewhere [17]. The two-layered composite scaffold was first soaked in the HCl solution (pH=1.5) before the casting of another cellulose nanofibrous layer. The preparation of cellulose nanofibrous solution and its application of fabricating a thin-film nanofibrous composite membrane, which was used as a pervaporation membrane support in this study, has also been described earlier [8]. Ultra-fine cellulose nanofibers were prepared from the wood pulp sample by the TEMPO/NaBr/NaClO oxidation method [19, 20], which usually contained the carboxyl group at around 1~1.3 mg/mole (we termed this unmodified cellulose

nanofibers). The modified ultra-fine cellulose nanofibers were prepared by using a lower oxidizing condition resulting in a lower concentration of carboxyl group (0.5 mg/mole) on the fiber surface. After the casting of cellulose nanofibrous layer, the three-layered composite scaffold was dried in oven at 70°C for one hour. The resulting cellulose/PAN/PET composite membrane was taped on a glass plate and then subsequently coated with a PVA/GA solution either by hands or by an automated drawdown machine. The final membrane was dried in an incubator at room temperature for 12 hours. The dried membrane was first washed with acetone/water to completely stop the cross-linking reaction, and was then cured at 130°C for one hour and cooled down to 25°C. The thickness of the top layer was usually controlled at around 5-8 micrometers.

§ 3.2.3 Evaluation of pervaporation properties

A custom pervaporation apparatus was used to evaluate the pervaporation properties of these membranes. The schematic design of the pervaporation apparatus is shown in Figure 2-1(a) and the photograph of this apparatus is shown in Figure 2-1(b). The unique feature of this apparatus is that the system was designed and constructed in a vertical fashion to possess a small footprint. The membrane cell assembly was purchased directly from Sulzer Chemtech Figure 2-2, where its design was capable of reducing the occurrence of concentration polarization near the barrier layer of the membrane [21]. The components used in this apparatus are summarized in Table 2-1.

The typical pervaporation evaluation procedures are as follows. The apparatus was firstly heated up to 70°C from room temperature, and was then equilibrated for one hour before use. After loading the test membrane in the sample cell, the apparatus was running for 1 hour to

precondition the membrane. During the evaluation, the permeate solution was collected in the cold trap that was cooled with liquid nitrogen during the experiment. The ethanol concentration of the collected permeate was analyzed using a gas chromatograph (GC) with a flame ionization detector (FID). The GC analyzer (Hewlett-Packard GC5890) consisted of a Carbowax-20M column (Agilent) packed with cross-linked polyethylene glycol.

When characterizing the pervaporation performance, two important parameters were evaluated: the permeant flux, J, and the separation factor, α, defined as below,

$$J = \frac{Q}{A\Delta t} \qquad \text{(Equation 3-1)}$$

$$\alpha = \frac{Y_W/Y_E}{X_W/X_E} \qquad \text{(Equation 3-2)}$$

where Q is the weight of the permeate collected in a time interval Δt; A is the effective membrane area; X and Y are the mass fractions in the feed and permeate, respectively; the subscripts W and E represent water and ethanol, respectively.

§ 3.3. Results and discussion

§ 3.3.1 Optimize the GA/PVA content for the barrier layer

Figure 3-2 shows that both permeant flux and separation factor exhibiting maximum values against the GA/PVA molar ratio used in cross-linking of the PVA barrier layer. This behavior can be explained as follows. At very low GA/PVA ratios, the degree of cross-linking is low. In this case, the PVA membrane can be easily swell in the ethanol/water solution, creating

a loose structure with high free volume. As a result, the separation factor is low and the permeation is high due to a high degree of swelling in non-crosslinked PVA. The separation factor increases rapidly with increasing degree of cross-linking, where the free volume in the barrier layer is decreased and the diffusion coefficient is also reduced [22]. However, at very high concentrations of GA, the degree of cross-linking may not be homogenous. As a result, the reaction can lead to a looser structure for pervaporation and high amorphous fraction in PVA, and consequently a poorer separation factor and low permeant flux. The optimal ratio of GA/PVA seems to be between 0.0125and 0.05 based on the results of permeant flux and separation factor. In this study, the GA/PVA ratio of 0.025 was chosen for the fabrication of high flux pervaporation membranes.

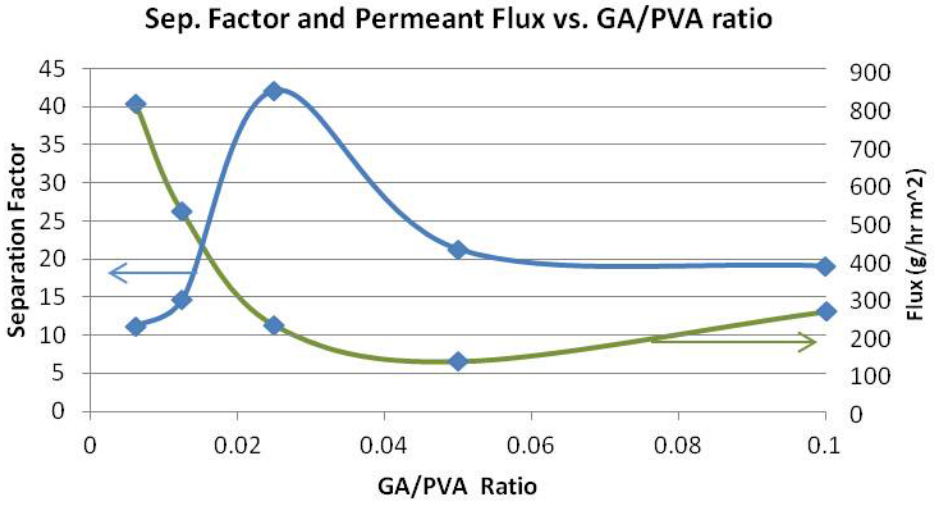

Figure 3-21 Membrane performance at different PVA/GA ratios (feed concentration = 80 wt. % ethanol solution, operated at 70 °C)

§ 3.3.2 Comparison of membranes based on different substrates

We compared the pervaporation performance of membranes based on different substrates, i.e., the new thin-film nanofibrous composite (TFNC) format versus the conventional thin-film composite formation. In this study, the TFNC membrane consisted of a cross-linked PVA barrier layer (using the optimal GA/PVA ratio), which was deposited on the cellulose nanofibrous scaffold layer that had the carboxyl group at around 1~1.3 (mg/mole). The cellulose nanofiber layer was supported by a composite support containing electrospun scaffold and non-woven substrate. The same optimally cross-linked PVA barrier layer was also coated on a nanofiltration membrane (NF270, Dow Chemical) and an ultrafiltration membrane (polyethersulfone (PES), Filtration Solutions Inc.). These three membranes were evaluated for pervaporation efficiency in ethanol dehydration using 70% ethanol as the feed solution and at 70 °C.

Figure 3-3 shows the pervaporation performance (i.e., the permeant flux and separation factor) of the above three membranes. The membrane based on the nanofibrous scaffolds showed the permeant flux of 1.34 (kg/m^2 hr), which was higher than the rest two membranes using the PES and NF supports. It is interesting to see that the separation factor was about the same for the nanofibrous scaffold and unmodified TFNC support, while that for the NF support was the highest. We note that the barrier layer thickness in these three membranes was about 5-8 microns, several times (about 5-8 times) thicker than that of the commercial Sulzer 1210 pervaporation membrane. Thus, the permeant flux of the nanofibrous membrane normalized by the barrier layer thickness based on the nanofibrous scaffold became substantially higher than that of the commercial pervaporation membrane (Sulzer 1210).

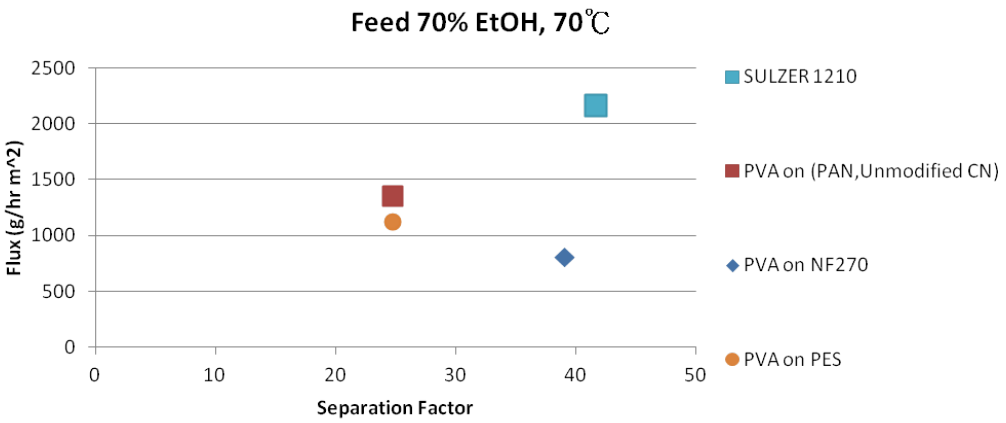

Figure 3-22 Comparison of pervaporation performance from membranes fabricated with the same PVA barrier layer but different support substrates.

Although the PVA based nanofibrous membrane exhibited a larger permeant flux than membranes based on other forms of substrate, the composite nanofibrous membrane could be further improved. Based on the Scanning Electron Microscopy (SEM) of the cross sectional morphology of the membrane, as shown in Figure 3-4, an intrusion of PVA from the barrier layer to the electrospun fibrous scaffold was observed. To be specific, when a composite nanofibrous membrane was annealed at high temperatures (as those in Figure 3-3), some parts of PVA barrier layer would usually penetrate into the electrospun nanofibrous scaffold. Often, the penetration (or PVA intrusion) resulted in a gap among the electrospun nanofibrous layer as shown in Figure 3-4.

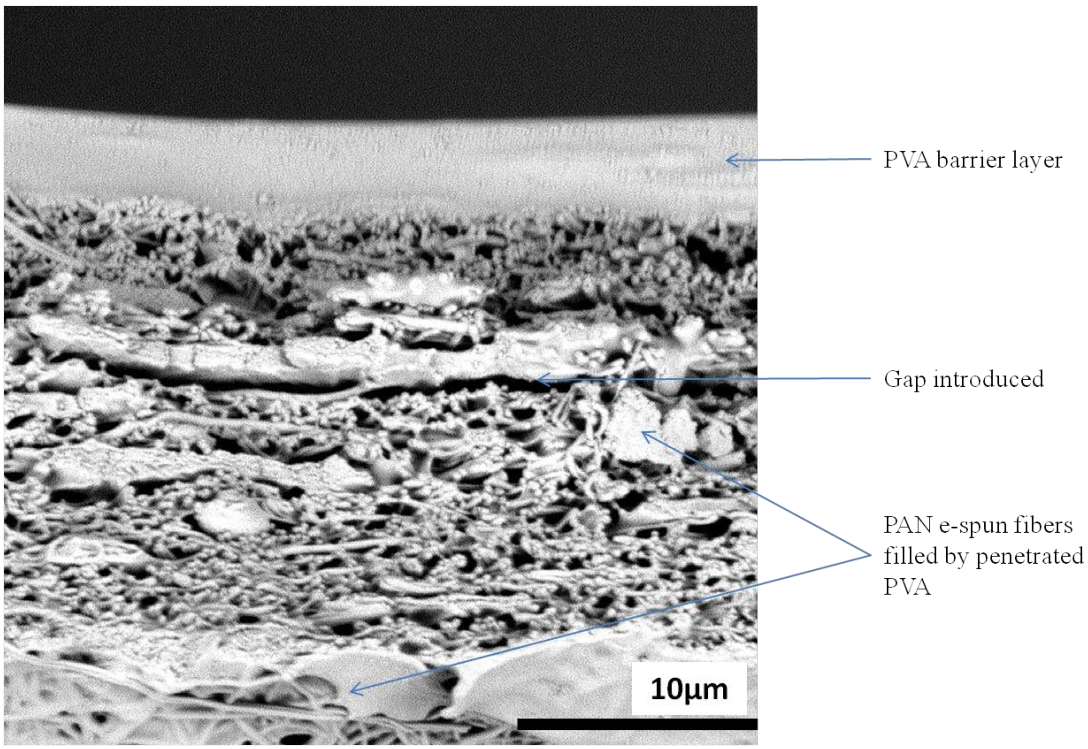

Figure 3-23 SEM cross-sectional view of the composite nanofibrous pervaporation membrane with the unmodified cellulous nanofibrous layer.

The presence of such a gap could significantly affect the overall diffusion rate, including the liquid transport in the barrier layer and gas transport in the substrate layer, even though the barrier layer is known as the rate-determining step. In addition, the filled fibers could promote condensation of the permeate vapor, affecting the Knudson flow. [7, 23] Hence, the obstruction of the diffusion path in the membrane would result in the decrease in selection ability in ethanol dehydration.

§ 3.3.3 Adoption of a modified cellulose nanofibrous layer

A pervaporation membrane, based on the adoption of a modified cellulose nanofibrous layer that can overcome the PVA intrusion problem, has been demonstrated, where it exhibited

superior permeant flux for ethanol dehydration than the one with unmodified cellulose nanofibers. Figure 3-5a shows when a cellulose nanofibrous layer was modified in a lower oxidization condition (the resulting carboxyl group was 0.5 mg/mole and thus more hydrophobic than the unmodified one), which could form a uniform more hydrophobic layer (thickness about 1 micron) on the electrospun nanofibrous scaffold (thickness about 40 microns). During to the increase in hydrophobicity of the cellulose nanofibrous support, the casting of PVA barrier layer could form a dense format (thickness about 4 microns) with less tendency to penetrate into the supporting scaffold. This is seen in Figure 3-5b, where the modified cellulose nanofibrous layer functions as a desired buffer to prevent the penetration (intrusion) of PVA into the electrospun nanofibrous scaffold, thereby permitting the electrospun nanofibrous scaffold to enhance the permeant flux of the membrane due to high porosity.

[a] 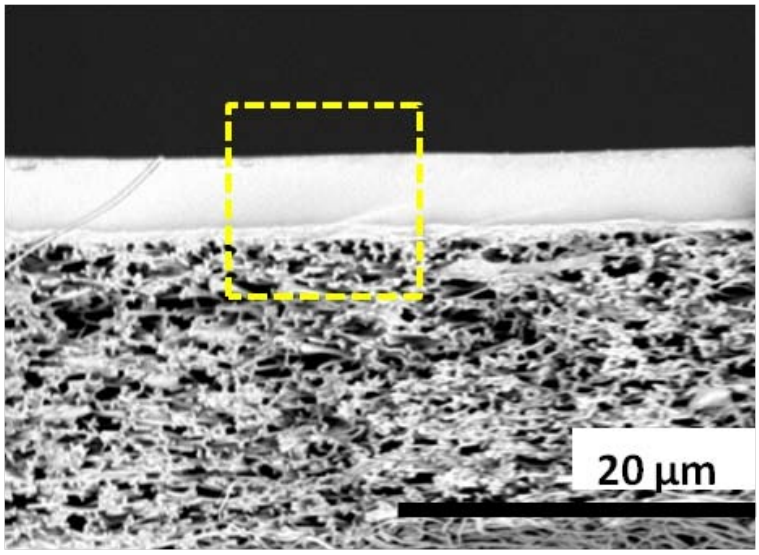

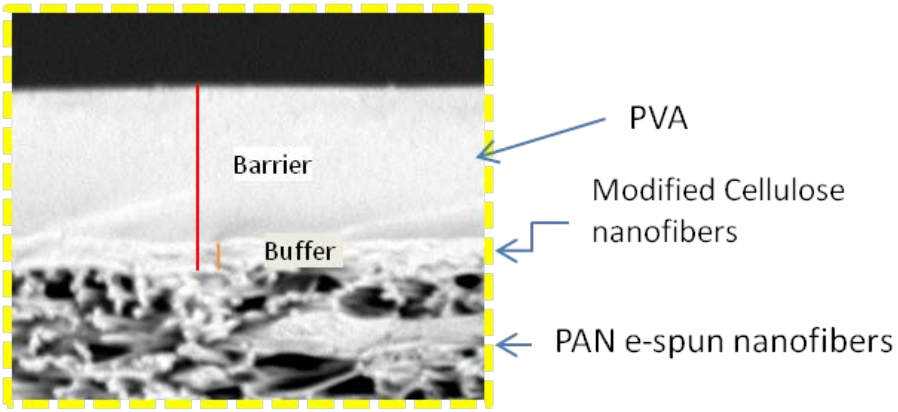

[b]

Figure 3-24 (a) SEM cross sectional view of composite nanofibrous membrane containing a modified cellulose nanofibrous layer, (b) enlarged local area near the electrospun scaffold. The measured membrane contained a PVA barrier with 4 microns thickness and a cellulose nanfiborus layer with 1 micron thickness.

In Figure 3-6, the separation factor of this membrane could reach 80.8, and the flux was 765 kg/m^2 hr. These two factors are significantly higher than those of the Sulzer 1210 membrane under the same operating conditions. With the thickness of the PVA barrier layer of the current membrane being around 10 times that of the Sulzer membrane, the current approach has the potential to increase the permeant flux further by reducing the PVA layer thickness.

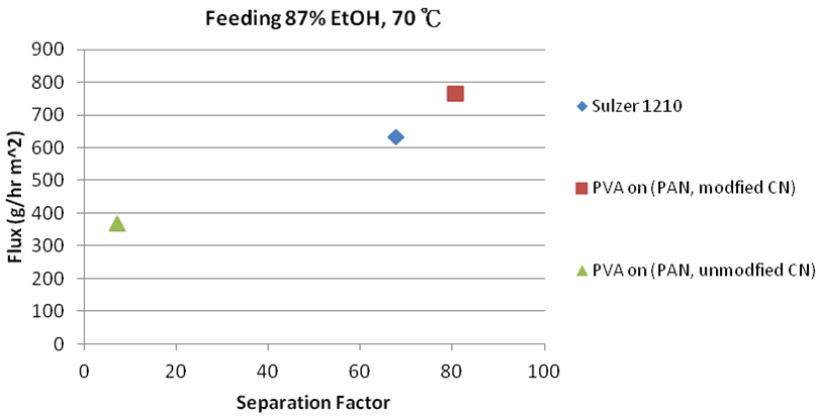

Figure 3-25 Comparison of pervaporation performance of Sulzer 1210 (with PVA as barrier), and the composite nanofibrous membranes containing a cellulose nanofibrous layer.

§ 3.4. Conclusions

In this study, we demonstrate that there are two unique features in nanofibrous membranes for pervaporation applications, such as the separation of water and ethanol. First, the membranes fabricated by using the composite nanofibrous scaffolds (such as ultra-fine cellulose nanofibers with diameters about a few nanometers and electrospun nanofibers with diameters about a few hundred nanometers) can have significantly higher permeant flux than those based on conventional porous membranes fabricated by the phase conventional method. Second, the modified cellulose nanofibers with lower hydrophilicity can effectively prevent the penetration of the barrier layer using cross-linked PVA to the nanofibrous scaffold. The combined features can lead to a new class of pervaporation membranes with simultaneous enhancements of permeant flux and separation factor.

§ 3.5. References

1. (EIA), U.E.I.A., *US ethanol comsumption statistics*. 2010.

2. Peter D. Chapman, T.O., Andrew G. Livingston, K. Li, *Membranes for the dehydration of solvents by pervaporation.* Journal of Membrane Science, 2008. **318**(1-2): p. 5-37.

3. Feng, X.S. and R.Y.M. Huang, *Liquid separation by membrane pervaporation: A review.* Industrial & Engineering Chemistry Research, 1997. **36**(4): p. 1048-1066.

4. Koops, G.H., et al., *Poly(vinyl chloride) polyacrylonitrile composite membranes for the dehydration of acetic acid.* Journal of Membrane Science, 2001. **81**(1-2): p. 14.

5. Pinnau, I. and W.J. Koros, *Relationship between substructure resistance and gas separation properties of defect-free integrally skinned asymmetric membranes.* Industrial & Engineering Chemistry Research, 1991. **30**(8).

6. Huang, R.Y.M.F., X., *Resistance model approach to asymmetric polyetherimide membranes for pervaporation of isopropanol/ water mixtures.* J. Membrane Sci. , 1993. **84**: p. 15.

7. Trifunović, O. and G. Tragardh, *The influence of support layer on mass transport of homologous series of alcohols and esters through composite pervaporation membranes.* Journal of Membrane Science, 2005(259): p. 122-134.

8. Ma, H.Y., et al., *High-flux thin-film nanofibrous composite ultrafiltration membranes containing cellulose barrier layer.* Journal of Materials Chemistry, 2010. **20**(22): p. 4692-4704.

9. Tang, Z.H., et al., *Design and Fabrication of Electrospun Polyethersulfone Nanofibrous Scaffold for High-Flux Nanofiltration Membranes.* Journal of Polymer Science Part B-Polymer Physics, 2009. **47**(22): p. 2288-2300.

10. Yoon, Y., B.S. Hsiao, and B. Chu, *High flux ultrafiltration nanofibrous membranes based on polyacrylonitrile electrospun scaffolds and crosslinked polyvinyl alcohol coating.* Journal of Membrane Science, 2009. **338**(1-2): p. 145-152.

11. Yoon, K., B.S. Hsiao, and B. Chu, *Formation of functional polyethersulfone electrospun membrane for water purification by mixed solvent and oxidation processes.* Polymer, 2009. **50**(13): p. 2893-2899.

12. Tang, Z.H., et al., *UV-cured poly(vinyl alcohol) ultrafiltration nanofibrous membrane based on electrospun nanofiber scaffolds.* Journal of Membrane Science, 2009. **328**(1-2): p. 1-5.

13. Yoon, K., B.S. Hsiao, and B. Chu, *High flux nanofiltration membranes based on interfacially polymerized polyamide barrier layer on polyacrylonitrile nanofibrous scaffolds.* Journal of Membrane Science, 2009. **326**(2): p. 484-492.

14. Yoon, K., B.S. Hsiao, and B. Chu, *Functional nanofibers for environmental applications.* Journal of Materials Chemistry, 2008. **18**(44): p. 5326-5334.

15. Chu, B., B.S. Hsiao, and K. Yoon, *Nanofiber and Nanocomposite-Fiber Technology for Environmental Applications.* AATCC Review, 2008. **8**.

16. Wang, X.F., et al., *High performance ultrafiltration composite membranes based on poly(vinyl alcohol) hydrogel coating on crosslinked nanofibrous poly(vinyl alcohol) scaffold.* Journal of Membrane Science, 2006. **278**(1-2): p. 261-268.

17. Yoon, K., et al., *High flux ultrafiltration membranes based on electrospun nanofibrous PAN scaffolds and chitosan coating.* Polymer, 2006. **47**(7): p. 2434-2441.

18. Wang, X.F., et al., *High flux filtration medium based on nanofibrous substrate with hydrophilic nanocomposite coating.* Environmental Science & Technology, 2005. **39**(19): p. 7684-7691.

19. Fukuzumi, H., et al., *Transparent and high gas barrier films of cellulose nanofibers prepared by TEMPO-mediated oxidation.* Biomacromolecules, 2009. **10**(1): p. 4.

20. Ma, H., et al., *Ultra-fine Polysaccharide Nanofibrous Membranes for Water Purification.* Biomacromolecules, 2011. **12**: p. 7.

21. Wijmans, J.G., et al., *The role of boundary layers in the removal of volatile organic compounds from water by pervaporation.* J. Membr. Sci. . **1-10**(109): p. 135-146.

22. Shao, P. and R.Y.M. Huang, *Polymeric membrane pervaporation.* Journal of Membrane Science, 2007. **287**(2): p. 162-179.

23. Rautenbach, R. and R. Albrecht, *On the behaviour of asymmetric membranes in pervaporation.* J. Membr. Sci., 1984(19): p. 1-22.

Chapter 4

Investigation of Nanofibrous Composite Membranes for Efficient Ethanol Dehydration

Table of Content

§ 4.1. Introduction

Ideally, for the current composite pervaporation (PV) membranes, the substrate layer should only provide the mechanical support to a thin dense barrier layer without affecting the mass transport of the permeate. The substrate should be porous to yield negligible resistance [1,2]. Otherwise, the substrate resistance would lead to decreases in permeability and/or selectivity because of the significant pressure drop across the membrane, which is being driven from the vacuum state of the membrane [3]. Many studies [4-8] had demonstrated clearly that the support layer could have significant effects on pervaporation. Bai at al [9] and Trifunović [10] concluded that the components of the mass transfer coefficient could be enhanced by increasing the porosity and pore diameter of the support and by decreasing the length of the Knudsen region, where the permeate vapor could be possibly condensed and trapped in the area of tiny pores in the support. Tan et al [11] studied the influence of support layer in PV composite of PDMS-PSf membrane, and found when the resistance of the support is significant, it could dominate PV performance of the composite membrane.

Hence, we hypothesized that the use of thin film nanofibrous composite (TFNC) as the supporting scaffold instead of the conventional phase inversion substrate could achieve the least resistance of the support substrate. This TFNC membrane consisted of three layers: a cellulose ultra-fine nanofibrous top layer with an average pore size of 20 nm [12], a polyacrylonitrile

(PAN) electrospun nanofibrous mid-layer and a polyethylene terephthalate (PET) nonwoven microfibrous bottom layer. The electrospun nanofibrous layer has high bulk porosity (up to 80%) and high surface to volume ratio. It can be integrated with a hydrophilic cellulose nanofibrous layer to form a fully interconnected pore structure with an asymmetric pore structure across the composite membrane thickness. Practical applications of these TFNC membranes were well demonstrated in liquid filtration, such as microfiltration, ultrafiltration, and nanofiltration [13-20]. Besides, the earl studies [21, 22] revealed that it could also lead to an integrated PV composite membrane when it was coated either with a polymeric or inorganic barrier layer. In the meanwhile, it had enhanced the membrane performance during ethanol dehydration

To understand the reasons and advantages of TFNC scaffold in a PV membrane, in this study, the PVA-TFNC composite membrane was developed to show the efficient permeability in ethanol dehydration when the same cross-linked PVA barrier was coated on different supporting scaffolds, including commercial ultrafiltarion membranes with comparable parameters to TFNC membranes. Related characterizations and tests among these membranes, including the evaluated performance of PVA-TFNC composite membrane, are presented as the following..

§ 4.2. Experimental

§4.2.1 Materials

Polyvinyl alcohol (PVA, degree of hydrolysis = 98.5%, weight-average molecular weight = 145,500 g/mole), polyacrylonitrile (PAN, weight average molecular weight = 150,000 g/mol), fumaric acid, and dextran (2000,000 g/mole) was obtained from Sigma Aldrich Inc. Nonwoven polyethylene terephthalate (PET) substrate (Hollytex 3242) was kindly provided by the Ahlstrom Mount Holly Springs Company. Cellulose raw material in suspension (Biofloc 96 MV, 22% wt. of wood pulp) was supplied by the Tembec Tartas factory in France. Commercial ultrafiltration membrane containing polyethersulfone (PES) porous layer was provided by the Filtration Solutions Inc. Commercial ultrafiltration membrane PAN400, was obtained from Sepro Inc. Sulzer 1210, a PVA composite PV membrane, was obtained from Sulzer Chemtech.

§4.2.2 PV membrane preparations:

PVA aqueous solutions (2 wt% ~ 4 wt%) were prepared at 80 ℃. Then, fumaric acid in the amount of 0.05 molar ratio to PVA, was blended with the PVA aqueous solution. The PVA/fumaric acid solution (5g PVA) was casted on the support membrane and the TFNC, by using a coating knife to control the coating thickness. The casted membrane was dried in the incubator at 40℃overnight and cured in a vacuum oven at 150 ℃ for 2 hours to initiate the cross-linking reaction.

§4.2.3 Characterization and evaluation

Water contact angle was determined by using an optical contact angle meter (CAM200, KSV Instruments, LTD). SEM micrographs were obtained using the LEO 1550 instrument equipped with a Schottky field emission gun (20 kV) and a Robinson backscatter detector. The surface-peeled samples were also characterized by FTIR (Nicolet iS10 FTIR-ATR). In addition, the following characterization methods were also adopted.

Dead-end filtration

Water permeability and filtration experiments were conducted to compare the pore size of tested support membranes by using a Millipore stirred ultra-filtration cell (model 8050) with an effective filtration area of 0.00134 m^2 to perform the dead-end filtration. A type of dextran (from Leuconstoc mesenteroides, Sigma) with molecular weight of 2,000 KDa was dissolved in Milli-Q water to prepare 5,000 ppm of feed solution. The Stokes-Einstein radius of polydispersed dextran of 2,000 KDa could be calculated to be about 54.6 nm according to the equation [23].

Pressure drop test

In order to determinate the effluence of the supporting layer porosity to the permeation ability when used in pervaporation, a test apparatus was designed to evaluate the pressure drop across the membrane, as shown in Figure 4.1. It is well accepted that the pressure drop across the membrane is inversely related to the porosity of the membrane according literature [4, 24].

Hence the pressure drop across the membrane could be correlated with the porosity of the membrane

The apparatus was set up under one atmosphere pressure with one side of the membrane being connected to a vacuum pump, in order to depressurize and to maintain 150 milli torr, which was detected via gauge V1. The other end of the cell was isolated and the remaining pressure could be detected via gaugeV2. Then, the pressure drop across the test membrane could be obtained.

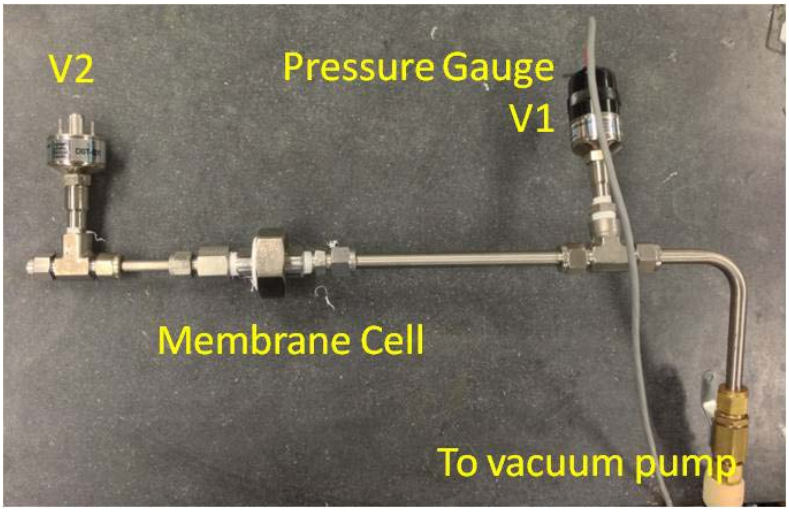

Figure 4-1 Schematic representation of test setup for pressure drop across the membrane

Pervaporation:

A custom pervaporation apparatus was used to evaluate the ethanol dehydration performance of the membranes. The detailed experimental procedure and setup were reported in an earlier publication. [10]

§ 4.3. Results and discussion

§4.3.1 Dead-end filtration and pressure drop evaluation

From the results of dead-end filtration experiments for tested membranes, as shown in the following table, the TFNC membrane had a permeation flux of 17.2 (L/m^2hrpsi), which was twice the flux with PAN400, and slighter higher than the flux of PES membrane. Moreover, the TFNC membrane also showed a rejection of dextran 2,000K at 87.6%, meaning that the sizes of 87.6% of pores on the CN layer of TFNC membrane were smaller than 54.6 nm, based on the Stokes-Einstein radius of polydispersed dextran [23]. The PAN400 carried slightly larger pores than the TFNC. The PES showed much larger pore sizes from only 60.8% of the rejection, which might also directly influence its water permeability.

The TFNC also had only about one-third of water contact angles to that of PAN400, and less than half that of PES membrane It was due to the hydrophilicity of cellulose nanofibers on the TFNC that were much greater than either the polyethersulfone of PES or polyacrylonitrile of PAN400. Hence, by comparison between TFNC and PAN400, the superior hydrophilicty of the TFNC enhanced greatly the water permeability, while the pore size of TFNC and of PAN400 were in the same range.

Table 4-1 Multitesting results of commercial UF membranes and TFNC membranes.

	Water Permeability (L/m^2hrpsi)	**Rejection % Dextran 2000(K Da)**	**Water contact angle**	**Pressure Drop (milli torr)**	**Note**
PAN400	7.9	83.9	47.9(+/- 0.5)	150	Sepro Inc.
PES	15.6	60.8	41.7(+/- 0.6)	230	Filtration Solution Inc.
TFNC	17.2	87.6	16.1 (+/- 0.5)	120	
E-spun layer	103.4	N/A	57.6 +-0.2	25	83.2 nm (pore size)
PVA-TFNC	N/A	N/A	64.8(+/-3.4)	N/A	N/A

The pressure drop test was conducted to try to elucidate the depletion of vacuum across the support layer during the pervaporation process. The pressure drop gradient could mainly be related to the porosity of the layer. The measurement was intended to help to evaluate the influence of the support layer to the pervaporation performance.

The TFNC had 150 milli torr of pressure drop, which was mainly attributed to the ultrafine cellulose nanofibers since the electro-spun PAN nanofinrsous scaffold could only cause a pressure drop of 25 milli torr. The PAN400 membrane and the PES membrane were made by using the phase inversion method, but the following one had a much higher pressure drop despite the fact that it carried larger sized pores on the surface according to the results of dead-end filtration experiments. The PAN400 pressure drop was at the same level of the TFNC membrane, meaning that both membranes had nearly the same degree of porosity.

After casting a dense barrier layer, such as “cross-linking PVA”, on the support layer, such as TFNC, PAN400 and PES, to form a pervaporation membrane, the pressure drop across these

PV membranes was dominant by the PVA layer and was responsible for the pressure difference between the vacuum side and the feed side (normally one bar)

§4.3.2 Fumaric acid cross-linking of the PVA barrier layer

From the mechanism in the following schematics, PVA losed hydroxyl groups to connect to fumaric acid by forming the ester group. It is well known that over cross-linking will lead to depletion in PVA hydrophilicty due to the loss of hydroxyl groups. The FTIR spectrum of cross-linked PVA indicated the presence of hydroxyl, carboxyl and epoxide functional groups (i.e., O—H stretch at 3430 cm^{-1}, C—H stretch at 2850 cm^{-1}, C=O at 1720 cm^{-1}, C—H bend at 1470 cm^{-1}, C—O stretch at 1300 cm^{-1}, —OH stretching at 1200 cm^{-1}, and O—H bend at 950 cm^{-1}).

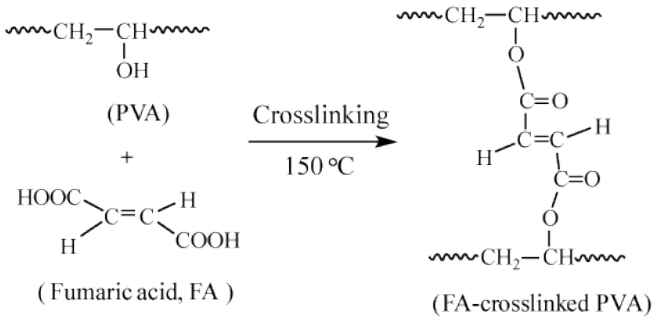

Figure 4-2 Schematic reaction mechanism of fumaric acid cross-linking of PVA

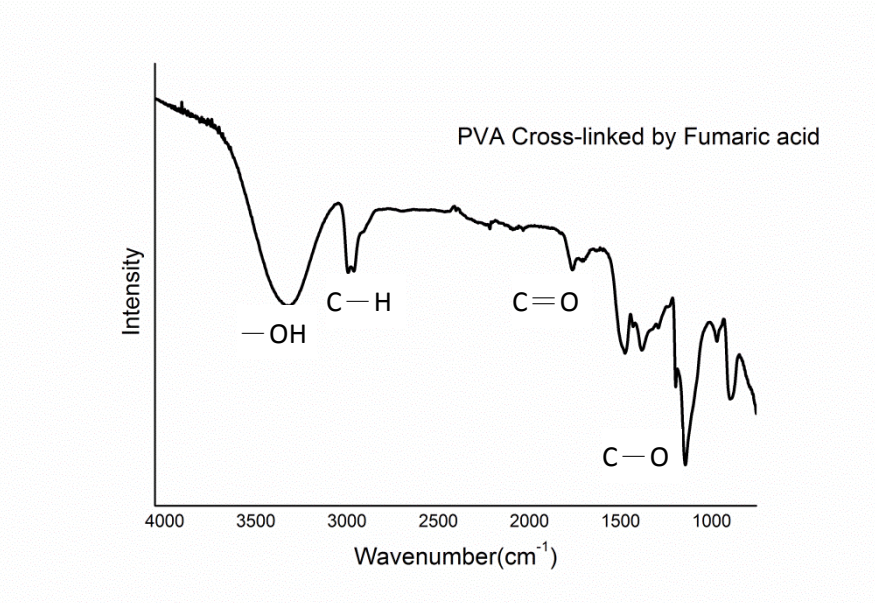

Figure 4-3 FTIR spectrum of PVA cross-linked by fumaric acid.

§4.3.3 Performance comparison of PV membranes on various supports

In order to fairly evaluate the influence of support mat to the performance during the pervaporation, the top layer of cross-linked PVA was controlled to a thickness of 2.06 μm, 2.11μm, and 2.09μm on PAN400, PES, and TFNC membrane, respectively. SEM images showed the cross-sectional morphology of membranes and the reference, “Sulzer 1210”, which was a composite membrane with a top layer of cross-linked PVA at 1.82 μm thickness on the phased-inversed PAN supporting mat. Except for the TFNC membrane, the other three membranes had phase-inversed supporting mat which was characterized as the non-homogeneous porous structure. The region with smaller pores existed near the top side. Because

the surface of the TFNC layer was composed of ultrafine cellulose nanofibers, the PVA could lie on the TFNC mat without intrusion into the e-spun scaffold [21]. Hence, in this fashion the cross-linked PVA layer could keep its integrity while the non-filling TFNC mat could also enhance the efficiency of water vapor transfer by taking advantage of its lower pressure drop.

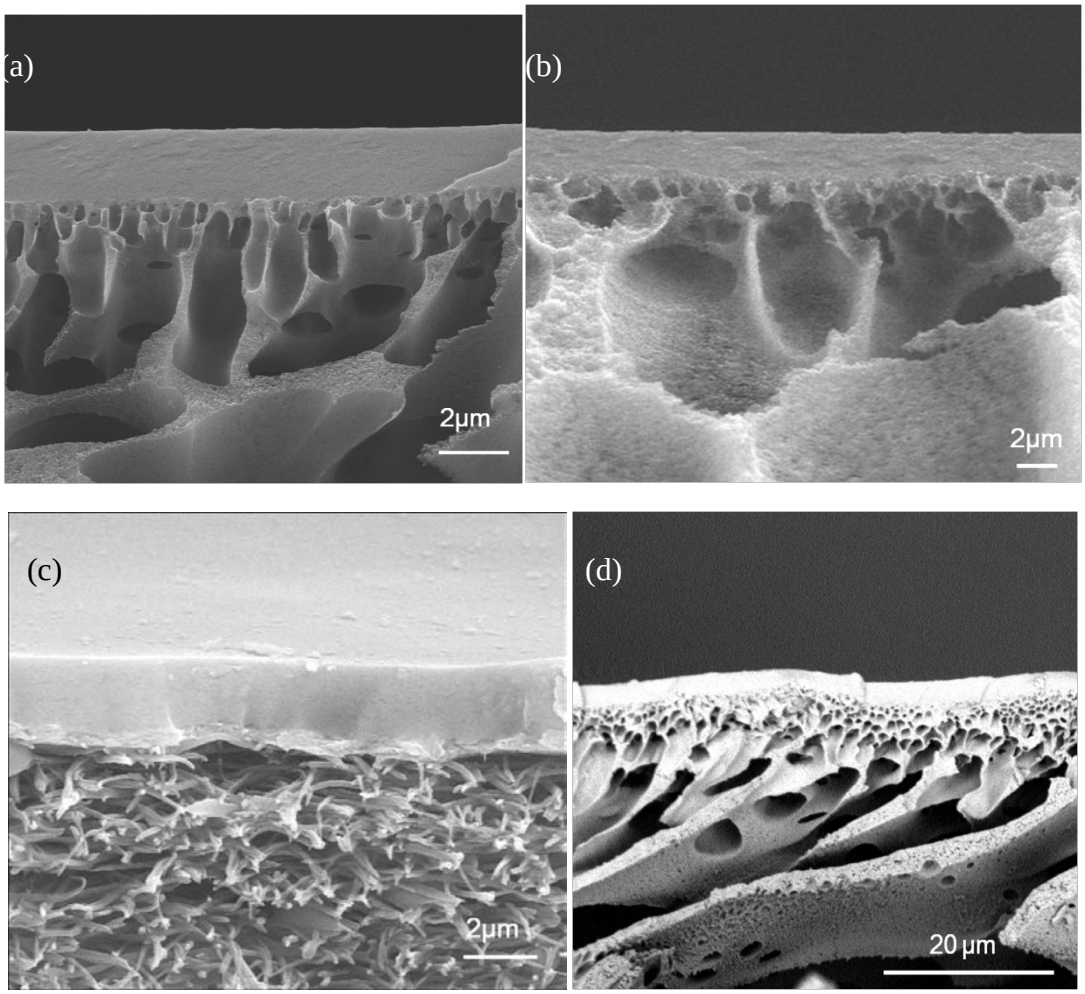

Figure 4-4 SEM cross-section imagine of a) PVA/PAN400 membrane, b) PVA/PES membrane, c) PVA/TFNC membrane, and d) Sulzer 1210 membrane

The membranes were evaluated in ethanol dehydration via pervaporation, with 80 wt% of ethanol feed, operating at 70 ℃. In the following plot, the PVA-TFNC membrane had permeate flux of 1.4 (kg/hrm^2) with the separation factor of 234, which was obviously superior toothers. The PVA-PAN400 membrane and PVA-PES membrane did not reach the same level of selectivity despite having the same barrier layer as that of the PVA-TFNC membrane. Since the PES had larger pores on the surface and lower porosity, it could have the higher possibility for intrusion of PVA. Then, the Knudsen diffusion could happen in the filled region to decrease the separation performance of the active layer. [10, 25]

The permeate flux of the membrane were in a reverse relationship with the pressure drop of the supporting mat. In comparison between TFNC and PAN400, the major difference was the hydrophilicity from the previous table; both membranes had similar pore sizes and pressure drop. However, the results of pure water flux and permeate flux in pervaporation revealed that the TFNC based membrane had the water flux being about twice higher in dead-end filtration, and lifting the performance index (PI: permeate flux multiply by separation factor) by 45% in pervaporation to the performance of the PAN400 based membrane. Therefore, it could be inferred that the water affinity of the support layer had an impact to the dehydration performance during pervaporation.

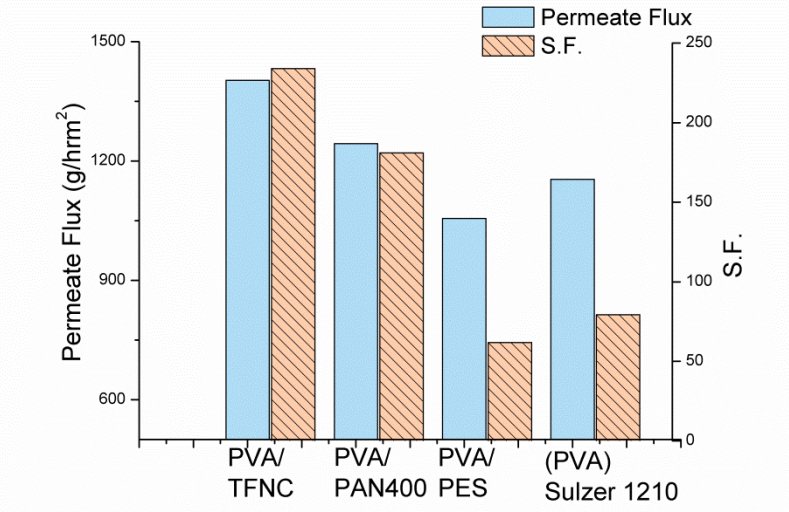

Figure 4-5 Comparison of performance of PV membranes used in ethanol dehydration, feed with 80 wt% ethanol, at 70 ℃

§4.3.4 Performance of PVA-TFNC under varying operating conditions

When feeding with concentrated ethanol aqueous solution, the PVA-TFNC membrane, with a PVA layer of 2.06 μm thickness, showed an increased separation factor but a decreased permeate flux. Due to lesser amount of water in the more concentrated ethanol aqueous solution, the diffusion tendency of water concentration gradient across the membrane was also decreased; therefore, the permeation flux was decreased in order to match the expectation of Fick's equation. When feeding with 90% of ethanol, the PVA-TFNC membrane had a flux of 0.88 (kg/m^2h) and a separation factor of 288, which was 30% more efficient in flux and 4.2 times higher in the separation factor, when compared with commercial Sulzer 12110 (see Chapter 2, Figure 2-3)

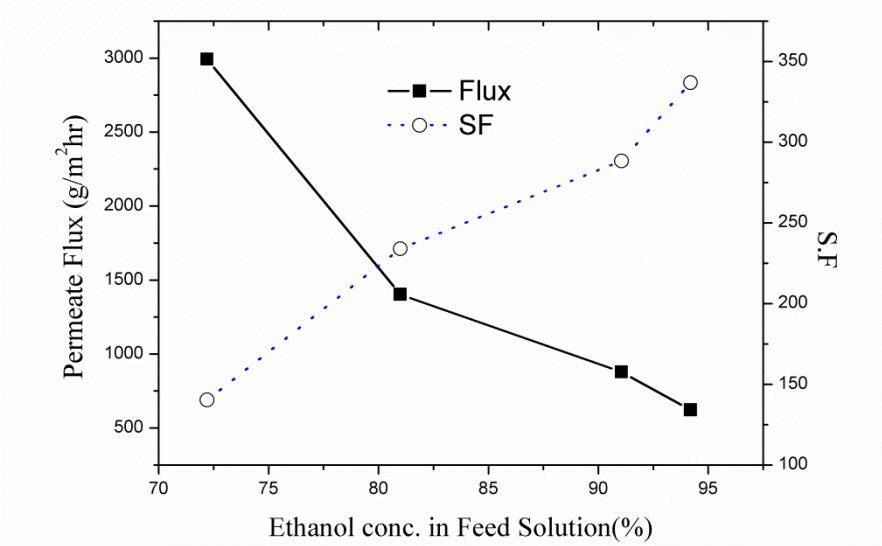

Figure 4-6 Performance of PVA-TFNC membrane in ethanol dehydration, feed with varying ethanol concentration, at 70 ℃

It was observed that the permeate flux was inversely dependent to the thickness of the PVA layer. Besides, there was a tradeoff between S.F. and permeate flux. The thinnest PVA layer in this study was 0.21±0.13 μm, where the limited thickness was related to the roughness of the TFNC. The average roughness of surface of TFNC was observed to be about 41 nm by using AFM [26] (e.g. 200 nm thick CN on the e-spun scaffold of 70 μm). Although the current PVA layer could be casted even thinner, it would be difficult to achieve a thinner coating by using the manual coating method as the thickness was less than 1 μm. The optimal and reliable range of the PVA layer thickness ranged from 1 μm to 2.5 μm, based on the current practice. (ex. Figure 4-4 (c) and Figure 4-8)

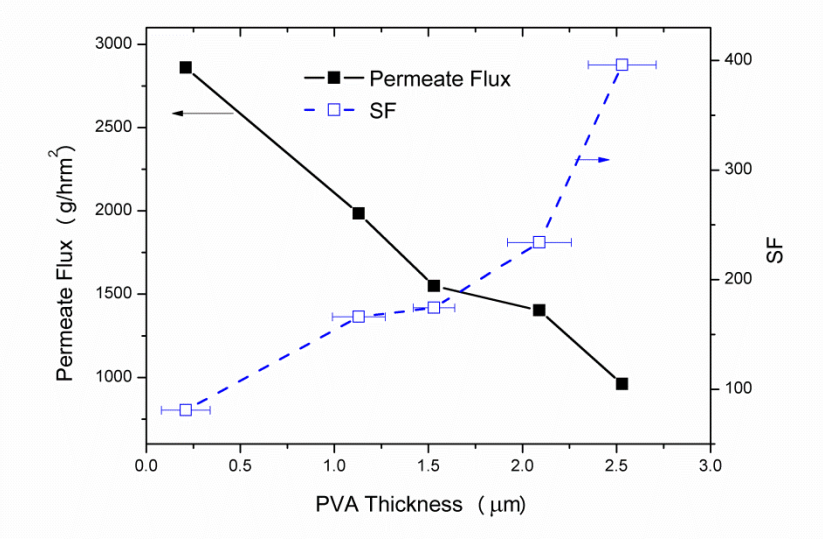

Figure 4-7 Performance vs. PVA layer thickness, feed with 80 wt% ethanol, at 70 ℃

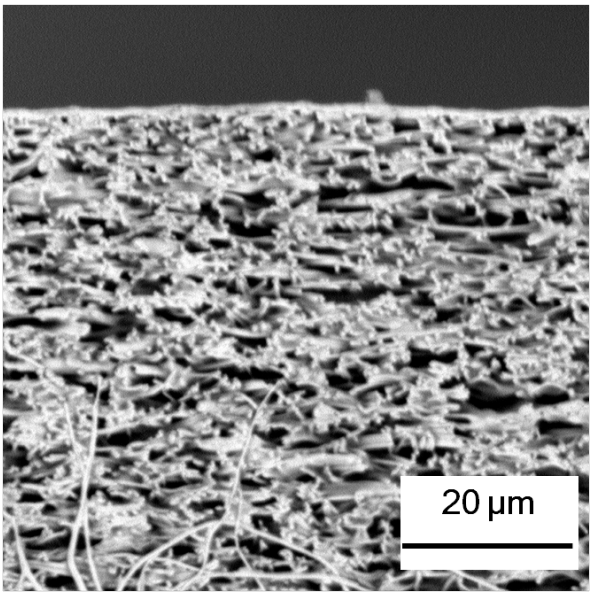

Figure 4-8 PVA-TFNC membrane with a PVA layer thickness of 1.13 μm

The increasing permeate flux was dependent on higher feeding temperature and a decreasing separation factor. Permeate molecules have higher energy to transfer under higher

thermal conditions. Besides, the free volume of the PVA layer could also be increased to enhance this effect when the polymer chains of PVA tended to move in the environment of higher temperatures [4, 25]. When the temperature was higher than that of the azeotrope point of ethanol aqueous mixture (78℃), the saturated ethanol/water stream pressurized the system to lead additional increments of permeate flux and a drop in the separation factor. On other hand, a lower feeding temperature could cause a counter effect on the membrane and the permeate molecules. Therefore, the practical operating temperature used in industry usually ranges from 50 - 70 ℃,in order to have more efficiency in performance and an acceptable selectivity.

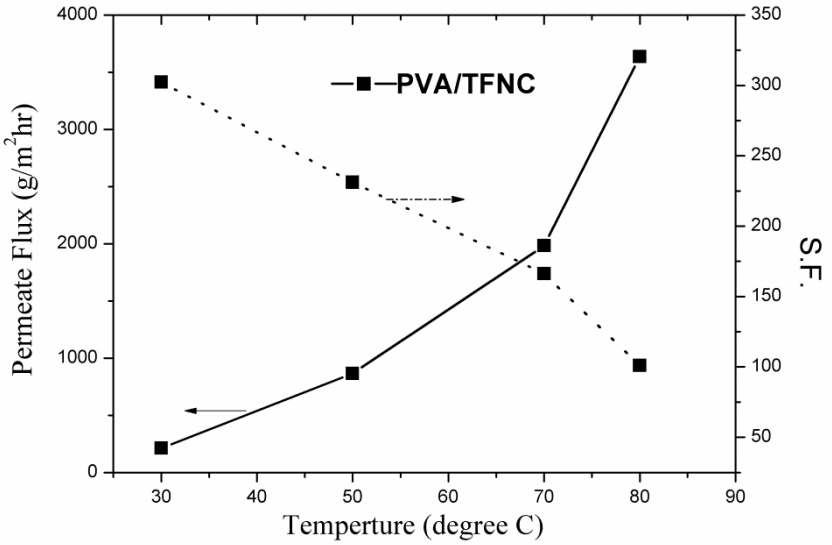

Figure 4-9 Performance vs. operating temperature, feed with 80 wt% ethanol

§ 4.4. Conclusions

The fumaric acid cross-linked PVA was coated on TFNC to form an efficient pervaporation membrane for ethanol dehydration. To investigate the influence of the supporting mat and the comparable commercial membrane, such as PES and PAN400, the performances were compared to the TFNC membrane in dead-end filtration and the pressure drop test. The supporting mats were coated with the same cross-linked PVA layer to form a pervaporation type membrane and were evaluated for ethanol dehydration via pervaporation

The TFNC membrane posed 50% ~ 80% of pressure drop compared to other commercial membranes due to its high porosity. Besides, TFNC only posed about one third water contact angles of other two membranes, meaning that the surface of TFNC was more hydrophilic. Hence, it enhanced the transfer of permeate vapor when used for pervaporation, resulting in 25% enhanced flux compared to the flux with PVA/PAN400 and 40% more efficient flux compared to the flux with PVA/PES.

The PVA-TFNC showed a tendency of increasing permeate flux when feeding with less concentrated ethanol aqueous solution, lowering the operating temperate, and using a thicker PVA layer. A tradeoff relationship between the separation factor and the permeate flux was also observed.

§ 4.5. References

1. (EIA), U.E.I.A., *US ethanol comsumption statistics*. 2011.

2. Koops, G.H., et al., *Poly(vinyl chloride) polyacrylonitrile composite membranes for the dehydration of acetic acid.* Journal of Membrane Science, 2001. **81**(1-2): p. 14.

3. Pinnau, I. and W.J. Koros, *Relationship between substructure resistance and gas separation properties of defect-free integrally skinned asymmetric membranes.* Industrial & Engineering Chemistry Research, 1991. **30**(8).

4. Feng, X.S. and R.Y.M. Huang, *Liquid separation by membrane pervaporation: A review.* Industrial & Engineering Chemistry Research, 1997. **36**(4): p. 1048-1066.

5. Huang, R.Y.M.F., X., *Resistance model approach to asymmetric polyetherimide membranes for pervaporation of isopropanol/ water mixtures.* J. Membrane Sci. , 1993. **84**: p. 15.

6. Lipnizki, F., et al., *Hydrophobic pervaporation: influence of the support layer of composite membranes on the mass transfer.* Separation Science and Technology, 2002. **37**(8): p. 1747-1770.

7. Gudernatsch, W., T. Menzel, and H. Strathmann, *Influence of composite membrane structure on pervaporation.* Journal of Membrane Science, 1991. **61**(0): p. 19-30.

8. Bode, E. and C. Hoempler, *Transport resistances during pervaporation through a composite membrane: experiments and model calculations.* Journal of Membrane Science, 1996. **113**(1): p. 43-56.

9. Bai, J., et al., *A study on the preparation and performance of polydimethylsiloxane-coated polyetherimide membranes in pervaporation.* Journal of Applied Polymer Science, 1993. **48**(6): p. 999-1008.

10. Trifunović, O. and G. Tragardh, *The influence of support layer on mass transport of homologous series of alcohols and esters through composite pervaporation membranes.* Journal of Membrane Science, 2005(259): p. 122-134.

11. Tan, S., et al., *The influence of support layer structure on mass transfer in pervaporation of composite PDMS–PSF membranes.* Chemical Engineering Journal, 2010. **157**(2–3): p. 304-310.

12. Ma, H., et al., *Ultra-fine Polysaccharide Nanofibrous Membranes for Water Purification.* Biomacromolecules, 2011. **12**: p. 7.

13. Ma, H.Y., et al., *High-flux thin-film nanofibrous composite ultrafiltration membranes containing cellulose barrier layer.* Journal of Materials Chemistry, 2010. **20**(22): p. 4692-4704.

14. Tang, Z.H., et al., *Design and Fabrication of Electrospun Polyethersulfone Nanofibrous Scaffold for High-Flux Nanofiltration Membranes.* Journal of Polymer Science Part B-Polymer Physics, 2009. **47**(22): p. 2288-2300.

15. Yoon, K., B.S. Hsiao, and B. Chu, *Formation of functional polyethersulfone electrospun membrane for water purification by mixed solvent and oxidation processes.* Polymer, 2009. **50**(13): p. 2893-2899.

16. Tang, Z.H., et al., *UV-cured poly(vinyl alcohol) ultrafiltration nanofibrous membrane based on electrospun nanofiber scaffolds.* Journal of Membrane Science, 2009. **328**(1-2): p. 1-5.

17. Wang, X.F., et al., *High flux filtration medium based on nanofibrous substrate with hydrophilic nanocomposite coating.* Environmental Science & Technology, 2005. **39**(19): p. 7684-7691.

18. Liu, Y., et al., *High-flux microfiltration filters based on electrospun polyvinylalcohol nanofibrous membranes.* Polymer, 2013. **54**(2): p. 548-556.

19. Wang, R., et al., *Nanofibrous microfiltration membranes capable of removing bacteria, viruses and heavy metal ions.* Journal of Membrane Science, 2013. **446**(0): p. 376-382.

20. Ma, H., et al., *Highly Permeable Polymer Membranes Containing Directed Channels for Water Purification.* ACS Macro Letters, 2012. **1**(6): p. 723-726.

21. Yeh, T.-M., et al., *Polymeric nanofibrous composite membranes for energy efficient ethanol dehydration.* Journal of Renewable and Sustainable Energy, 2012. **4**(4): p. 041406.

22. Yeh, T.-M., et al., *High flux ethanol dehydration using nanofibrous membranes containing graphene oxide barrier layers.* Journal of Materials Chemistry A, 2013.

23. Venturoli, D. and B. Rippe, *Ficoll and dextran vs. globular proteins as probes for testing glomerular permselectivity: effects of molecular size, shape, charge, and deformability.* American Journal of Physiology - Renal Physiology, 2005. **288**(4): p. F605-F613.

24. Huang, R.Y.M., et al., *Pervaporation separation of water/isopropanol mixture using sulfonated poly(ether ether ketone) (SPEEK) membranes: transport mechanism and separation performance.* Journal of Membrane Science, 2001. **192**(1-2): p. 115-127.

25. Shao, P. and R.Y.M. Huang, *Polymeric membrane pervaporation.* Journal of Membrane Science, 2007. **287**(2): p. 162-179.

26. Wang, X., et al., *Nanofiltration Membranes Prepared by Interfacial Polymerization on Thin-Film Nanofibrous Composite Scaffold.* Polymer, 2013. **(in pressing)**.

Chapter 5

High Flux Ethanol Dehydration using Nanofibrous Membranes Containing Graphene Oxide (GO) Barrier Layer

Table of Content

§ 5.1. Introduction

Graphene oxide (GO) can be obtained by exfoliation of graphite oxide. Similar to graphene, GO also possesses one-atom thick sheets with high surface-to-volume ratio and extraordinary physical properties. [1, 2] In addition, GO can form a stable aqueous suspension due to the presence of carboxyl acid groups and hydroxyl groups on the edge or the side of GO sheets.[3] Since the pioneering studies of Geim et al. in 2004, who successfully obtained graphene sheets by physical peeling of concentrated graphite, many follow-up studies and applications of GO have been carried out. For example, Nair and Geim et al. reported that GO membranes, having a layer thickness in the submicron range,[4] allowed unimpeded permeation of water vapor, but they were totally impermeable to other liquid and gas molecules including helium. This unique behavior may be attributed to the phenomenon of "nanocapillaries" formed between the GO sheets. In other words, the hydrophilic nature of carboxyl acid groups and hydroxyl groups (which attracts water molecules) may create the tortuous network of confined water channels, allowing the transport of water molecules but preventing the diffusion of larger size and hydrophobic molecules. In this case, the GO membranes will be used for the separation of water and ethanol, which forms the base of the current study.

In this study, a GO barrier layer was laminated onto the surface of a thin-film nanofibrous composite (TFNC) membrane to fabricate a multilayered pervaporation membrane for ethanol dehydration. The GO barrier layer was formed by self-assembly of GO sheets, with the total layer thickness being controlled from 93 to 618 nm. The casting procedure included vacuum filtration and spin coating. To elucidate the mechanism of water transport in the GO layer, the morphological analysis of the GO barrier layer was carried out by using scanning electron microscopy (SEM), transmission electron microscopy (TEM) and grazing incidence wide-angle X-ray scattering (GIWAXS) methods. Measurements of the ethanol dehydration efficiency via pervaporation were performed using the GO-based TFNC membranes with different GO layer thicknesses. For example, the 93 nm thick GO membrane showed a permeate flux value of 2.2 (kg/m2hr) and a separation factor of 308 with a feed solution containing 80 wt% ethanol and 20% water at 70°C. These results are notably superior to those obtained with commercial polymeric membranes for pervaporation (e.g., the water flux increased by a factor of two and the selectivity increased by a factor of four). The GO thickness dependent relationship of the separation factor and the water flux was also observed, indicating that further improvements of GO-based TFNC membranes may be obtained by optimizing the barrier layer thickness.

§ 5.2. Experimental

§ 5.2.1 Materials:

The dispersed GO aqueous solution, in concentration of 5 g/L and flakes of 0.5-5 μm size, were received from Graphene Supermarket, Inc. and subsequently treated with the Hummer method. [6] Nonwoven polyethylene terephthalate (PET) substrate (Hollytex 3242) was purchased from the Ahlstrom Mount Holly Springs Company. Cellulose raw material in suspension (Biofloc 96 MV, 22% wt. of wood pulp) was supplied by Tembec Tartas Company in France. Sulzer 1210, a PVA composite membrane, was obtained from Sulzer Chemtech. 95 vol. % of ethanol in water was purchased from Sigma Aldrich, Inc.

§ 5.2.2 Membrane fabrication

The chosen scaffold (mat) to support the GO barrier layer was an experimental thin-film nanofibrous composite (TFNC) membrane containing an average pore size of 20 nm in the top layer [7]. This TFNC membrane consisted of three layers: a cellulose ultra-fine nanofibrous top layer, a polyacrylonitrile (PAN) electrospun nanofibrous mid-layer and a polyethylene terephthalate (PET) nonwoven microfibrous substrate. Practical applications of these TFNC membranes include high-flux microfiltration and ultrafiltration, as well as pervaporation.[7-11] In general, TFNC membranes exhibit several advantages over conventional polymeric

membranes made by the phase inversion method. These advantages include large bulk porosity (80%) and fully interconnected pore structures, which are especially useful to avoid the Knudsen diffusion in gas separation and pervaporation. The schemes to prepare TFNC membranes have been described in several publications elsewhere. [7-9]

A spin coating or vacuum filtration method [2, 4, 12] was used to cast the GO barrier layer on the TFNC membrane. These two methods provide an economical and practical pathway to produce defect-free films on a nanoporous support, when compared with other casting methods such as chemical vapor deposition (CVD) [13, 14], Langmuir-Blodgett assembly [15], layer-by-layer coating [18] and evaporation coating [17].

The tested GO-based TFNC membranes were prepared by using the following procedures. The GO dispersion solution (Graphene Supermarket inc.), containing flakes in the size range of 0.5~5 microns, was first treated by the Hummer method. [25] Varying concentration of GO solutions were prepared and sonicated to disperse the GO sheets/particulates before casting. The resulting GO solutions were cast on the chosen three-layered TFNC membrane using either spin-coating or vacuum filtration method to prepare the GO barrier layer of different thicknesses. A representative experimental GO/TFNC membrane was shown in Fig. 5-1c (the membrane diameter was 3.8 cm). This membrane possessed a water contact angle of 68 ± 3° and an ethanol

contact angle of 8 ± 3°. We believe that the low ethanol contact angle value does not mean the surface of GO membrane was ethanol-philic. Instead, it was probably due to the low surface tension force of ethanol itself. For other hydrophilic dense membranes, such as typical RO and NF membranes, they tend to have a smaller alcohol contact angle than water contact angle.

With the higher GO concentration, a longer curing time was needed to produce a thicker GO layer thickness. However, in a prolonged process, some defects could occur, including the uneven aggregation of GO flakes. On the other side, the lower GO concentration could lead to voids or cracks. Hence, the operating parameters in the casting procedure, which were strongly dependent on the properties of the chosen TFNC membrane (e.g. hydrophilicity and average pore size of the cellulose layer), should be carefully optimized in order to prepare a thin and uniform barrier layer consisting of GO.

§ 5.2.3 Characterization

Water contact angle was determined by using an optical contact angle meter (CAM200, KSV Instruments, LTD). SEM micrographs were obtained using the LEO 1550 instrument equipped with a Schottky field emission gun (20 kV) and a Robinson backscatter detector. The TEM sample was first surface-peeled from the demonstrated membrane, embedded in the mold with epoxy resin and subsequently polymerized at 70°C. The epoxy-fixed samples were then

microtome sectioned and were imaged by the Tecnai12 BioTwinG2 (FEI company) instrument at 80 kV. Digital images were acquired using a digital camera system (AMT XR-60 CCD). The surface-peeled samples (without epoxy setting) were also characterized by FTIR (Nicolet iS10 FTIR-ATR) and XRD (Bruker AXS D8) using a copper source (λ=1.54Å). A GO layer (about 300 nm thick) spin-coated on the silicon wafer support was characterized by GIWAXS, which was performed at the X9 beamline in the National Synchrotron Light Source, Brookhaven National Laboratory.[17]

§ 5.2.4 Pervaporation

A custom pervaporation apparatus was used to evaluate the ethanol dehydration performance of the membranes. The detailed experimental procedure and setup were reported in an earlier publication.[10]

§ 5.3. Results and discussion

Fig. 5-1a illustrates the proposed “ideal” mechanism for water-ethanol transport in a perfectly stacked GO barrier layer. In this diagram, each hydrophilic GO sheet is represented by an orange color bar, where the topological representation of the barrier layer with multilayered GO sheets is illustrated in Fig. 5-1b. The distance “D” in Fig. 5-1a represents the GO inter-sheet

spacing, which determines the selectivity performance and can be adjusted by changing the moisture content or by modifying the spacing with chemicals.[12] The water molecular pathway is represented by the blue dashed line, along which water travels in a tortuous manner through the phenomenon of nanocapillary. As outlined earlier, the passage of the ethanol molecule is blocked by the formation of confined spacing between the GO sheets.

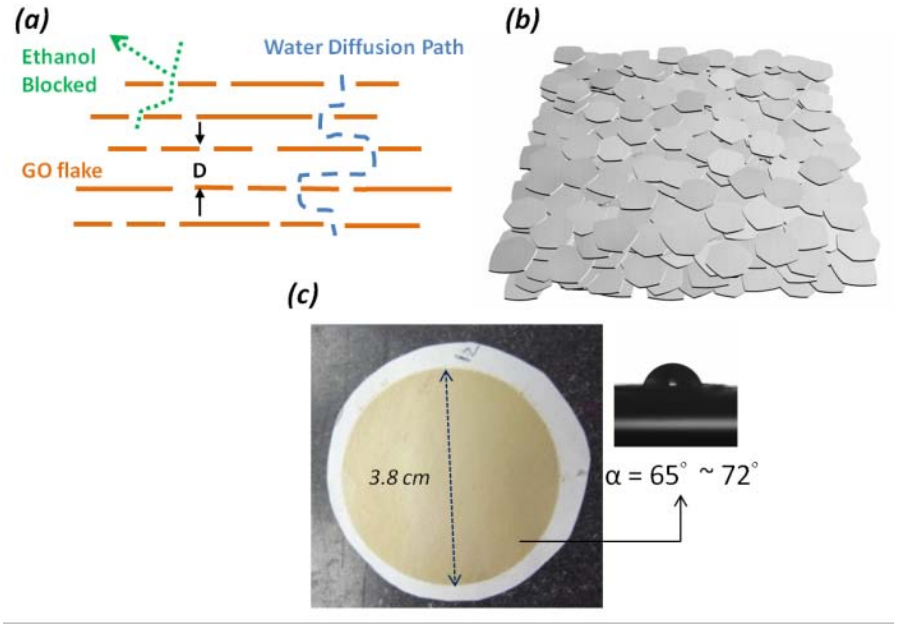

Figure 5-1 Water transport in the graphene oxide (GO) barrier layer. (a) The proposed mechanism for water-ethanol separation within the GO barrier layer based on perfectly stacked GO sheets (orange bars), in which the inter-sheet spacing was greatly expanded. (b) Topological representation of the barrier layer with multilayered GO sheets based on (a). (c) A representative experimental permeation membrane (diameter 3.8 cm) based on the GO barrier layer, the membrane possessed a water contact angle of 68 ± 3°.

§ 5.3.1 GO-TFNC membrane characterization

In Fig. 5-1c, the resulting TFNC membrane with the GO barrier layer had a circular shape with a diameter 3.8 cm. The thickness of the GO layer ranged from 93 nm to 618 nm, controlled by changing the operating parameters during casting, including the water suction rate, spinning time and spinning speed. The surface of the tested GO-based TFNC membranes exhibited an average water contact angle of 68 ± 3 degrees under an ideally non-leaking condition.

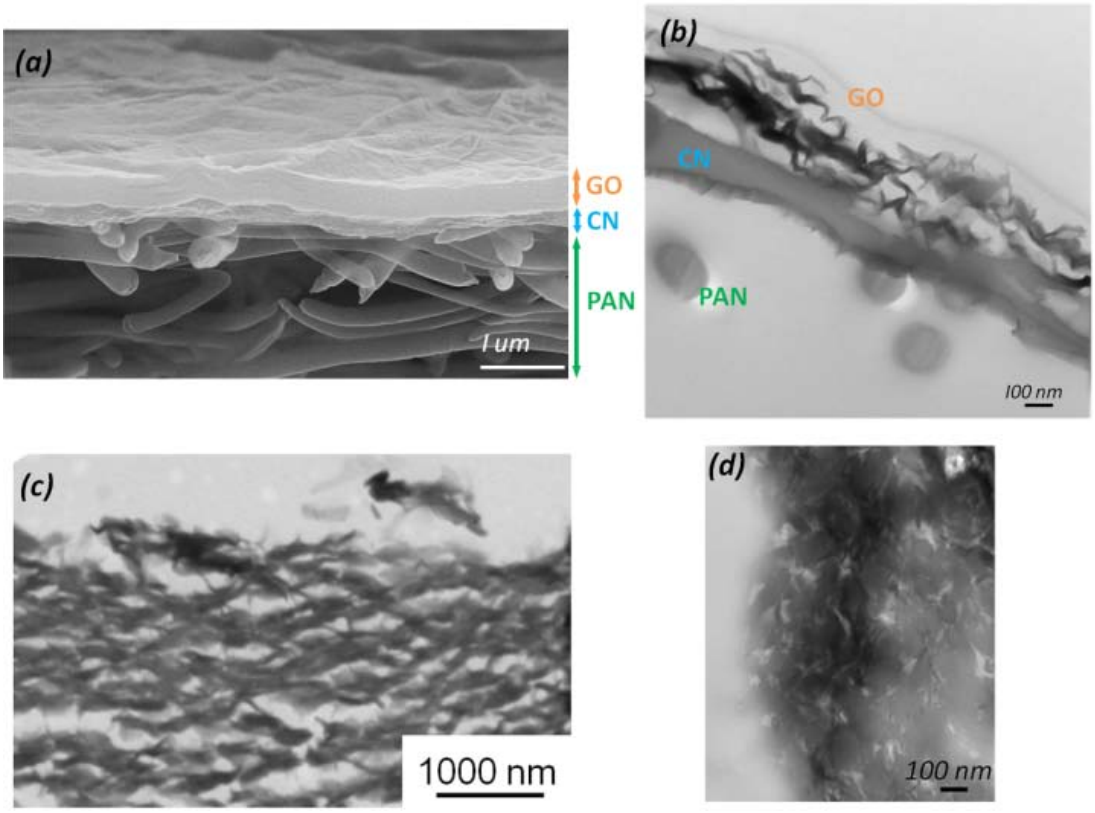

Figure 5-2 (a) SEM image of a cross-sectioned TFNC membrane with a GO barrier layer. (b) and (c) TEM images of the cross-sectioned GO barrier layer with the different thickness. (d) TEM top-view image of the GO barrier layer.

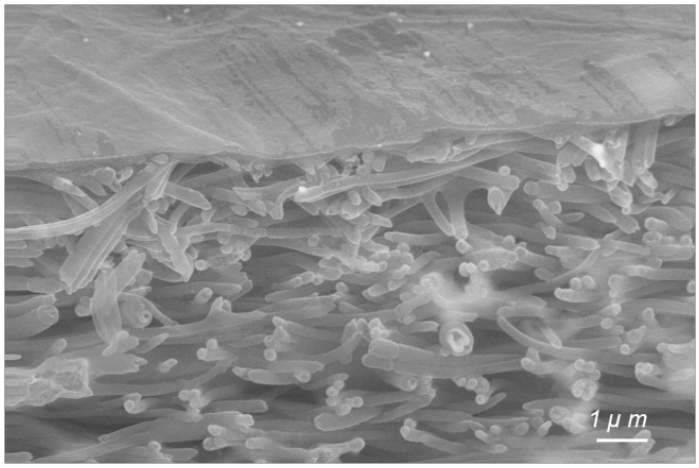

Figure 5-3 SEM image of a cross-sectioned TFNC membrane with a GO barrier, which reveals the real morphology without the waviness effect as seen in Figure 5-2b.

A representative cross-sectional scanning electron microscopy (SEM) image of the tested membrane sample is shown in Fig. 5-2a, which clearly reveals the discrete GO layer supported by a TFNC scaffold. Cross-sectional and top-viewed TEM images of the GO layer (Fig. 52b – 5-2d) revealed more detailed information about the GO morphology, suggesting that the GO sheets probably formed unaligned stacks in the barrier layer. The schematic diagram of the corresponding GO structure is illustrated in Fig. 5-4a, in which randomly oriented GO stacks (the GO sheet is not shown in scale with respect to the nanofibrous scaffold) are the dominant morphology. The waviness of GO sheets shown in the TEM micrograph of the cross-sectioned sample (Fig. 5-2b and 2c) could be attributed to the relief of the stress during microtome sectioning of the sample. [16] The morphology without waviness effect of the same piece of GO membrane in Fig. 5-2b can be seen in Fig. The top-view TEM image (Fig. 5-2d) shows some

lighter gray areas being present between the platelets (with lengths from 0.3~0.8 μm). We speculate that the variations of color could possibly be due to voids or thinly covered areas, being deposited by less oriented sheets or intercalating flakes.

To understand the surface topography of the GO barrier layer, grazing incidence wide-angle X-ray scattering (GIWAXS) measurements was carried out on the GO layer cast on a silicon wafer support. The results indicated the appearance of a ring pattern (Fig. 5-4c), suggesting the absence of any preferred orientation between the layered GO stacks. This finding concurred with the GO structure observed by TEM (Fig. 5-2d), but differed from the ideal expectation of the GO arrangement in a parallel fashion (Fig. 5-1b). Thus, the logical mechanism of water transport in the GO barrier is more likely illustrated in Fig. 5-4b

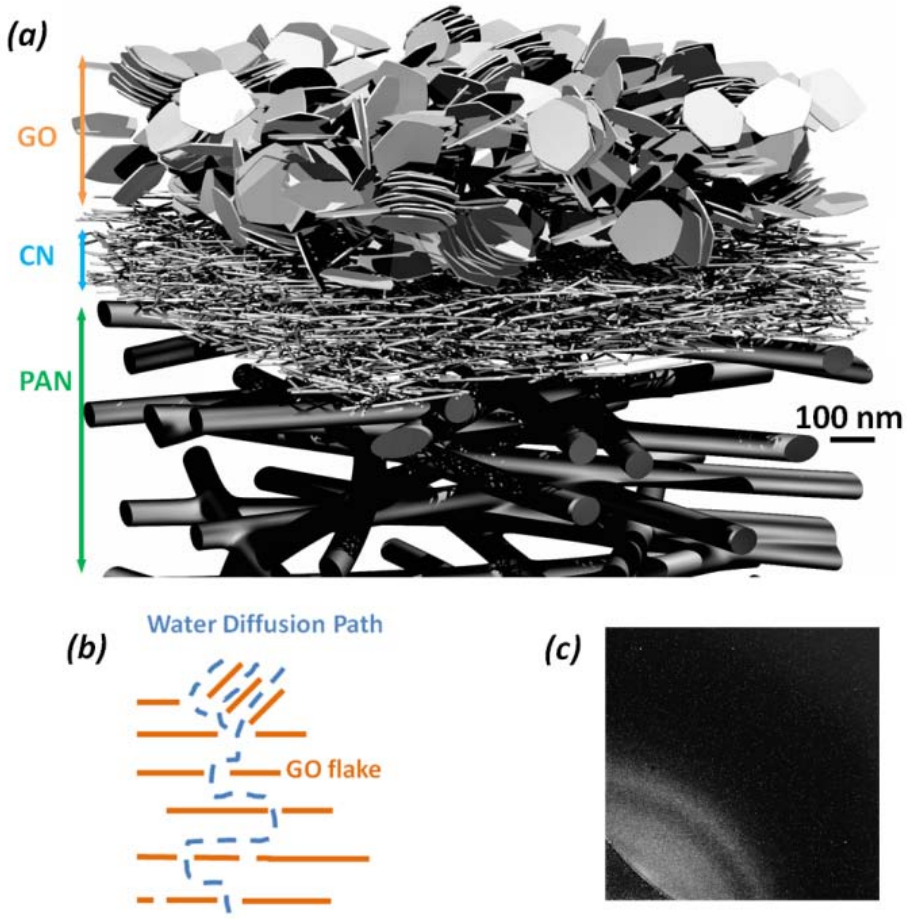

Figure 5-4 (a) The schematic diagram indicating the morphological arrangement of GO sheets (not shown in correct scale) and the supporting TFNC membrane scaffold. (b) The revised mechanism for water-ethanol separation within the GO barrier layer after the morphology characterization (the inter-sheet spacing was greatly expanded). The misaligned stack was shown as an example. (c) A ring pattern of GIWAXS result on a GO layer.

§ 5.3.2 Morphology analysis

Fig. 5-2a (SEM image) and 2b (TEM image) show the morphology of the GO barrier layer supported by a TFNC membrane at different length scales. The SEM image (Fig. 5-2a) clearly indicated the supporting layer consisting of electrospun PAN nanofibers (the mean diameter was

about 100 nm), where the total layer thickness was about 40 μm. The higher resolution TEM image (Fig. 5-2b) indicated that a layer (thickness about 100 nm) of ultra-fine cellulose nanofibers (CN, the mean diameter was about 5 nm but the fibers could not be identified individually) was sandwiched between the electrospun layer and the GO barrier layer. The properties of the CN layer were characterized by our laboratory earlier.[7] In brief, the CN layer is hydrophilic and has a very high degree of crystallinity (> 80%), where this layer has an average pore size about 20 nm and the maximum pore size about 50 nm. Fig. 5-4a illustrates a schematic diagram of the hierarchical structure arrangement of the tested membrane, consisting of four different layers: (1) the top GO barrier layer with randomly organized GO stacks, (2) the ultrafine cellulose nanofiber supporting layer (with diameters of about 5 nm), (3) the electrospun PAN nanofibrous scaffold (diameters of about 100 nm), and (4) the nonwoven PET fibrous substrate (omitted in Fig. 5-4a) which provides the mechanical strength of this membrane system.

The average spacing between two adjacent GO sheets (schematically illustrated as “D” in Fig. 5-1a) in the layered GO stack was calculated to be 8.53 Å from the XRD data (Fig. 5-5), taken at a relative humidity of 30%. The FTIR spectrum of the GO barrier layer (Fig. 5-5) indicated the presence of hydroxyl, carboxyl and epoxide functional groups (i.e., O－H at 3430 cm-1, C＝O at 1720 cm-1, C－OH stretching at 1200 cm-1, C－O stretching at 1000 cm-1), resulting from the oxidation process and leading to the hydrophilic nature of GO [19].

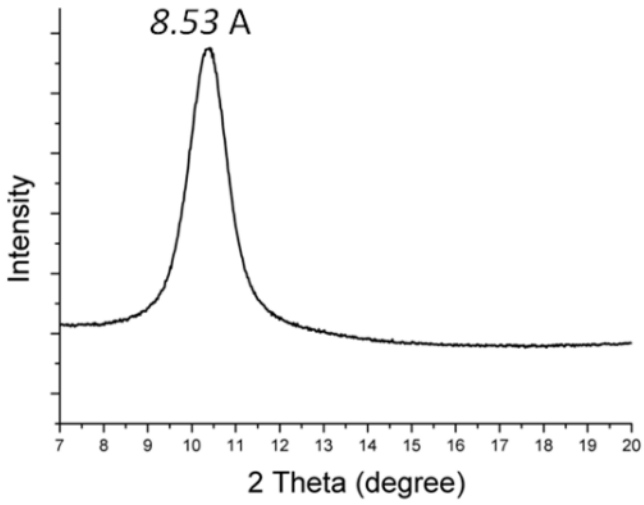

Figure 5-5: XRD pattern of graphene oxide

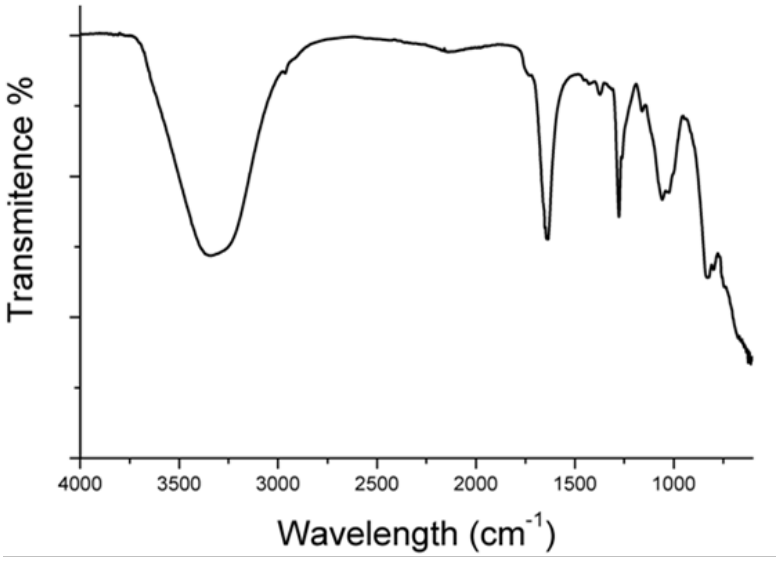

Figure 5-6: FTIR spectrum of graphene oxide

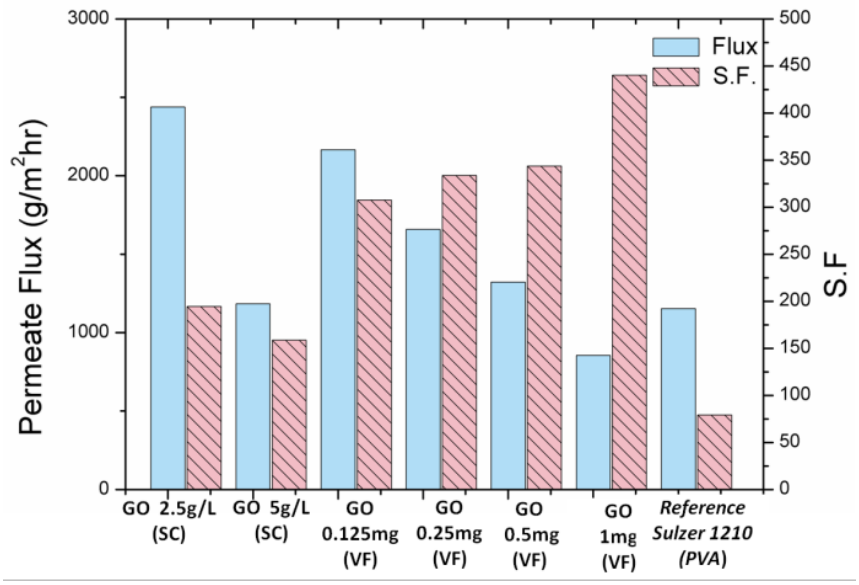

Figure 5-7 Permeate flux and separation factor (SF) obtained from the ethanol dehydration experiment via pervaporation using an 80 wt% ethanol feed solution at 70°C. Comparison of various GO-based TFNC membranes and a commercial reference. GO layers were casted by SC (spin coating) or VF (vacuum filtration) methods according to various prescribed recipes.

§ 5.3.3 Pervaporation performance

The GO-based TFNC membranes with different GO layer thicknesses were evaluated for ethanol dehydration via pervaporation using a feed aqueous solution containing 80 wt% of ethanol in water at 70°C. Table 5-1 summarizes the composition, GO layer thickness, and experimental data of tested membranes. The permeate flux and separation factor (SF) results for the GO-based TFNC membranes and a commercial pervaporation membrane (as a reference) are shown in Fig. 5-7. The data revealed that all tested GO-based TFNC membranes had a higher separation factor than the commercial membrane, e.g., the SF value of GO based membranes was

at least 159, much higher than 79 from the reference. The better SF performance could be due to the retardation of ethanol transport within the GO barrier layer. The maximum and minimum water flux values of the tested membranes were 2.4 kg/m2hr and 0.9 kg/m2hr, respectively; these values are significantly better or at least comparable to the flux (1.1 kg/m2hr) from the commercial membrane. It was found that the GO1 and GO3 membranes showed the best overall performance, i.e., the water flux values of 2.4 kg/m2hr and 2.2 kg/m2hr, and SF values of 195 and 308, respectively. We verified that the TFNC membrane itself did not contribute toward the separation of ethanol and water (see Table S1), but its unique support structure could enhance the transport of vapor water molecules through the membrane during pervaporation [10].

Table 5-1: Sample preparation schemes for various GO-based TFNC membranes, and their corresponding GO layer thickness and pervaporation results.

Sample	GO Casting Method	Aqueous GO Concentration [a] [mg/L]	GO Layer Thickness [nm]	Permeate [b]	
				Water conc.[c] [wt %]	Total Flux [kg/m^{2}hr]
GO_1	Spin coating	2500	N/A	97.8	2.4
GO_2	Spin coating	5000	N/A	97.2	1.2
GO_3	Vacuum filtration	0.5	93	98.7	2.2
GO_4	Vacuum filtration	1.0	187	98.7	1.7
GO_5	Vacuum filtration	2.0	300	98.8	1.3
GO_6	Vacuum filtration	4.0	618	99.0	0.9
TFNC Membrane		N/A	100 (Cellulose)	19.9	27.6
Sulzer 1210 (PVA based)		N/A	1.81μm (PVA)	95.9	1.1

[a] The designated concentration of GO solution used for casting of the top barrier layer

[b] Permeate data were measured by pervaporation experiment with a feed solution containing 80 wt% ethanol and water at 70 °C

[c] The concentration was quantitatively analyzed by using gas chromatograph (Hewlett-Packard GC5890) with a flame ionization detector and a Carbowax-20M column (Agilent)

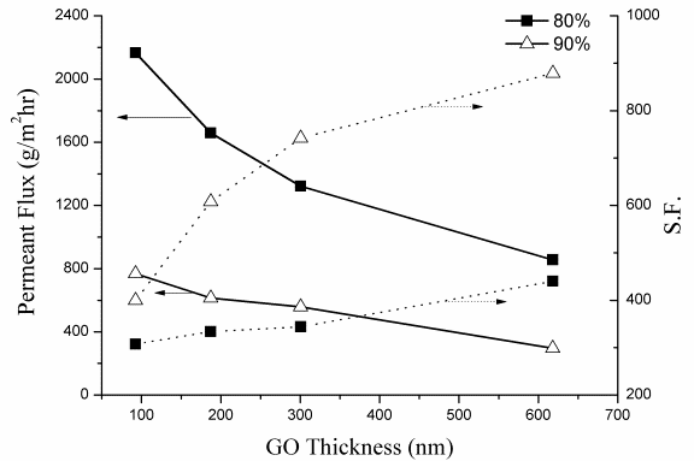

Figure 5-8 Relationship between the permeate flux and SF as a function of the GO layer thickness when using 80 wt% and 90 wt% ethanol aqueous feed solution at 70°C

Fig. 5-8 illustrates the relationship between SF and water flux with 80 wt% and 90 wt% ethanol aqueous as feeds. It was seen that water flux increased with decreasing SF as the thickness of the GO layer became thinner (especially with the thickness value below 200 nm). This observation suggests that water permeability is greatly influenced by the thickness of the GO layer, but SF depends less strongly on the GO layer thickness since the difference between the permeate concentrations collected in this study were within 2 wt%. There are two possible

explanations for this finding. (1) The density of the assembled GO sheets was not homogeneous along the deposited direction using the current casting methods, whereas the barrier layer thickness did not produce a linear relationship with SF. (2) The mechanism for water/ethanol separation within the GO layer are correlated not only to the layer thickness, but also to other characteristics such as hydrophilicity, inter-sheet spacing, and alignment of stacks of GO. We believe explanation (2) may be a more dominant factor.

The permeation flux of the membrane in 90% ethanol feed solution was greatly decreased with increasing separation factor when compared with results of 80% ethanol feed solution. It should be noted that the inter-sheet spacing among GO sheets became narrower as the water content in GO sheets was reduced. Thus, the membrane in 90% ethanol feed solution would have smaller 'nanocapilaries' within the GO sheets than the ones within the GO sheets in 80% ethanol feed solution, [20] resulting in having the membrane in 90% ethanol feed solution becoming denser to carry the higher separation factor with lower permeation flux.

The above evaluation experiments were operated for at least three hours with stable performance. The performance of our GO-based membranes at higher temperatures (e.g., 90 °C) could become less stable when compared with a typical operating temperature of $\leqq$ 70 °C because the GO layer was fabricated without further chemical modifications. The slight

decomposition of the GO layer, due to possible loss of some hydroxyl or/and carboxyl groups at higher temperatures, could affect the membrane performance. Cross-linking modifications on GO trying to improve mechanical property and stability have been mentioned [3, 21-23] However, attention to the hydrophilic nature of GO, the layer morphology, and their corresponding effects on water transport requires further study.

We infer the separate mechanism in GO partially from its non-oriented morphology as shown in Fig. 5-4a and 4b, respectively. It suggested that there were more possible pathways for water (even ethanol) to permeate into the GO stacks from the spacing of intercalating flakes in comparison with water permeating in an ideally orientated GO layer as shown in Fig. 5-1a. On the other side, the ideal model of orientated GO layer might reach more effective separation with thinner GO deposition as compared with the non-oriented GO model. Further, we speculate that the ideally oriented GO layer could still possibly be achieved through some specific fabrication process, and the influence of the size and functional groups of GO flakes to the layer morphology needs to be investigated and coordinated as well.

§ 5.4. Conclusions

In conclusion, the fabricated membranes based on TFNC scaffold and the GO barrier layer showed high water permeability and excellent selectivity for ethanol dehydration through

pervaporation. A membrane with the GO barrier layer thickness of 93 nm exhibited a water permeate flux of 2.2 kg/m2hr that is two times higher than the commercialized pervaporation membrane, and a separation factor of 308 that is nearly four times higher than the commercialized membrane. The structure characterization of the GO barrier layer indicated the GO sheets were aggregated into layered stacks and there was no preferred orientation between these stacks. The demonstrated membrane system, based on the TFNC support and a GO barrier layer, is suitable for the ethanol dehydrate application. However the membrane performance for pervaporation can be further optimized by a better control of the GO stack orientation and the total layer thickness, perhaps through a different coating method. [24]

§ 5.5. References

1. N. R. Wilson, P.A. Pandey, R. Beanland, R. J. Young, I. A. Kinloch, L. Gong, Z. Liu, K. Suenage, J. P. Rourke, S. J. York, J. Solan. *Acs Nano*. **2009**, 3, 2457-2556..
2. G. Eda, M. Chhowalla. *Adv. Mater*. **2010**. 22, 2392-2415.
3. S. Park, K. Lee, G. Bozoklu, W. Cai, S. T. Nguyen, R. S. Ruoff. *Acs Nano*. **2008**, 2, 572-578.
4. R. R. Nair, Wu, H. A, P. N Jayaram, I. V. Grigorieva, A. K Geim, *Science*, **2012**, 335, 442-444.
5. U.S. Energy Information Administration (EIA), *US ethanol comsumption statistics*. **2011**.
6. J. William, S. Hummers, R. E. Offeman, J. Am. Chem. Soc. **1958**, 80, 1339.
7. H. Ma, C. Burger, B. S. Hsiao, B. Chu, *Biomacromolecules*, **2011**, 12, 970-976.
8. H. Ma, K. Yoon, L. Rong, Y. Mao, Z. Mo, D. Fang, Z. Hollander, J. Gaiteri, C. Burger, B. S. Hsiao, B. Chu, *J. Mater. Chem.* **2010**, 20, 4692-4707.
9. H. Ma, K. Yoon, L. Rong, M. Sokralla, A. Kopot, X. Wang, D. Fang, B. S. Hsiao, B. Chu, *Ind. Eng. Chem. Res*. **2010**, 49, 11978-11984.
10. T. Yeh, D. Mahajan, B. S. Hsiao, B. Chu, *JRSE*. **2012**, 4, 041406.
11. H. Ma, C. Burger, B. S. Hsiao, B. Chu, *Acs Macro Lett.* **2012**, 1, 723-726.
12. K. W. Putz, O. C. Compton, M. J. Palmeri, S. T. Nguyen, L. C. Brinson, *Adv. Func. Mater*. **2010**, 20, 3322-3329.
13. A. Reina, X. Jia, J. Ho, D. Nezich, H. Son, V. Bulovic, M. S. Dresselhaus, J. Kong, *Acs Nano***. 2008**. 9, 30-35.
14. V. López, R. S. Sundaram, C. Gómez-Navarro, D. Olea, M. Burghard, J. Gómez-Herrero, F. Zamora, K. Kern, *Adv. Mater.* **2009**, 21, 4683-4686.
15. X. Li, G. Zhang, X. Bai, X. Sun, X. Wang, E. Wang, H. Dai, *Nat. Nano.* **2008**, 3, 538-542.
16. Y. Yang, L. Bolling, M. A. Priolo, J. C. Grunlan, *Adv. Mater.* **2013**, 25, 503-508.

17. C. Chen, Q. Yang, W. Lv, Y. Wen, P. Hou, M. Wang, H. Cheng, *Adv. Mater*. **2009**, 21, 3007-3011.

18. L. Yang, *J. Synchrotron Rad.* **2013**. 20, 211-218.

19. J. I. Paredes, S. Villar-Rodil, A. Martínez-Alonso, J. M. D. Tascón, *Langmuir*, **2008**, 24, 10560-10564.

20. A. Buchsteiner, A. Lerf, J. Pieper, *J. Phys. Chem. B*, **2006,** 110, 22328-22338.

21. Z. An, O. C. Compton, K. W. Putz, L. C. Brinson, S. T. Nguyen, *Adv. Mater*. **2011**, 23, 3842-3846.

22. Q. Cheng, M. Wu, M. Li, L. Jiang, Z. Tang, *Angew. Chem. Int. Ed.* **2013**, 52, 3750-3755.

23. A. Satti, P. Larpent, Y. Gun'ko, *Carbon*, **2010**, 48, 3376-3381.

24. D. R. Paul, *Science*, **2012**, 335, 413-414

25. J. William, S. Hummers, R. E. Offeman, *J. Am. Chem. Soc.* **1958**, 80, 1339.

Chapter 6

Borate Cross-linked of Graphene Oxide Membrane for Pervaporation

Table of Content

§ 6.1. Introduction

A pristine graphene oxide (GO) layer was successfully developed on a thin film nanofibrous composite (TFNC) mat to form a new type of pervaporation PV membrane. It showed impressive performance when using in ethanol dehydration. However, a pristine GO layer in an assembled structure based on the hydrogen bonding and Van der Waals forces [1], would partly collapse due to high temperature environment or external forces, such as in a pervaproation system, which involves cross-flow filtration under relatively high temperature thermal conditions. Hence, the GO flakes within the layer should be cross-linked to maintain its structure firmly under cross-flow in hot ethanol aqueous solution.

GO flakes could be cross-linked to form a connecting structure by taking advantage of reactions involving hydroxyl groups, carboxyl groups, and epoxide groups on the edges and sides of the flakes. (Figure 6-1) In particular, for the reactions with epoxide, the ring opening of aromatic carbon bonding is regarded as the reduction to grahene [2-4]. Several studies in the past pointed out that the cross-linking of GO could enhance its mechanical property by using common agents, such as divalent metal cations [5, 6], amine compounds [2, 7-9], glutaraldehyde[10], and borate [11]. However, aside from mechanical and conductive properties, the influence of cross-linking to GO in many respect have not been studied thoroughly, like the influence to its thermal stability, the hydrophilicty, and the inter-sheet spacing within the GO

stacks. These effects should be clarified when GO is used as a filter material.

Based on the previous development by us on the pristine GO/TFNC membrane [12], the GO layer cross-linked by different agents,(e.g. calcium chloride, ethylenediamine, and borate) was developed and analyzed, to investigate the effects of thermal stability, mechanical strength , surface affinity, and morphology of the GO layer.

Borate cross-linking of GO was chosen for the GO layer on the TFNC mat to form a PV membrane and was evaluated in ethanol dehydration under different thermal conditions. Related discussions and results are reported as follows.

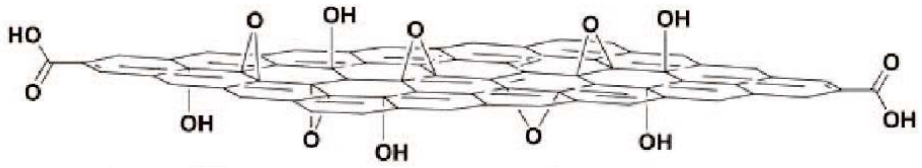

Figure 6-9 Schematic of assumed chemical structure of graphene oxide [5]

§ 6.2. Experimental

§ 6.2.1 Materials

The dispersed GO aqueous solution, at a concentration of 5 g/L and with flakes of 0.5~5 microns in size, were received from the Graphene Supermarket, Inc. and subsequently treated with the Hummer method. [6] Nonwoven polyethylene terephthalate (PET) substrate (Hollytex 3242) was purchased from the Ahlstrom Mount Holly Springs Company. Cellulose raw material in suspension (Biofloc 96 MV, 22% wt. of wood pulp) was supplied by Tembec Tartas Company in France. Sulzer 1210, a PVA composite membrane, was obtained from Sulzer Chemtech. 95 vol. % of ethanol in water, calcium chloride, ethylenediamine, and borate were purchased from Sigma Aldrich, Inc.

§ 6.2.2 Membrane fabrication

The tested GO-based TFNC membranes were prepared by using the following procedures. The GO dispersion solution (Graphene Supermarket inc.), containing flakes in the size range of 0.5~5 microns, was first treated by the Hummer method. [13] Varying concentrations of GO solutions were prepared and sonicated to disperse the GO sheets/particulates before casting. The resulting GO solutions were casted on the chosen three-layered TFNC membrane using the vacuum filtration method [21] to prepare the GO barrier layer of different thicknesses.

The chosen scaffold (mat) to support the GO barrier layer was an experimental thin-film nanofibrous composite (TFNC) membrane containing an average pore size of 20 nm in the top layer [14]. This TFNC membrane consisted of three layers: a cellulose ultra-fine nanofibrous top layer, a polyacrylonitrile (PAN) electrospun nanofibrous mid-layer and a polyethylene terephthalate (PET) nonwoven microfibrous substrate. Practical applications of these TFNC membranes include high-flux microfiltration and ultrafiltration, as well as pervaporation. [14-18] In general, TFNC membranes exhibit several advantages over conventional polymeric membranes made by the phase inversion method. These advantages include large bulk porosity (80%) and fully interconnected pore structures, which are especially useful to avoid the Knudsen diffusion in gas separation and pervaporation. The schemes to prepare TFNC membranes have been described in several publications elsewhere. [14-20]

The preparation of cross-linked GO layer was similar to the above description. The specific concentration of cross-linking solution was blended with the GO suspension, as shown in Table 6-1, and then the GO layer was casted by vacuum filtration on the substrate, which could also be cellulose acetate based commercial membrane. (e.g. Millipore GSW 0.22μm) Subsequently, distilled (di) water was filled in the funnel to rinse the GO layer to remove residual cross-linking agents. After curing the membrane in the oven at 70~90°C, the free-standing cross-linked GO film could be obtained by immersing the dried membrane in acetone to remove the cellulose

acetate substrate. For the test, the cross-linked GO film in a round shape with a diameter of 3.8 cm, theoretically contained 15~30 mg of pristine GO with a certain ratio of cross-linking agent. For the membranes used in pervaporation, the borate cross-linked GO, containing ~0.25 mg of GO (thickness about 0.18 μm [21]), was coated on the TFNC mat instead.

Table 6-2 Composition of modified GO.

Sample	**Theoretical cross-linker molar ratio to GO amount (mole/mg)**
GO/Borate X[a]	2.5×10^{-7}
GO/Borate 2X	5.0×10^{-7}
GO/Borate 8X	2.0×10^{-6}
GO/Borate 40X	1.0×10^{-5}
GO/ Amine[b]	5.0×10^{-5}
GO/ Ca^{2+}[c]	5.0×10^{-5}

[a] X represents the unit of borate dose as the right column in the table.

[b] Use ethylenediamine (EDA) as the cross-linking agent

[c] Use calcium chloride as the cross-linking agent

§ 6.2.3 Characterization

Water contact angle was determined by using an optical contact angle meter (CAM200, KSV Instruments, LTD). SEM micrographs were obtained by using the LEO 1550 instrument equipped with a Schottky field emission gun (20 kV) and a Robinson backscatter detector. Surface-peeled samples were also characterized by FTIR (Nicolet iS10 FTIR-ATR) and XRD (Bruker AXS D8) by using a copper source (λ=1.54 Å). Raman analysis was conducted by using a Nicolet Almega dispersive spectrometer coupled to an Olympus microscope, with the laser wave length of 532 nm. A modified tensile instrument was conducted with the initial sample length between the clamps being 10~30 mm. Total organic carbon analyzer (TOC-V CPN, Shimadzu Scientific Instruments) could analyze the peeling amount of GO stacks in water during the thermal bath experiment (see §6.3.2). Thermo gravimetric analysis (TGA) was conducted (TGA-7, Perkin Elmer) from 30 °C to 900 °C over a 90-minute interval under air.

§ 6.2.4 Pervaporation

A custom-made pervaporation apparatus was used to evaluate the ethanol dehydration performance of the membranes. The detailed experimental procedure and setup were reported in earlier publications [17, 21].

§ 6.3. Results and discussion

§ 6.3.1 Characterization of cross-linked GO

We previously mentioned the types of reaction mechanisms between cross-linking agents and GO. The reduction of GO could possibly be accompanied by the cross-linking process due to the ring opening of epoxide on the aromatic carbon bonding, such as the tested EDA cross-linking of GO. The XRD pattern showed that all cross-linked GO could still keep the characteristic peak around 10° except the GO/amine cross-linking. Instead of having the peak corresponding to the d-spacing of GO stacks (002), the GO/amine cross-linking had much stronger peaks at 14.2°, 16.9, and 25.6° where the characteristic peak of grapheme was. Therefore, the EDA used for this cross-linking obviously changed the nature of GO, even partly reducing the GO to graphene by reaction with epoxide on the aromatic carbon domain [7].

The main peak of GO/Ca^{2+} was weakened and slightly shifted, meaning that the d-spacing of GO was decreased to 0.828 nm, while it had clear peaks at 14.2° and 16.9°. Our finding matched the published results [5], indicating that parts of the divalent metal ions on the GO sheets would be removed after rinsing with water. .Hence, the cross-linking of GO sheets could be depleted by losing ionic Ca^{2+} between oxidized groups during water rinsing. Moreover, the increment of peaks at 14.2° and 16.9° revealed that the structure of GO was changed when comparing with GO/borate and pristine GO.

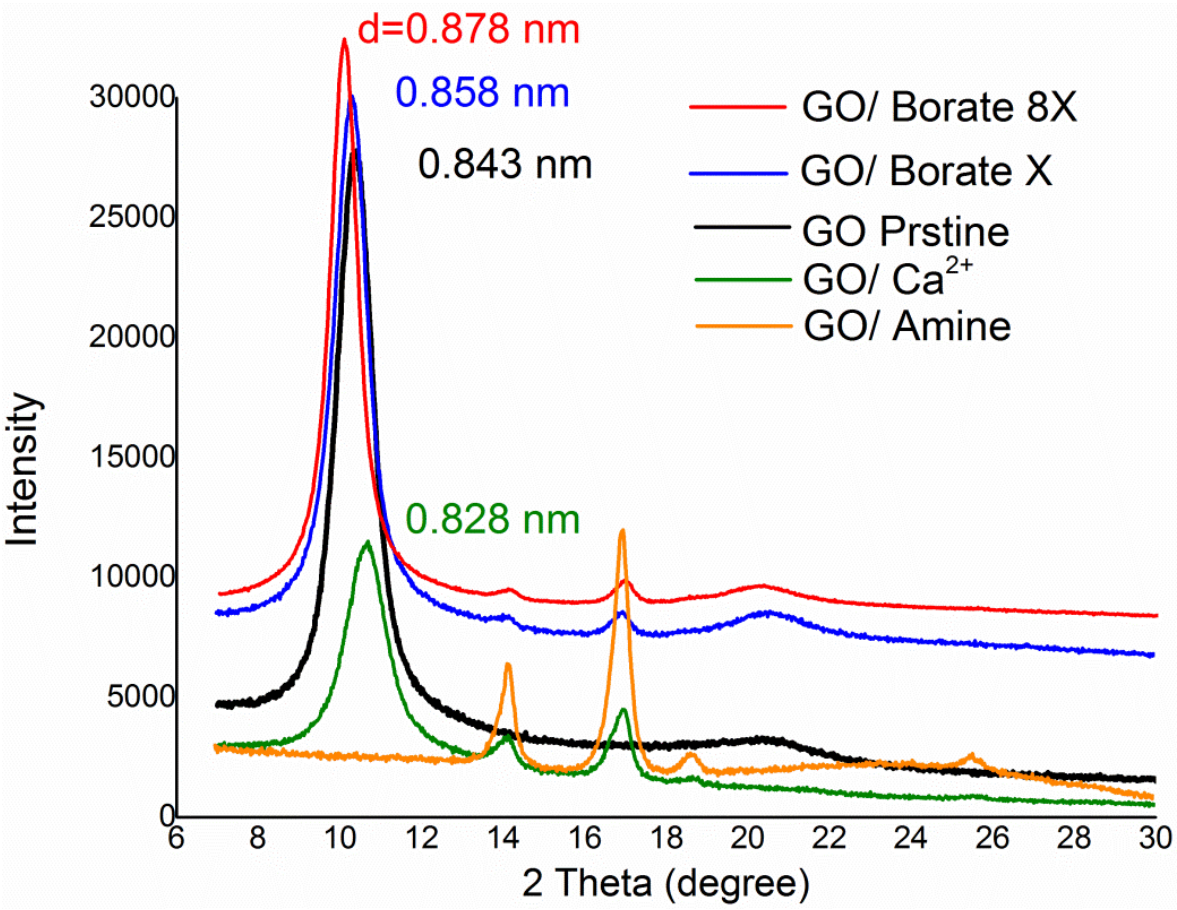

Figure 6-10 XRD spectra of pristine graphene oxide and borate/Ca^{2+}/amine cross-linked graphene oxide

When more borate was used to cross-link the GO layer, larger d-spacing was obtained from the XRD analysis, meaning that the dimension of nanocapillaries [21] within the GO stacks of the layer was expanded with increasing borate incorporation. Besides, the XRD results showed that the borate cross-linking did not accompany an apparent reduction on GO.

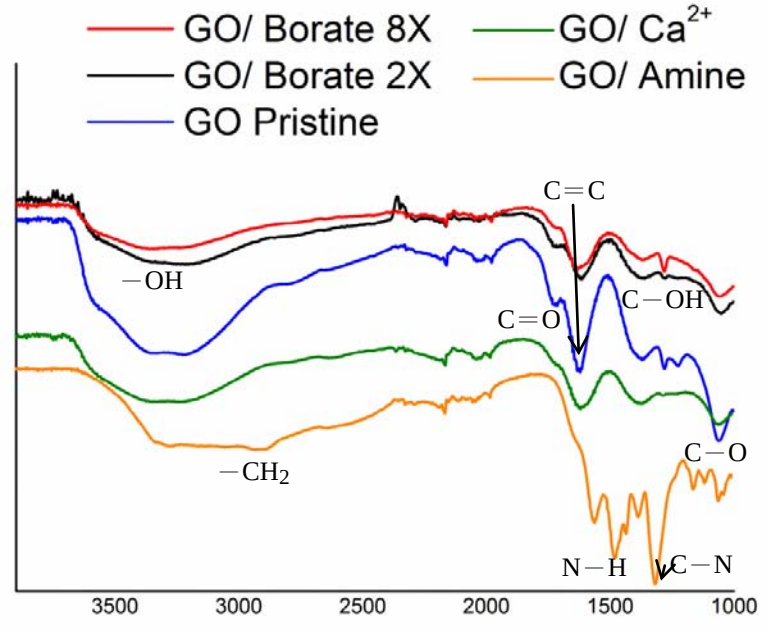

Figure 6-11 FTIR spectra of pristine GO and modified GO.

The FTIR spectrum of the GO layers indicated the presence of hydroxyl, carboxyl, epoxide groups, and etc. (i.e., −OH at 3430 cm^{-1}, $-CH_2$ stretching at 2900 cm-1, C=O at 1720 cm^{-1}, C=C at 1622 cm^{-1}, C−H bend at 1470 cm^{-1}, C−OH stretching at 1200 cm^{-1}, C−O stretching at 1000 cm^{-1}) The peaks of GO/ amine at 1490cm^{-1} and 1310 cm^{-1} were attributed to the stretching of the N−H and C−N, respectively. According to these spectrum of GO layers, it confirm that GO/ borate could mostly keep the chemical characteristic of GO, and the intensity of hydroxyl would deplete as more borate incorporation.

In the Raman spectrum from the following figure, only the band D of GO/ amine shifted from 1326cm^{-1} to 1309cm^{-1}, and had the highest ratio of band D/ band G because the EDA change vigorously the basal plane of GO.[8, 9]

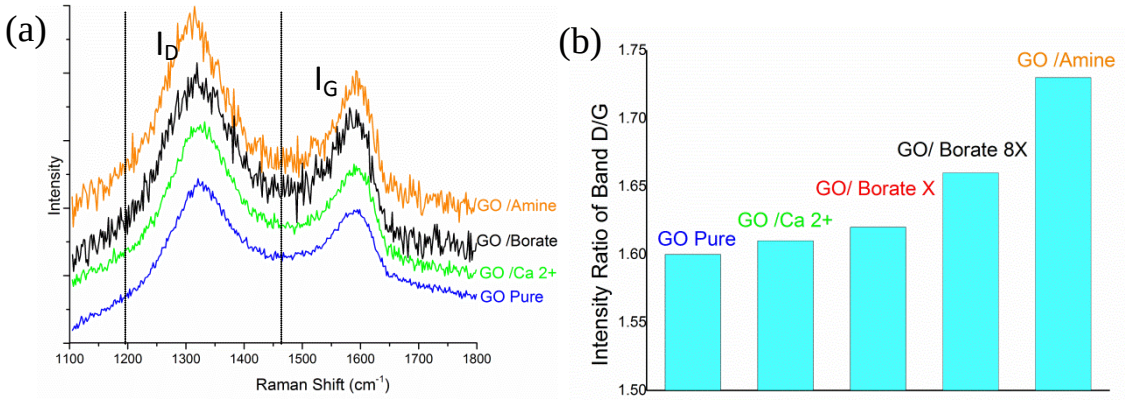

Figure 6-12 (a)Raman spectra of pristine graphene oxide and borate/ Ca^{2+}/amine cross-linked graphene oxide. (b) Plot for ratio of I_D/I_G of pristine GO and types of cross-linked GO

The SEM cross-sectional images of GO/borate showed that the layered morphology of GO seemed to get loosen and appeared with more slits because the material became more brittle when increasing borate ratio, as shown in Figure 6-4 (b) and (c).

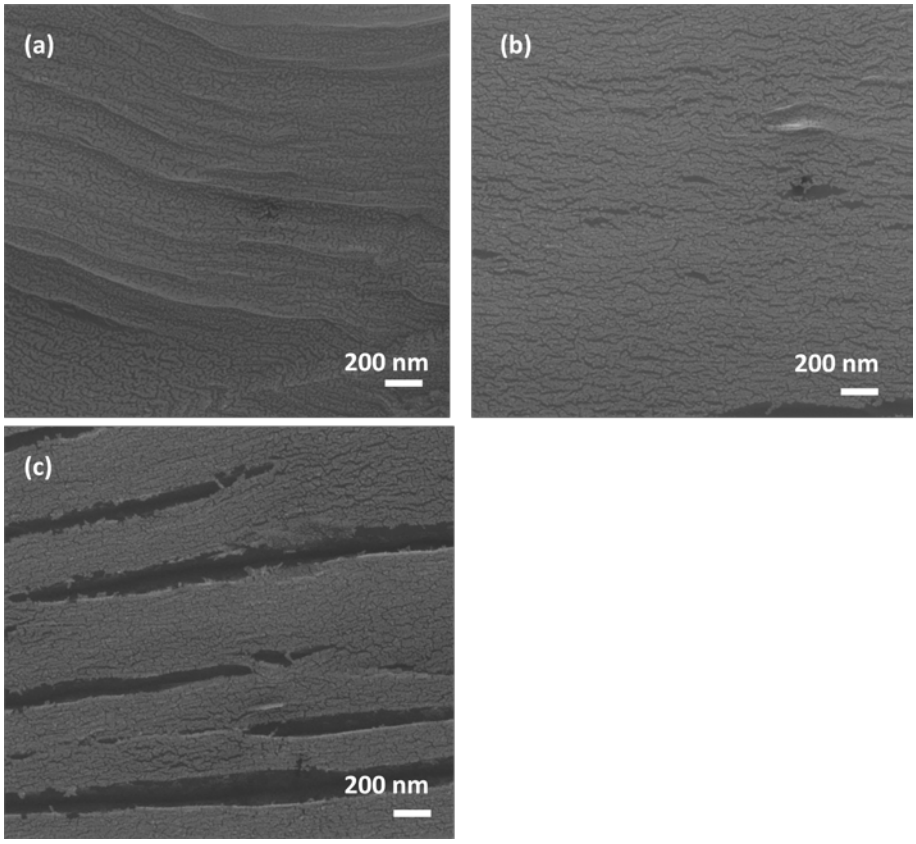

Figure 6-13 SEM images of cross-sectional view of (a) pristine GO, (b) GO/Borate 8X, and (c) GO/Borate 40X

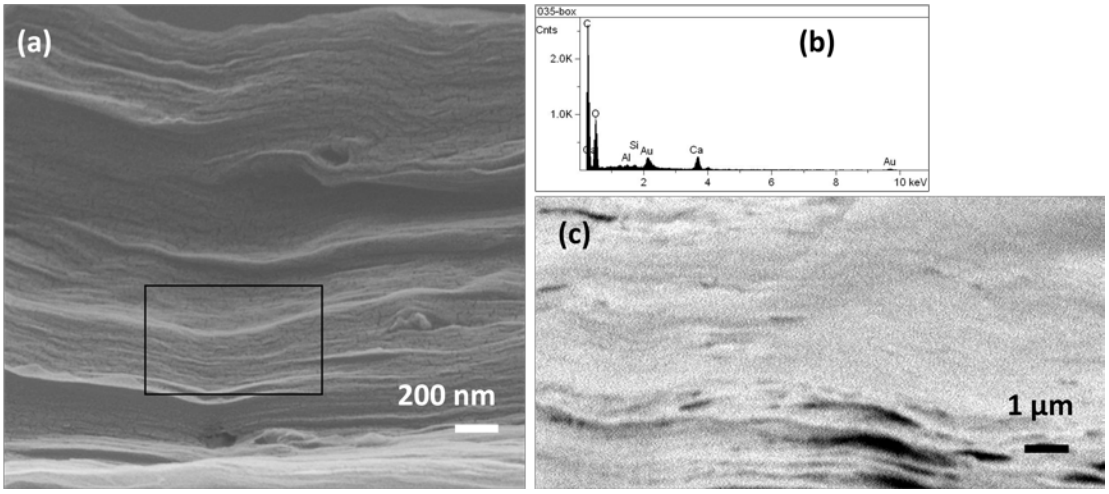

Figure 6-14 SEM imagines of cross-sectional view of (a) GO/Ca^{2+} and (c) GO/amine. (b) EDS spectra for the local area in (a), while the elemental ratio of C:O:Ca = 10:4:1

EDS spectra of the local area in SEM cross-sectional images of GO/ Ca^{2+} showed the ratio of elements, such as carbon: oxygen: calcium = 10:4:1. The white (light color) region of the Figure 6-5 (a) is believed the area with more amount of calcium element (or GO/ Ca^{2+})[5] Figure 6-5 (c) displayed the morphology of GO/ amine with barely layered structure.

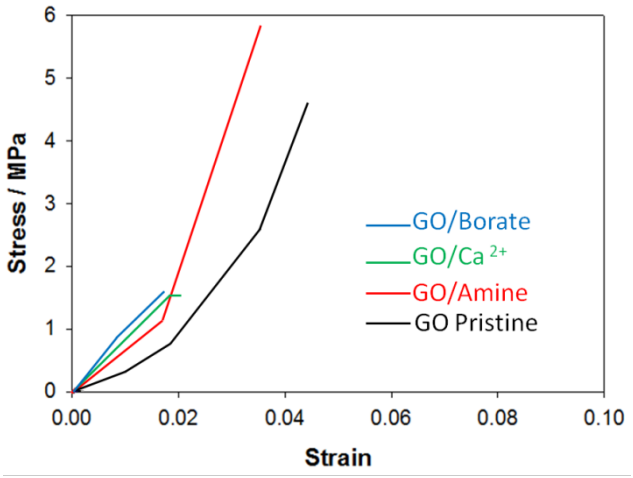

Figure 6-15 Plot of tensile test for GO pristine and various cross-linked GO films

The GO layers were cut into strips with appropriate dimensions (Table 6-2) for the tensile test (Figure 6-7). All cross-linked GO samples had higher Young's modules than the pristine GO, meaning that the cross-linking reaction had stiffened the GO to increase its tensile strength. Among these tests, GO/borate 8X presented the highest stress/strain, which could be attributed to the more effective bonding between GO sheets and borate. However, the GO/borate 8X also showed lower breaking point for its brittleness. In terms of fragility and defects on the GO film,

the sample strips were more difficult to prepare. Hence, the samples did not appear to have comparable breaking points by using the current stretching tester. Nano-indentation should be an ideal method to analyze fragile thin film materials such as GO [22, 23].

Table 6-3 Dimension of sample strips for tensile test

Sample	Length (mm)	Width (mm)	Thickness (mm)	Cross-section Area (mm)
GO Prstine	20	15	0.0533	0.800
GO/ Amine	10	7.5	0.0254	0.191
GO/ Ca^{2+}	15	10	0.0127	0.127
GO/Borate 8X	20	6.8	0.0381	0.259

According to the above characterization of cross-linked GO layers, the borate was selected as an ideal cross-linking agent for effective bonding and for keeping the GO characteristics without changing the basal planes of GO. In the following tests and evaluation, the GO/borate layers were prepared and integrated with the TFNC mat to form a pervaporation class membrane used in ethanol dehydration.

§ 6.3.2 Analysis of GO/ borate layer

The water contact angles analysis for GO/borate membranes revealed that more borate incorporation could lead to a less hydrophilic surface of the GO layer due to the consumption of hydroxyl groups during the cross-linking between the GO sheets.

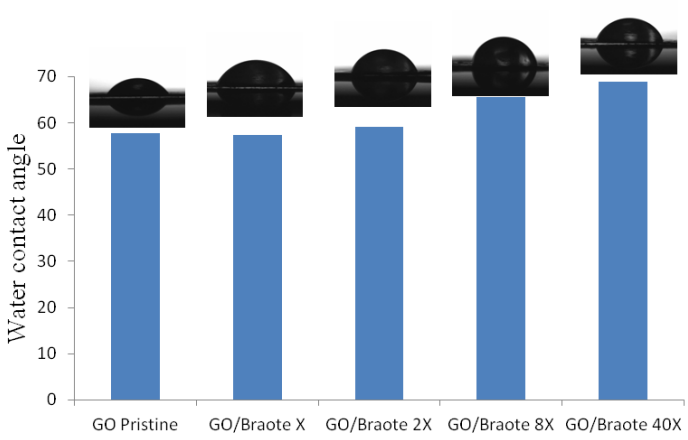

Figure 6-16 Comparison of water contact angles of borate cross-linking of GO layers

In order to optimize the incorporation on the amount of borate for improving the thermal stability during pervaporation, 5 mg of GO layer which were incorporated with varying amounts of borate were prepared and then immersed in di-water at 70 °C for 3 hours. After removing the GO/borate sample from the water solution, the aqueous solution was vigorously sonicated to disperse the peeling GO flakes, subsequently; the residual carbon content in the aqueous solution was obtained by TOC, as shown in Table 6-3. More borate incorporation caused less carbon content remaining in the aqueous solution, meaning that more cross-linking of GO would effectively increase its thermal stability in aqueous solution.

(a)  (b) 

Figure 6-17 (a) GO/Borate film showed improved ductility; (b) GO/Borate film immersed in water for the thermal stability test.

Table 6-4 Remaining carbon content in the di-water after thermal bath test[a]

Sample	Average carbon concentration (ppm) [b]
Pristine GO	10.20
GO/ Borate X	9.06
GO/ Borate 2X	6.11
GO/ Borate 8X	5.63
GO/ Borate 40X	4.34
H_2O	4.27

[a] Thin borate cross-linked GO membranes in 20 ml water at 70 °C for 3 hours

[b] Total organic carbon (TOC) analysis for carbon content

The TGA analysis showed in Figure 6-10, indicating that the GO/ borate 8X raised about 10 wt% of the maintaining mass compared to the mass of pristine GO at 100 °C under air

atmosphere. The weight loss lower 150 °C was loss of moisture and water in the sample, and then the weight loss higher.250 °C was from oxygen compounds. Besides, the GO/borate did not have a major mass loss at 500 °C that the pristine GO did

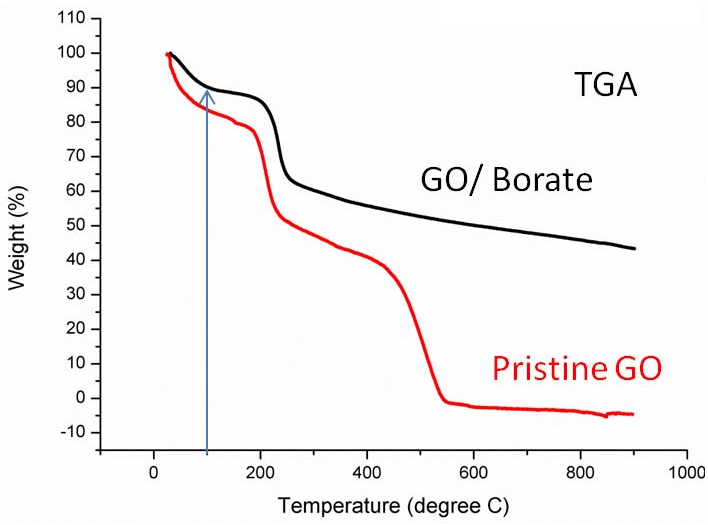

Figure 6-18 TGA curves of pristine GO and GO/Borate 8X. Borate cross-linking markedly increased thermal stability of GO

§ 6.3.3 Evaluation of TFNC based membrane with GO/Borate barrier layer for ethanol dehydration

The GO/borate suspension was coated onto the TFNC to form pervaporation membranes for ethanol dehydration. Figure 6-14 (b) illustrates the assumed formation of cross-linked networks of GO/borate. The distance between GO sheets was expanded by the borate bonding when compared with that of pristine GO, as shown in Figure 6-14 (a). Figure 6-11 illustrates the

hierarchical structure arrangement of the GO-TFNC membrane, consisting of four different layers: (1) the top GO/borate barrier layer with randomly organized GO stacks [21], (2) the ultrafine cellulose nanofiber supporting layer (with fiber diameters of about 5 nm) where the thickness was about 100 nm, (3) the electrospun PAN nanofibrous scaffold (diameters of about 100 nm) where the thickness was about 40 μm, and (4) the nonwoven PET fibrous substrate (omitted in Figure 6-10) which provided the mechanical strength of this membrane system.

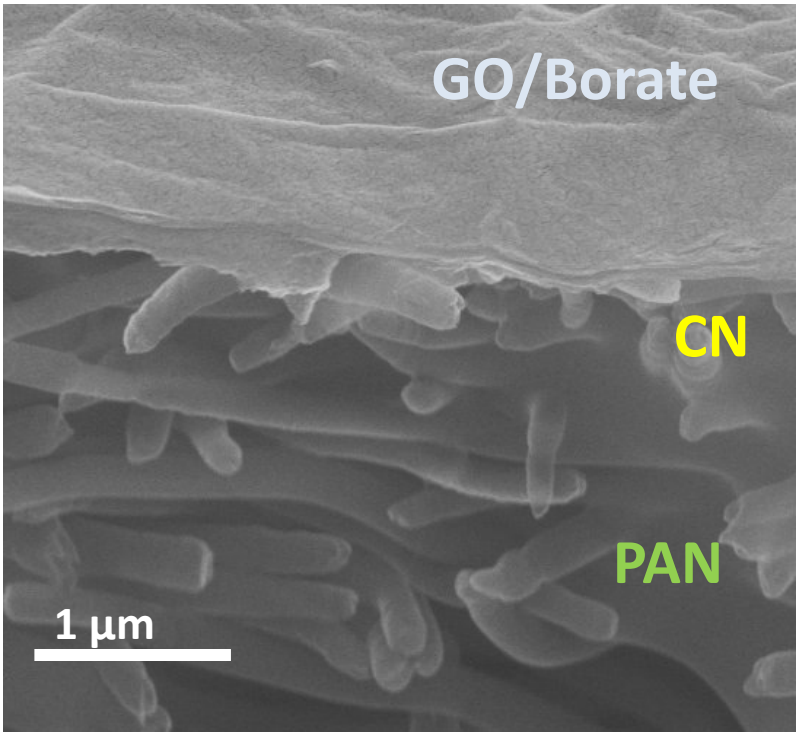

Figure 6-19 SEM imagines of cross-sectional view of GO-TFNC membrane

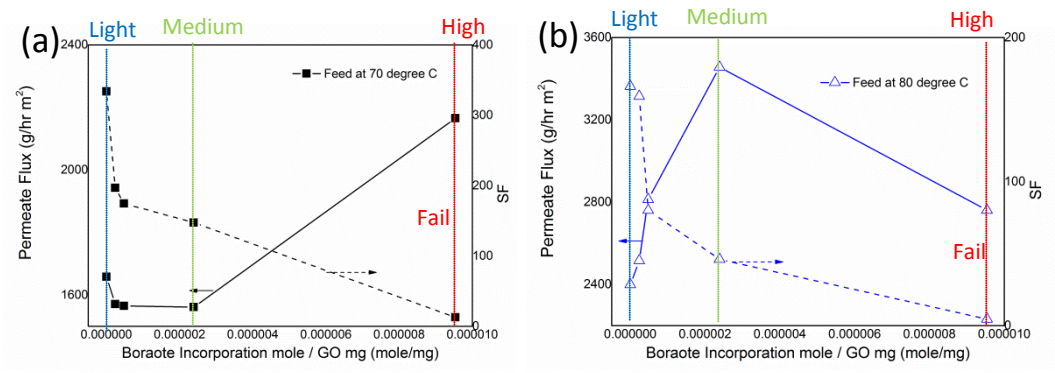

Figure 6-20 Comparison of flux and SF for the GO layer incorporated with varying amounts of borate when feeding with 80 wt% ethanol aqueous solution, (a) at 70 °C, and (b) 80°C.

A series of TFNC based membranes containing GO/borate barrier layers where individually incorporated with varying amounts of borate, were evaluated in ethanol dehydration by pervaporation at 70 °C and 80 °C. According to the results shown above, the membrane with highest borate incorporation (GO/borate 40X) failed with a low separation factor (SF) in terms of possible leaks or loosening of structure from the modified GO layer, with the cross-sectional SEM image being shown in Figure 6-5 (c). It was expected that the highly cross-linked layer could lead to defects, like polymeric cross-linking [17]; More borate cross-linking caused the depletion of membrane selectivity at both temperatures (SF decreased). However, for membranes in the range between GO/borate X to GO/ borate 8X (light to medium cross-linking), the permeate flux of lightly cross-linked GO/borate membranes decreased as increasing borate does till borate 8X (2.0×10^{-6} mole/mg) at 70 °C. But at 80°C, the flux raised as well as increasing borate does till borate 8X.

The permeate flux of GO membranes was closely influenced by the loss of hydrophilicty and the increment of nanocapillaries [21] in the GO layer when incorporating more borate into the GO. Increasing the size of nanocapillaries within GO stacks would not only enhance the permeate flux but also weaken the membrane selectivity (see Figure 6-14 c, d). Besides, the kinetic energy of permeates s (water/ethanol) would vary according to the thermal condition. Hence, at 70 °C, the decrease in hydrophilicty could supersede the effects from nanocapillaries and thereby leading toward a decrease in the flux, as shown in Figure 6-12 (a). On other hand, at 80 °C, energetic permeate molecules, were able to overcome the surface barrier to penetrate into the GO stacks, and lead toward an enhancement in the flux shown in Figure 6-11 (b).

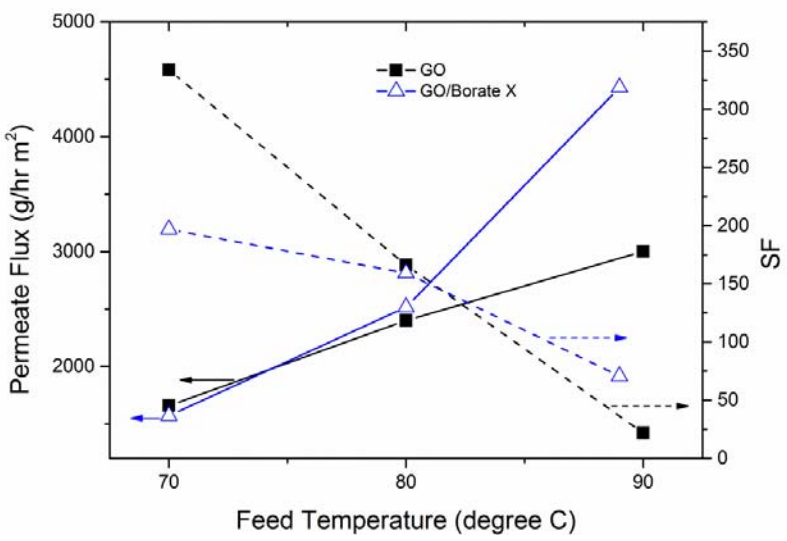

Figure 6-21 Comparison of permeate flux and SF for pristine GO and borate cross-linked GO when feed with 80 wt% ethanol aqueous solution, at varying temperatures.

In considering the amount of incorporated borate, the lightly cross-linked GO membrane, "GO/borate X", was chosen to compare with pristine GO membranes under varying thermal conditions. At 90 °C, the cross-linked GO membrane had a SF value of 70.5 which was about three times higher than the pristine GO membrane. It also achieved a higher flux of 4.4 kg/hrm^2. Therefore, by using an appropriate amount of borate to cross-link GO could improve the thermal stability as well as the membrane selectivity at high temperatures. However, An over dose of borate could lead to defects and less hydrophilicty in the GO layer, resulting in a decrease in the membrane performance.

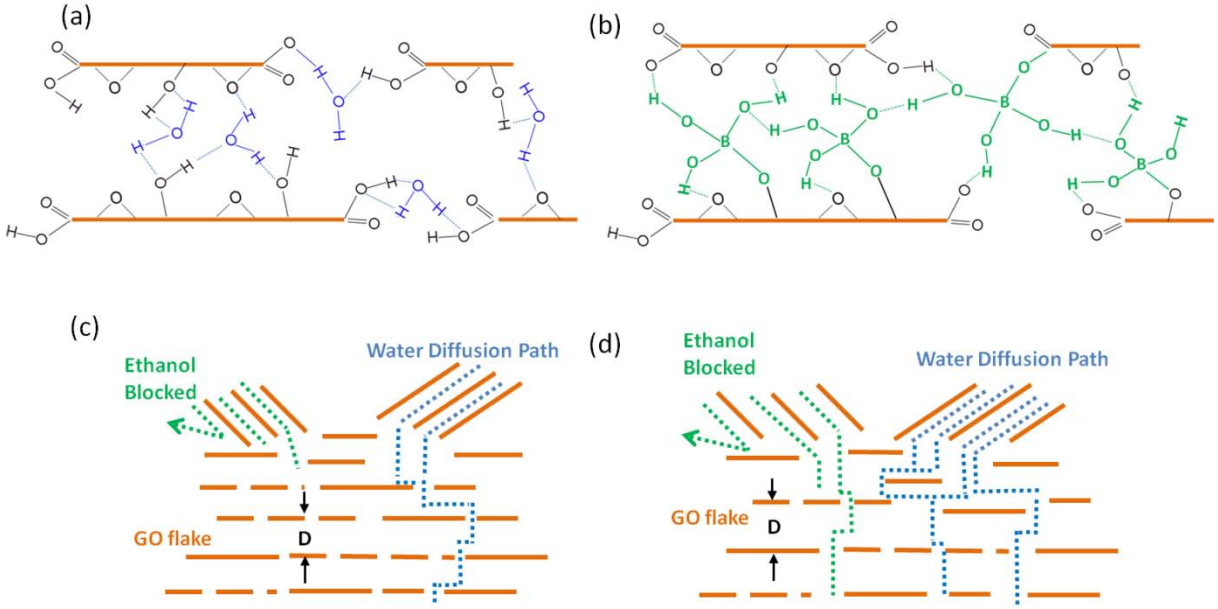

Figure 6-22 Schematic illustration of formation of network for pristine GO and water (a), and formation of network for borate cross-linked GO (b). Assumed mechanism for water-ethanol separation within the pristine GO barrier layer (c), and cross-linked GO layer.

§ 6.4. Conclusions

Graphene oxide was cross-linked by EDA, calcium chloride, and borate, and various characterizations and analysis were conducted to compare GO and modified GO effectiveness. In conclusion, the amine groups and a divalent metal ion, Ca^{2+}, might lead to reduction by reaction with epoxide groups on the aromatic carbon domain, to deplete the original characteristics of GO, resulting in undesirable structures when using such membranes as a filter.

Only borate as the cross-linker was effective in enhancing the Young's modulus and the thermal stability of the GO layer while keeping pertinent and unique properties of GO intact. As more borate was incorporated, the size of nanocapillaries within the GO stacks expanded, but the hydrophilicty of GO also decreased. Furthermore, with, the permeate ability of molecules depending on the operating temperature, it was observed that the amount of borate incorporation could affect the membrane permeability while operating under different thermal conditions. An appropriate amount of borate to cross-link GO (e.g. less than 2.0×10^{-6} mole/ mg GO) could lead to an improvement in performance at higher operating temperatures in the ethanol dehydration via the pervaporation process. For instance, the TFNC membrane including a barrier layer of GO/borate X (2.5×10^{-7} mole/mg GO) was demonstrated to show a SF value of 70.5 and a higher flux of 4.4 kg/hr.m^2 at 90 °C, which was much superior to the pristine GO membrane (e.g. SF of 21.8 and the flux of 3.8 kg/hr.m^2).

§ 6.5. References

1. Zhu, Y., et al., *Graphene and Graphene Oxide: Synthesis, Properties, and Applications.* Advanced Materials, 2010. **22**(35): p. 3906-3924.

2. Park, S., et al., *Graphene Oxide Sheets Chemically Cross-Linked by Polyallylamine.* The Journal of Physical Chemistry C, 2009. **113**(36): p. 15801-15804.

3. Kuila, T., et al., *Chemical functionalization of graphene and its applications.* Progress in Materials Science, 2012. **57**(7): p. 1061-1105.

4. Dreyer, D.R., et al., *The chemistry of graphene oxide.* Chemical Society Reviews, 2010. **39**(1): p. 228-240.

5. Park, S., et al., *Graphene Oxide Papers Modified by Divalent Ions—Enhancing Mechanical Properties via Chemical Cross-Linking.* Acs Nano, 2008. **2**(3): p. 572-578.

6. Jiang, X., et al., *Self-Assembly of Reduced Graphene Oxide into Three-Dimensional Architecture by Divalent Ion Linkage.* The Journal of Physical Chemistry C, 2010. **114**(51): p. 22462-22465.

7. Stankovich, S., et al., *Systematic Post-assembly Modification of Graphene Oxide Paper with Primary Alkylamines.* Chemistry of Materials, 2010. **22**(14): p. 4153-4157.

8. Ma, H.-L., et al., *Chemical reduction and removal of Cr(vi) from acidic aqueous solution by ethylenediamine-reduced graphene oxide.* Journal of Materials Chemistry, 2012. **22**(13): p. 5914-5916.

9. Lee, D.W., et al., *Highly controllable transparent and conducting thin films using layer-by-layer assembly of oppositely charged reduced graphene oxides.* Journal of Materials Chemistry, 2011. **21**(10): p. 3438-3442.

10. Gao, Y., et al., *The Effect of Interlayer Adhesion on the Mechanical Behaviors of Macroscopic Graphene Oxide Papers.* Acs Nano, 2011. **5**(3): p. 2134-2141.

11. An, Z., et al., *Bio-Inspired Borate Cross-Linking in Ultra-Stiff Graphene Oxide Thin Films.* Advanced Materials, 2011. **23**(33): p. 3842-3846.

12. Yeh, T.-M., et al., *High flux ethanol dehydration using nanofibrous membranes containing graphene oxide barrier layers.* Journal of Materials Chemistry A, 2013. **1**(41): p. 12998-13003.

13. Hummers, W.S. and R.E. Offeman, *Preparation of Graphitic Oxide.* Journal of the American Chemical Society, 1958. **80**(6): p. 1339-1339.

14. Ma, H., et al., *Ultra-fine Polysaccharide Nanofibrous Membranes for Water Purification.* Biomacromolecules, 2011. **12**: p. 7.

15. Ma, H., et al., *High-flux thin-film nanofibrous composite ultrafiltration membranes containing cellulose barrier layer.* JOURNAL OF MATERIALS CHEMISTRY, 2010. **20**(22): p. 4692-4704

16. Ma, H., et al., *Thin-film nanofibrous composite ultrafiltration membranes based on polyvinyl alcohol barrier layer containing directional water channels.* Industry & Engineering Chemistry Research, 2010. **49**: p. 7.

17. Yeh, T.-M., et al., *Polymeric nanofibrous composite membranes for energy efficient ethanol dehydration.* Journal of Renewable and Sustainable Energy, 2012. **4**(4): p. 041406.

18. Ma, H., et al., *Highly Permeable Polymer Membranes Containing Directed Channels for Water Purification.* ACS Macro Letters, 2012. **1**(6): p. 723-726.

19. Wang, R., et al., *Nanofibrous microfiltration membranes capable of removing bacteria, viruses and heavy metal ions.* Journal of Membrane Science, 2013. **446**(0): p. 376-382.

20. Liu, Y., et al., *High-flux microfiltration filters based on electrospun polyvinylalcohol nanofibrous membranes.* Polymer, 2013. **54**(2): p. 548-556.

21. Yeh, T.-M., et al., *High flux ethanol dehydration using nanofibrous membranes containing graphene oxide barrier layers.* Journal of Materials Chemistry A, 2013.

22. Bunch, J.S. and M.L. Dunn, *Adhesion mechanics of graphene membranes.* Solid State Communications, 2012. **152**(15): p. 1359-1364.

23. Jayasena, B., C.D. Reddy, and S. Subbiah, *Separation, folding and shearing of graphene layers during wedge-based mechanical exfoliation.* Nanotechnology, 2013. **24**(20): p. 205301.

Chapter 7

Summary and Outlook

The present study focused on finding energy efficient solutions to global challenges of clean water scarcity and managing CO_2 through substitution of renewable fuels such as ethanol. The principle of low-carbon and green materials was applied to develop a membrane-based process, namely “pervaporation” that utilized a new type of nanofibrous membrane.

Specific to the study, a custom pervaporation apparatus was built to produce fuel-grade ethanol which could remove 31.3 L/ h water at less than 1.2 wt.% ethanol from a 80 wt.% ethanol feed at 70°C. Additionally, it was built in a vertically compact fashion with extendable digital control by using testing devices and interfaces for ease of use and compactness.

A new class of pervaporation (PV) membrane combined a thin-film nanofibrous composite (TFNC) mat and a hydrophilic barrier layer. The TFNC mat consisted of three layers: a cellulose ultra-fine (CN) nanofibrous top layer, a polyacrylonitrile (PAN) electrospun nanofibrous mid-layer and a polyethylene terephthalate (PET) nonwoven microfibrous substrate. The TFNC membrane achieved 50% - 80% less pressure drop compared to other commercial membranes by taking advantage of its high porosity and tunable pore size of the hierarchical fibrous structure. A PV class membrane, including a barrier layer of fumaric acid cross-linked polyvinyl alcohol (PVA) on the TFNC membrane, showed superior performance, compared to commercial membranes for ethanol dehydration: for example, a 25% increase in efficient flux and 40% efficient flux, compared to PVA-PAN400 and PVA-PES, respectively. To understand the

mechanism, characterization and analysis of the prepared membranes were conducted and discussed.

Graphene oxide (GO) was successfully demonstrated as an efficient filter material for ethanol dehydration due to the presence of natural hydrophilic nanocapillaries within the stacks. The hypothesized mechanism of diffusion within the GO and morphology of the layer was evaluated and characterized by using various techniques, such as electron scattering at the NSLS at BNL. The influence of cross-linking of GO was studied to find that specific cross-linking process would accompany reduction by reacting with epoxide groups on the aromatic carbon domains, such as amine based agents. The reduction would lead to loss of the GO's nature characteristic in a negative effect to self–assembled film formation. Moreover, borate cross-linked GO could effectively format networking structure without changing much intrinsic features of GO. The GO/ borate layer showed improved thermal stability and higher Young's modulus compared to pristine GO. The amount of borate incorporated into GO and its influence on the membrane's performance in ethanol dehydration were studied.

To conclude this study, the novel application of nanofibrous membrane for ethanol dehydration via pervaporation was successfully demonstrated. This type of membranes is capable of showing superior performance in liquid separation, which has been well proven or in semi-vapor separation process such as pervaporation. Based on these results, the nanofibrous membranes could be extendable to a vapor-related separation process such as desalination by membrane distillation. In addition, GO is promising as a filter though there are still challenges that need to be overcome, such as development of synthesis method to produce a defect-free large-area film. Modification of GO will be a crucial issue to shape GO to match the requirement of various types of filtration processes.

List of References

1. Bauen, A., *Future energy sources and systems acting on climate change and energy security.* J. Power Sources, 2006. **157** p. 893–901.
2. Sissine, F., *Energy Independence and Security Act of 2007: A Summary of Major Provisions*, in *United States Senate Committee on Energy & Natural Resources*. 2007.
3. (EIA), U.E.I.A., *US ethanol comsumption statistics*. 2011.
4. *National Petroleum Council*. 2007.
5. http://www.abengoabioenergy.com/corp/web/en/nuevas_tecnologias/proyectos/planta_biomasa/index.html.
6. Fadden, K.M. *Hydrophobic front end Membranes for BiofuelSeparations*. 2009.
7. Simo, M., Brown, C.J., and Hlavacek, V.,, Simulation of Pressure Swing Adsorption in *Fuel Ethanol Production Process.* Comput. Chem. Eng., 2008. **32**(7): p. 1635–1649.
8. Ladisch, M.R., *Cornmeal Adsorber for Dehydrating Ethanol Vapors.* Ind. Eng.Chem. Proc. Des. Dev., 1983. **23**: p. 437-445.
9. Available from: http://www.ethanolindia.net/.
10. Neuhause.S and F. Wolf, *Separation of Alkylpyridine Mixtures .1. Separation of Beta-Gamma-Picoline Fractions by Azeotropic Distillation.* Brennstoff-Chemie, 1968. **49**(12): p. 355-&.
11. Frolkova, A.K. and V.M. Raeva, *Bioethanol dehydration: State of the art.* Theoretical Foundations of Chemical Engineering, 2010. **44**(4): p. 545-556.
12. Pucci, A., *Phase-Equilibria of Alkanol Alkane Mixtures in New Oil and Gas Process-Development.* Pure and Applied Chemistry, 1989. **61**(8): p. 1363-1372.
13. Kaminski, W., J. Marszalek, and A. Ciolkowska, *Renewable energy source - Dehydrated ethanol.* Chemical Engineering Journal, 2008. **135**(1-2): p. 95-102.
14. Li, N.N. and J.M. Calo, *Separation and purification technology*. 1992, New York: M. Dekker. viii, 310 p.

15. Bowen, T.C., R.D. Noble, and J.L. Falconer, *Fundamentals and applications of pervaporation through zeolite membranes.* Journal of Membrane Science, 2004. **245**(1-2): p. 1-33.

16. A.M. Urtiaga, E.D.G., G. Ruiz, I. Ortiz, *Parallelism and differences of pervaporation and vacuum membrane distillation in the removal of VOCs from aqueous streams.* Separation and Purification Technology, 2001. **22-23**: p. 327–337.

17. Smuleac, V., et al., *Novel perfluorinated polymer-based pervaporation membranes for the separation of solvent/water mixtures.* Journal of Membrane Science, 2010. **352**(1-2): p. 41-49.

18. Hyder, M.N., R.Y.M. Huang, and P. Chen, *Effect of selective layer thickness on pervaporation of composite poly(vinyl alcohol)-poly(sulfone) membranes.* Journal of Membrane Science, 2008. **318**(1-2): p. 387-396.

19. Shao, P. and R.Y.M. Huang, *Polymeric membrane pervaporation.* Journal of Membrane Science, 2007. **287**(2): p. 162-179.

20. Okada, T. and T. Matsuura, *A New Transport Model for Pervaporation.* Journal of Membrane Science, 1991. **59**(2): p. 133-150.

21. Cabasso, I., E. Korngold, and Z.Z. Liu, *On the Separation of Alcohol Water Mixtures by Polyethylene Ion-Exchange Membranes.* Journal of Polymer Science Part C-Polymer Letters, 1985. **23**(11): p. 557-581.

22. Huang, R.Y.M., et al., *Pervaporation separation of water/isopropanol mixture using sulfonated poly(ether ether ketone) (SPEEK) membranes: transport mechanism and separation performance.* Journal of Membrane Science, 2001. **192**(1-2): p. 115-127.

23. Yeom, C.K. and K.H. Lee, *Pervaporation separation of water-acetic acid mixtures through poly(vinyl alcohol) membranes crosslinked with glutaraldehyde.* Journal of Membrane Science, 1996. **109**(2): p. 257-265.

24. Praptowidodo, V.S., *Influence of swelling on water transport through PVA-based membrane.* Journal of Molecular Structure, 2005. **739**(1-3): p. 207-212.

25. Kang, Y.S., et al., *Pervaporation of Water Ethanol Mixtures through Cross-Linked and Surface-Modified Poly(Vinyl Alcohol) Membrane.* Journal of Membrane Science, 1990. **51**(1-2): p. 215-226.

26. Zhang, W., et al., *Maleic anhydride surface-modification of crosslinked chitosan membrane and its pervaporation performance.* Journal of Membrane Science, 2007. **295**(1-2): p. 130-138.

27. Huang, R.Y.M., R. Pal, and G.Y. Moon, *Crosslinked chitosan composite membrane for the pervaporation dehydration of alcohol mixtures and enhancement of structural stability of chitosan polysulfone composite membranes.* Journal of Membrane Science, 1999. **160**(1): p. 17-30.

28. Shieh, J.J. and R.Y.M. Huang, *Pervaporation with chitosan membranes .2. Blend membranes of chitosan and polyacrylic acid and comparison of homogeneous and composite membrane based on polyelectrolyte complexes of chitosan and polyacrylic acid for the separation of ethanol-water mixtures.* Journal of Membrane Science, 1997. **127**(2): p. 185-202.

29. Nam, S.Y. and Y.M. Lee, *Pervaporation and properties of chitosan poly(acrylic acid) complex membranes.* Journal of Membrane Science, 1997. **135**(2): p. 161-171.

30. Chapman, P.D., et al., *Membranes for the dehydration of solvents by pervaporation.* Journal of Membrane Science, 2008. **318**(1-2): p. 5-37.

31. Yeom, C.K., J.G. Jegal, and K.H. Lee, *Characterization of relaxation phenomena and permeation behaviors in sodium alginate membrane during pervaporation separation of ethanol-water mixture.* Journal of Applied Polymer Science, 1996. **62**(10): p. 1561-1576.

32. Yeom, C.K. and K.H. Lee, *Characterization of permeation behaviors of ethanol-water mixtures through sodium alginate membrane with crosslinking gradient during pervaporation separation.* Journal of Applied Polymer Science, 1998. **69**(8): p. 1607-1619.

33. Yeom, C.K. and K.H. Lee, *Characterization of sodium alginate and poly(vinyl alcohol) blend membranes in pervaporation separation.* Journal of Applied Polymer Science, 1998. **67**(5): p. 949-959.

34. Yeom, C.K. and K.H. Lee, *Characterization of sodium alginate membrane crosslinked with glutaraldehyde in pervaporation separation.* Journal of Applied Polymer Science, 1998. **67**(2): p. 209-219.

35. Huang, R.Y.M., R. Pal, and G.Y. Moon, *Characteristics of sodium alginate membranes for the pervaporation dehydration of ethanol-water and isopropanol-water mixtures.* Journal of Membrane Science, 1999. **160**(1): p. 101-113.

36. Chen, S.H., et al., *Pervaporation separation of water/ethanol mixture by sulfonated polysulfone membrane.* Journal of Membrane Science, 2001. **183**(1): p. 29-36.

37. Hung, M.Y., et al., *Pervaporation separation of Water/Ethanol mixture by a sodium sulfonate polysulfon membrane.* Journal of Applied Polymer Science, 2003. **90**(12): p. 3374-3383.

38. Hung, M.Y., et al., *Pervaporation separation of water/ethanol mixture by TGN/PSF blending membrane.* European Polymer Journal, 2003. **39**(12): p. 2367-2374.

39. Qiao, X.Y. and T.S. Chung, *Diamine modification of P84 polyimide membranes for pervaporation dehydration of isopropanol.* Aiche Journal, 2006. **52**(10): p. 3462-3472.

40. Wang, Y.C., et al., *Preparation and pervaporation performance of 3,3-bis[4-(4-aminophenoxy)phenyl] phthalide based polyimide membranes.* Journal of Applied Polymer Science, 2005. **96**(6): p. 2046-2052.

41. Lee, K.R., R.Y. Chen, and J.Y. Lai, *Plasma Deposition of Vinyl-Acetate onto Nylon-4 Membrane for Pervaporation and Evaporation Separation of Aqueous Alcohol Mixtures.* Journal of Membrane Science, 1992. **75**(1-2): p. 171-180.

42. Xu, Z.K., et al., *Microporous polypropylene hollow fiber membranes Part II. Pervaporation separation of water/ethanol mixtures by the poly(acrylic acid) grafted membranes.* Journal of Membrane Science, 2003. **214**(1): p. 71-81.

43. Ball, I.J., et al., *The pervaporation of ethanol water feeds with polyaniline membranes and blends.* Synthetic Metals, 1999. **102**(1-3): p. 1311-1312.

44. Chiang, W.Y. and Y.H. Lin, *Properties of modified polyacrylonitrile membranes prepared by copolymerization with hydrophilic monomers for water-ethanol mixture separation.* Journal of Applied Polymer Science, 2003. **90**(1): p. 244-250.

45. Svang-Ariyaskul, A., et al., *Blended chitosan and polyvinyl alcohol membranes for the pervaporation dehydration of isopropanol.* Journal of Membrane Science, 2006. **280**(1-2): p. 815-823.

46. Rao, K.S.V.K., et al., *Blend membranes of chitosan and poly(vinyl alcohol) in pervaporation dehydration of isopropanol and tetrahydrofuran.* Journal of Applied Polymer Science, 2007. **103**(3): p. 1918-1926.

47. Kurkuri, M.D., U.S. Toti, and T.M. Aminabhavi, *Syntheses and characterization of blend*

membranes of sodium alginate and poly(vinyl alcohol) for the pervaporation separation of water plus isopropanol mixtures. Journal of Applied Polymer Science, 2002. **86**(14): p. 3642-3651.

48. Dong, Y.Q., et al., *Preparation of poly(vinyl alcohol)-sodium alginate hollow-fiber composite membranes and pervaporation dehydration characterization of aqueous alcohol mixtures.* Desalination, 2006. **193**(1-3): p. 202-210.

49. Song, K.M. and W.H. Hong, *Dehydration of ethanol and isopropanol using tubular type cellulose acetate membrane with ceramic support in pervaporation process.* Journal of Membrane Science, 1997. **123**(1): p. 27-33.

50. Peters, T., et al., *Thin high flux ceramic-supported PVA membranes.* Desalination, 2006. **200**(1-3): p. 37-39.

51. Peters, T.A., et al., *Ceramic-supported thin PVA pervaporation membranes combining high flux and high selectivity; contradicting the flux-selectivity paradigm.* Journal of Membrane Science, 2006. **276**(1-2): p. 42-50.

52. Van Veen, H.M., et al., *Dewatering of organics by pervaporation with silica membranes.* Separation and Purification Technology, 2001. **22-3**(1-3): p. 361-366.

53. Sommer, S. and T. Melin, *Performance evaluation of microporous inorganic membranes in the dehydration of industrial solvents.* Chemical Engineering and Processing, 2005. **44**(10): p. 1138-1156.

54. Zhen Huanga, H.-m.G., Wee lee Tan , Xiang-Yi Qiao , Santi Kulprathipanja, *Pervaporation study of aqueous ethanol solution through zeolite-incorporated multilayer poly(vinyl alcohol) membranes Effect of zeolites.* Journal of Membrane Science 2006. **276**: p. 260-271.

55. Van Den Berg, A.W.C., et al., *Zeolite A membranes synthesized on a UV-irradiated TiO2 coated metal support: the high pervaporation performance.* Journal of Membrane Science, 2003. **224**(1-2): p. 29-37.

56. Tanaka, K., et al., *Application of zeolite membranes to esterification reactions.* Catalysis Today, 2001. **67**(1-3): p. 121-125.

57. Zhang, Q.G., et al., *Structure and permeation of organic-inorganic hybrid membranes composed of poly(vinyl alcohol) and polysilisesquioxane.* Journal of Materials Chemistry, 2008. **18**(39): p. 4646-4653.

58. Uragami, T., et al., *Structure and permeation characteristics of an aqueous ethanol solution of organic-inorganic hybrid membranes composed of poly(vinyl alcohol) and tetraethoxysilane.* Macromolecules, 2002. **35**(24): p. 9156-9163.

59. Uragami, T., H. Matsugi, and T. Miyata, *Pervaporation characteristics of organic-inorganic hybrid membranes composed of poly(vinyl alcohol-co-acrylic acid) and tetraethoxysilane for water/ethanol separation.* Macromolecules, 2005. **38**(20): p. 8440-8446.

60. Koops, G.H., et al., *Poly(Vinyl Chloride)Polyacrylonitrile Composite Membranes for the Dehydration of Acetic-Acid.* Journal of Membrane Science, 1993. **81**(1-2): p. 57-70.

61. Pinnau, I. and W.J. Koros, *Relationship between Substructure Resistance and Gas Separation Properties of Defect-Free Integrally Skinned Asymmetric Membranes.* Industrial & Engineering Chemistry Research, 1991. **30**(8): p. 1837-1840.

62. Feng, X.S. and R.Y.M. Huang, *Liquid separation by membrane pervaporation: A review.* Industrial & Engineering Chemistry Research, 1997. **36**(4): p. 1048-1066.

63. Huang, R.Y.M.F., X., *Resistance model approach to asymmetric polyetherimide membranes for pervaporation of isopropanol/ water mixtures.* J. Membrane Sci. , 1993. **84**: p. 15.

64. Ma, H.Y., et al., *High-flux thin-film nanofibrous composite ultrafiltration membranes containing cellulose barrier layer.* Journal of Materials Chemistry, 2010. **20**(22): p. 4692-4704.

65. Tang, Z.H., et al., *Design and Fabrication of Electrospun Polyethersulfone Nanofibrous Scaffold for High-Flux Nanofiltration Membranes.* Journal of Polymer Science Part B-Polymer Physics, 2009. **47**(22): p. 2288-2300.

66. Yoon, Y., B.S. Hsiao, and B. Chu, *High flux ultrafiltration nanofibrous membranes based on polyacrylonitrile electrospun scaffolds and crosslinked polyvinyl alcohol coating.* Journal of Membrane Science, 2009. **338**(1-2): p. 145-152.

67. Yoon, K., B.S. Hsiao, and B. Chu, *Formation of functional polyethersulfone electrospun membrane for water purification by mixed solvent and oxidation processes.* Polymer, 2009. **50**(13): p. 2893-2899.

68. Tang, Z.H., et al., *UV-cured poly(vinyl alcohol) ultrafiltration nanofibrous membrane based on electrospun nanofiber scaffolds.* Journal of Membrane Science, 2009. **328**(1-2): p. 1-5.

69. Yoon, K., B.S. Hsiao, and B. Chu, *High flux nanofiltration membranes based on*

interfacially polymerized polyamide barrier layer on polyacrylonitrile nanofibrous scaffolds. Journal of Membrane Science, 2009. **326**(2): p. 484-492.

70. Yoon, K., B.S. Hsiao, and B. Chu, *Functional nanofibers for environmental applications.* Journal of Materials Chemistry, 2008. **18**(44): p. 5326-5334.

71. Chu, B., B.S. Hsiao, and K. Yoon, *Nanofiber and manocomposite-fiber technology for environmental applications.* Aatcc Review, 2008. **8**(2): p. 31-33.

72. Wang, X.F., et al., *High performance ultrafiltration composite membranes based on poly(vinyl alcohol) hydrogel coating on crosslinked nanofibrous poly(vinyl alcohol) scaffold.* Journal of Membrane Science, 2006. **278**(1-2): p. 261-268.

73. Yoon, K., et al., *High flux ultrafiltration membranes based on electrospun nanofibrous PAN scaffolds and chitosan coating.* Polymer, 2006. **47**(7): p. 2434-2441.

74. Wang, X.F., et al., *High flux filtration medium based on nanofibrous substrate with hydrophilic nanocomposite coating.* Environmental Science & Technology, 2005. **39**(19): p. 7684-7691.

75. Wijmans, J.G., et al., *The role of boundary layers in the removal of volatile organic compounds from water by pervaporation.* J. Membr. Sci. . **1-10**(109): p. 135-146.

76. Koops, G.H., et al., *Poly(vinyl chloride) polyacrylonitrile composite membranes for the dehydration of acetic acid.* Journal of Membrane Science, 2001. **81**(1-2): p. 14.

77. Pinnau, I. and W.J. Koros, *Relationship between substructure resistance and gas separation properties of defect-free integrally skinned asymmetric membranes.* Industrial & Engineering Chemistry Research, 1991. **30**(8).

78. Trifunović, O. and G. Tragardh, *The influence of support layer on mass transport of homologous series of alcohols and esters through composite pervaporation membranes.* Journal of Membrane Science, 2005(259): p. 122-134.

79. Fukuzumi, H., et al., *Transparent and high gas barrier films of cellulose nanofibers prepared by TEMPO-mediated oxidation.* Biomacromolecules, 2009. **10**(1): p. 4.

80. Ma, H., et al., *Ultra-fine Polysaccharide Nanofibrous Membranes for Water Purification.* Biomacromolecules, 2011. **12**: p. 7.

81. Rautenbach, R. and R. Albrecht, *On the behaviour of asymmetric membranes in*

pervaporation. J. Membr. Sci., 1984(19): p. 1-22.

82. Lipnizki, F., et al., *Hydrophobic pervaporation: influence of the support layer of composite membranes on the mass transfer.* Separation Science and Technology, 2002. **37**(8): p. 1747-1770.

83. Gudernatsch, W., T. Menzel, and H. Strathmann, *Influence of composite membrane structure on pervaporation.* Journal of Membrane Science, 1991. **61**(0): p. 19-30.

84. Bode, E. and C. Hoempler, *Transport resistances during pervaporation through a composite membrane: experiments and model calculations.* Journal of Membrane Science, 1996. **113**(1): p. 43-56.

85. Bai, J., et al., *A study on the preparation and performance of polydimethylsiloxane-coated polyetherimide membranes in pervaporation.* Journal of Applied Polymer Science, 1993. **48**(6): p. 999-1008.

86. Tan, S., et al., *The influence of support layer structure on mass transfer in pervaporation of composite PDMS–PSF membranes.* Chemical Engineering Journal, 2010. **157**(2–3): p. 304-310.

87. Liu, Y., et al., *High-flux microfiltration filters based on electrospun polyvinylalcohol nanofibrous membranes.* Polymer, 2013. **54**(2): p. 548-556.

88. Wang, R., et al., *Nanofibrous microfiltration membranes capable of removing bacteria, viruses and heavy metal ions.* Journal of Membrane Science, 2013. **446**(0): p. 376-382.

89. Ma, H., et al., *Highly Permeable Polymer Membranes Containing Directed Channels for Water Purification.* ACS Macro Letters, 2012. **1**(6): p. 723-726.

90. Yeh, T.-M., et al., *Polymeric nanofibrous composite membranes for energy efficient ethanol dehydration.* Journal of Renewable and Sustainable Energy, 2012. **4**(4): p. 041406.

91. Venturoli, D. and B. Rippe, *Ficoll and dextran vs. globular proteins as probes for testing glomerular permselectivity: effects of molecular size, shape, charge, and deformability.* American Journal of Physiology - Renal Physiology, 2005. **288**(4): p. F605-F613.

92. Wang, X., et al., *Nanofiltration Membranes Prepared by Interfacial Polymerization on Thin-Film Nanofibrous Composite Scaffold.* Polymer, 2013. **(in pressing)**.

93. N. R. Wilson, P.A. Pandey, R. Beanland, R. J. Young, I. A. Kinloch, L. Gong, Z. Liu, K.

Suenage, J. P. Rourke, S. J. York, J. Solan. *Acs Nano*. **2009**, 3, 2457-2556..

94. G. Eda, M. Chhowalla. *Adv. Mater.* **2010**. 22, 2392-2415.

95. S. Park, K. Lee, G. Bozoklu, W. Cai, S. T. Nguyen, R. S. Ruoff. *Acs Nano*. **2008**, 2, 572-578.

96. R. R. Nair, Wu, H. A, P. N Jayaram, I. V. Grigorieva, A. K Geim, *Science*, **2012**, 335, 442-444.

97. J. William, S. Hummers, R. E. Offeman, J. Am. Chem. Soc. **1958**, 80, 1339.

98. H. Ma, K. Yoon, L. Rong, M. Sokralla, A. Kopot, X. Wang, D. Fang, B. S. Hsiao, B. Chu, *Ind. Eng. Chem. Res*. **2010**, 49, 11978-11984.

99. H. Ma, C. Burger, B. S. Hsiao, B. Chu, *Acs Macro Lett.* **2012**, 1, 723-726.

100. K. W. Putz, O. C. Compton, M. J. Palmeri, S. T. Nguyen, L. C. Brinson, *Adv. Func. Mater*. **2010**, 20, 3322-3329.

101. A. Reina, X. Jia, J. Ho, D. Nezich, H. Son, V. Bulovic, M. S. Dresselhaus, J. Kong, Acs Nano. 2008. 9, 30-35.

102. V. López, R. S. Sundaram, C. Gómez-Navarro, D. Olea, M. Burghard, J. Gómez-Herrero, F. Zamora, K. Kern, Adv. Mater. 2009, 21, 4683-4686.

103. X. Li, G. Zhang, X. Bai, X. Sun, X. Wang, E. Wang, H. Dai, *Nat. Nano.* **2008**, 3, 538-542.

104. Y. Yang, L. Bolling, M. A. Priolo, J. C. Grunlan, *Adv. Mater.* **2013**, 25, 503-508.

105. C. Chen, Q. Yang, W. Lv, Y. Wen, P. Hou, M. Wang, H. Cheng, *Adv. Mater.* **2009**, 21, 3007-3011.

106. L. Yang, *J. Synchrotron Rad.* **2013**. 20, 211-218.

107. J. I. Paredes, S. Villar-Rodil, A. Martínez-Alonso, J. M. D. Tascón, *Langmuir*, **2008**, 24, 10560-10564.

108. A. Buchsteiner, A. Lerf, J. Pieper, *J. Phys. Chem. B,* **2006,** 110, 22328-22338.

109. Z. An, O. C. Compton, K. W. Putz, L. C. Brinson, S. T. Nguyen, *Adv. Mater.* **2011**, 23, 3842-3846.

110. Q. Cheng, M. Wu, M. Li, L. Jiang, Z. Tang, *Angew. Chem. Int. Ed.* **2013**, 52, 3750-3755.

111. A. Satti, P. Larpent, Y. Gun'ko, Carbon, 2010, 48, 3376-3381.

112. D. R. Paul, *Science*, **2012**, 335, 413-414

113. J. William, S. Hummers, R. E. Offeman, *J. Am. Chem. Soc.* **1958**, 80, 1339.

114. Zhu, Y., et al., *Graphene and Graphene Oxide: Synthesis, Properties, and Applications.* Advanced Materials, 2010. **22**(35): p. 3906-3924.

115. Park, S., et al., *Graphene Oxide Sheets Chemically Cross-Linked by Polyallylamine.* The Journal of Physical Chemistry C, 2009. **113**(36): p. 15801-15804.

116. Kuila, T., et al., *Chemical functionalization of graphene and its applications.* Progress in Materials Science, 2012. **57**(7): p. 1061-1105.

117. Dreyer, D.R., et al., *The chemistry of graphene oxide.* Chemical Society Reviews, 2010. **39**(1): p. 228-240.

118. Park, S., et al., *Graphene Oxide Papers Modified by Divalent Ions—Enhancing Mechanical Properties via Chemical Cross-Linking.* Acs Nano, 2008. **2**(3): p. 572-578.

119. Jiang, X., et al., *Self-Assembly of Reduced Graphene Oxide into Three-Dimensional Architecture by Divalent Ion Linkage.* The Journal of Physical Chemistry C, 2010. **114**(51): p. 22462-22465.

120. Stankovich, S., et al., *Systematic Post-assembly Modification of Graphene Oxide Paper with Primary Alkylamines.* Chemistry of Materials, 2010. **22**(14): p. 4153-4157.

121. Ma, H.-L., et al., *Chemical reduction and removal of Cr(vi) from acidic aqueous solution by ethylenediamine-reduced graphene oxide.* Journal of Materials Chemistry, 2012. **22**(13): p. 5914-5916.

122. Lee, D.W., et al., *Highly controllable transparent and conducting thin films using layer-by-layer assembly of oppositely charged reduced graphene oxides.* Journal of Materials Chemistry, 2011. **21**(10): p. 3438-3442.

123. Gao, Y., et al., *The Effect of Interlayer Adhesion on the Mechanical Behaviors of Macroscopic Graphene Oxide Papers.* Acs Nano, 2011. **5**(3): p. 2134-2141.

124. An, Z., et al., *Bio-Inspired Borate Cross-Linking in Ultra-Stiff Graphene Oxide Thin Films.* Advanced Materials, 2011. **23**(33): p. 3842-3846.

125. Yeh, T.-M., et al., *High flux ethanol dehydration using nanofibrous membranes containing graphene oxide barrier layers.* Journal of Materials Chemistry A, 2013. **1**(41): p. 12998-13003.

126. Hummers, W.S. and R.E. Offeman, *Preparation of Graphitic Oxide.* Journal of the American Chemical Society, 1958. **80**(6): p. 1339-1339.

127. Ma, H., et al., *High-flux thin-film nanofibrous composite ultrafiltration membranes containing cellulose barrier layer.* Jounral of Materials Chemistry, 2010. **20**(22): p. 4692-4704

128. Ma, H., et al., *Thin-film nanofibrous composite ultrafiltration membranes based on polyvinyl alcohol barrier layer containing directional water channels.* Industry & Engineering Chemistry Research, 2010. **49**: p. 7.

129. Bunch, J.S. and M.L. Dunn, *Adhesion mechanics of graphene membranes.* Solid State Communications, 2012. **152**(15): p. 1359-1364.

130. Jayasena, B., C.D. Reddy, and S. Subbiah, *Separation, folding and shearing of graphene layers during wedge-based mechanical exfoliation.* Nanotechnology, 2013. **24**(20): p. 205301.